



**Politecnico
di Torino**

Department of Environment, Land and Infrastructure Engineering
Master of Science in Environmental and Land Engineering – Climate Change

Master Thesis

A geomatics approach to assess the environmental impact of lithium mining

Supervisor:

Prof. Piero Boccardo

Co-Supervisor:

Prof. Giovanni Andrea Blengini

Candidate:

Alberta Pavone

July 2022

Abstract

Nowadays, the economic development is still heavily dependent on raw materials extraction: future trends predict that the extraction of mineral resources will increase in the next decades, due to the increase in the global population and to the transition towards clean energy. Lithium is one of the critical minerals in the ecological transition, because fundamental for electric vehicles lithium-ion batteries. Its demand is expected to soar in a sustainable scenario that wants the global temperature rising to stay below 2°C with respect to the pre-industrial levels. Natural resources extraction generates environmental pressures both at the local and global level, causing environmental and social impacts. Therefore, more studies are needed to evaluate the implications caused by lithium mining and production. The aim of this study is to show the important role of Remote Sensing and Geographic Information System (GIS) to study lithium mining and its supply chain, underlining the need to use geospatial data and tools to quantify the carbon emissions of transportation and the environmental impacts of mining activity on the land use. Two case studies have been considered, representing the two different lithium mining technologies: one in the Salar de Atacama (Chile) where lithium is extracted from brine and the other one at Greenbushes (Western Australia) where lithium is extracted from ore. In Chile, an automatic way of extraction of the land disturbed by the mining activity has been carried out using several indices, evaluating which of them performs better through an accuracy assessment. In Western Australia, a manual extraction of the mine area has been performed in GIS since a lower time-consuming process is needed. Sentinel-5P satellite images have been analysed to detect if eventual atmospheric emissions can be quantified at mine sites to be integrated in the Life Cycle Assessment (LCA) analysis. Land and sea routes in the lithium supply chain have been studied and kilometres travelled by trucks and vessels have been quantified. Land disturbed by the mine activity has been linked to the production rate of the mine site, generating an indicator of the Land Use Intensity (LUI) using both mass and economic allocation methods. The global impact of carbon emissions generated from the transportation in lithium production have been estimated, through the integration in a LCA analysis, using the ILCD 2011 Midpoint+ characterization method. Among all the indices used to extract the mine area in Chile, the MNDWI computed with the SWIR shows the highest accuracy, followed by the NDVI. Sentinel-5P satellite images have a spatial resolution that do not allow the identification of emissions belonging to the mine sites, underlining the need to develop higher spatial resolution data products. Land Use Intensity results are highly dependent on allocation methods: considering the results obtained with economic allocation, LUI is higher for lithium products extracted from brine in Salar de Atacama (133.4 - 142.7 m²/ton) with respect to the ones

extracted from ore at Greenbushes (42.7 - 48.6 m²/ton). The results of the carbon emissions analysis estimated that transportation in lithium supply chain accounts for 12.5% for lithium carbonate and 5.05% for lithium hydroxide in the Chilean pathway and respectively 3.32% and 4.29% in the Australian one. LCA results also shows that a shorter supply route in Western Australia lower the emission from 0.70 tonCO₂eq/ton of lithium product to 0.18 tonCO₂eq/ton. The results obtained in this work underline the importance to adopt a multidisciplinary approach in the study of mining sector and to define a common methodology and criteria to assess its environmental impacts, integrating Remote Sensing and GIS tools in the analysis.

Table of Contents

List of Figures	7
List of Tables	10
Abbreviations	12
1 Introduction	13
1.1 Objectives of the study.....	15
2 Lithium in a nutshell	17
3 Characterization of the study sites	22
3.1 Salar de Atacama, Chile	22
3.1.1 Lithium extraction process from brine	23
3.1.2 The importance of the unique ecosystem	25
3.1.3 Social and political framework.....	27
3.2 Greenbushes, Western Australia	28
3.2.1 Lithium extraction process from ore	30
4 Data products	33
5 Methodology	38
5.1 Indices analysis for evaporation ponds area extraction in Chile.....	38
5.2 Mine area analysis in Western Australia	45
5.3 Atmospheric emissions analysis	46
5.4 Transportation Routes Analysis.....	46
5.5 Environmental impact assessment of lithium mining on land	47
5.6 Carbon emissions from lithium products: the contribution of transportation	49
6 Results and discussions	53
6.1 Indices analysis for evaporation ponds area extraction in Chile.....	53
6.2 Mine area analysis in Western Australia	56
6.3 Atmospheric emissions analysis	58
6.4 Transportation Routes Analysis.....	60

6.5	Environmental impact assessment of lithium mining on land	67
6.6	Carbon emissions from lithium products: the contribution of transportation	70
7	Conclusions	73
	References	75
	Appendix	79
I.	Indices Analysis for evaporation ponds area extraction in Chile	79
II.	Transportation Routes Analysis.....	84
III.	Environmental impact assessment of lithium mining on land	86
IV.	Carbon emissions from lithium products: the contribution of transportation	95

List of Figures

Figure 1. Mineral demand for clean energy technologies by scenario: Sustainable Development Scenario (SDS) and Net-zero by 2050 Scenario (NZE). (Source: IEA, 2021).....	14
Figure 2. Main global end-use markets of lithium in 2021 according to USGS data (USGS, 2022). .	17
Figure 3. Main countries where lithium resources are located in 2021 according to USGS data (USGS, 2022).	18
Figure 4. Timeseries of lithium resources and reserves, expressed in million tons (left axis), and of lithium production and consumption, expressed in thousand tons (right axis). Data shown in the graph come from the Annual Publication of Lithium Statistics and Information by National Minerals Information Center, USGS.	19
Figure 5. Location of the Salar de Atacama, in northern Chile, shown by a Landsat 8 satellite image acquired on the 27 th of September 2016. (Source: Marazuela et al., 2020).....	23
Figure 6. SQM mine plant in the Salar de Atacama, Chile. (Source: SQM, https://www.sqmlithium.com/en/nosotros/).....	24
Figure 7. Sentinel-2 satellite image acquired on the 16 th of January 2022 showing SQM processing plant in the Salar de Carmen (left) and Albemarle processing plant, called Planta Química La Negra (right).	25
Figure 8. Topographic Map of the Salar de Atacama, showing National Reserves, Human Settlements, Rivers, and Streams. (Source: Liu et al., 2019).	26
Figure 9. Aerial image showing the town of Greenbushes and the close spodumene mine site. (Source: Talison Lithium https://www.talisonlithium.com/greenbushes-project).....	29
Figure 10. Sentinel-2 satellite image acquired on the 6 th of April 2022 showing the area of Fremantle and the Kwinana processing plant.	31
Figure 11. Sentinel-2 satellite image acquired on the 11 th of April 2022 showing the Kemerton lithium processing plant.	31
Figure 12. Spectral signatures of three different evaporation pond classes in ENVI software. On the x axis, the bands considered in the analysis are shown; on the y axis, the Surface Reflectance value acquired by the MSI sensor is shown.	41
Figure 13. Flow diagram showing the steps carried out to process each satellite image in ArcGIS Pro and in ENVI.....	43
Figure 14. Flow diagram showing the steps followed to create ground truth data.	44
Figure 15. Flow diagram showing the steps followed to perform the accuracy assessment in ArcGIS Pro.....	45

Figure 16. Flow processes and system boundaries for the Chilean brine pathway. Road Transport (RT) in Chile and in China and Ship Transport (ST) are also indicated.	49
Figure 17. Flow processes and system boundaries for the Australian ore pathway. Road Transport (RT) in Western Australia and in China and Ship Transport (ST) are also indicated.....	50
Figure 18. Graph illustrating all the origin and destination locations for each transportation stage for the Chilean brine pathway.....	50
Figure 19. Graph showing all the origin and destination locations for each transport stage for the Western Australian ore pathway.	51
Figure 20. Graph showing all the origin and destination locations for each transport stage for the near future Western Australian ore pathway.	52
Figure 21. True Color Image Sentinel-2 satellite images acquired on the 3 rd of January 2022 showing the area over the Salar de Atacama, Chile.	53
Figure 22. NDVI image (left) and NDWI (McFeeter) image (right) showing the Salar de Atacama area.	54
Figure 23. Sentinel-2 satellite image acquired on the 17 th of February 2022 showing the mine site of Greenbushes and the identified active area with a red dotted line.	56
Figure 24. False Color of the satellite image acquired by Sentinel-2 on the 17 th of February 2022 showing the Greenbushes mine site and the area affected by the fire (in brownish).....	57
Figure 25. Aerosol Index (AER AI) image obtained from TOPOMI sensor (Sentinel-5P), acquired on the 1 st of January 2022 over the Chilean area.	59
Figure 26. Nitrogen Dioxide (NO ₂) image obtained from TOPOMI sensor (Sentinel-5P), acquired on the 8 th of February 2022 over the Chilean area.....	59
Figure 27. Nitrogen Dioxide (NO ₂) image obtained from TOPOMI sensor (Sentinel-5P), acquired on the 5 th of February 2022 over the Greenbushes area in Western Australia.	60
Figure 28. Map showing the stops and the transportation routes in Chile for the SQM trucks (green) and for the Albemarle ones (brown).	61
Figure 29. Map showing the stops and the transportation route in Western Australia for the trucks transporting concentrated spodumene from the Greenbushes mine site.	62
Figure 30. Map showing the stops and the transportation routes in China for the trucks in the Chilean lithium brine pathway (yellow), in the Australian ore pathway (brown), and in the near future Australian ore pathway (green).....	63
Figure 31. Sea routes travelled by the vessels both for lithium production from brine in Chile (green) and from ore in Western Australia (red).	65

Figure 32. Multitemporal land use images showing the area of the port of Mejillones in Chile, retrieved from the GlobeLand30 database. The upper left image refers to the year 2000, the upper right one to the year 2010, and the bottom one to the year 2020.66

Figure 33. Results of the LCA analysis, where the absolute value of carbon emission related to transport is shown in yellow. Carbon emissions coming from the lithium production, shown in blue, have been retrieved from literature (Kelly et al., 2021).70

Figure 34. Percentage of carbon emissions related to transport in lithium production for lithium carbonate and for lithium hydroxide extracted from brine in Chile and from ore in Western Australia.71

Figure 35. True Color Images of the processed satellite images showing the Salar de Atacama during the years.79

Figure 36. NDVI image computed for each year considered in the analysis.80

Figure 37. Indices image (NDWI, MNDWI, ...) computed for the satellite image related to the year 2022. The two bottom images show the ground truth data (left) and the binary image (right) for the year 2022.81

Figure 38. Binary images (0,1) for all the indices considered (NDVI, NDWI, MNDWI, ...) for the analysis of the satellite image relative to the year 2022.82

Figure 39. Travel Mode properties and Restriction settings related to the trucks transportation route analysis computed in ArcGIS Pro.85

Figure 40. Binary Image obtained through the NDVI analysis showing the Salar de Atacama area, identifying the SQM operations (red circle) and the lithium evaporation ponds section (blue circle).86

Figure 41. Flow chart showing the different mass required to produce 1 ton of lithium carbonate and lithium hydroxide, starting from the mass of the extracted brine from the Salar de Atacama.87

Figure 42. Flow chart showing the different mass required to produce 1 ton of lithium carbonate and lithium hydroxide, starting from the mass of the spodumene ore extracted at Greenbushes mine site.92

List of Tables

Table 1. Spectral bands and spatial resolution of the Thematic Mapper (TM) sensor mounted on board of Landsat 5. (Source: USGS https://www.usgs.gov/landsat-missions/landsat-5).....	33
Table 2. Spectral bands and spatial resolution of the Operational Land Imager (OLI) sensor mounted on board of Landsat 8. (Source: USGS https://www.usgs.gov/landsat-missions/landsat-8).....	34
Table 3. Wavelengths and Bandwidths of the three Spatial Resolutions of the MSI instruments mounted on board of Sentinel-2. (Source: https://sentinel.esa.int/web/sentinel/missions/sentinel-2/instrument-payload/resolution-and-swath)	35
Table 4. Level 2 geophysical products of the TROPOspheric Monitoring Instrument (TROPOMI) mounted on board of Sentinel 5P. (Source: https://sentinels.copernicus.eu/web/sentinel/technical-guides/sentinel-5p/products-algorithms)	36
Table 5. List of all the satellite images used for this analysis, showing the acquisition date, the sensor type, and the cloud cover of the data products.	37
Table 6. Bands correspondence between the Band Number proper of Sentinel-2 Nomenclature and the one assigned in ENVI during the analysis.	41
Table 7. Thresholds that have been used to create all the binary images, estimated area (in squared kilometres) occupied by the evaporation ponds, and Kappa Coefficient resulting from the accuracy analysis shown for each index in relation to the Sentinel-2 satellite image acquired in 2022.	55
Table 8. Confusion matrix relative to the NDVI analysis.....	55
Table 9. Results of the estimated area according to the multitemporal NDVI analysis, together with the Kappa Coefficient accuracy indicator.	56
Table 10. Results of the Land Routes Transportation Analysis, showing distances expressed in kilometres.	64
Table 11. Results of the Sea Routes Transportation Analysis, showing the distance covered by the vessels in kilometres, together with the days of travelling.	65
Table 12. Results of the Land Use Intensity (LUI) analysis, showing the squared metres per ton of product of lithium carbonate and of lithium hydroxide both for the brine extraction in the Salar de Atacama and for the ore extraction at Greenbushes. Mass allocation and economic allocation results are also shown for the brine extraction in Chile, together with the land use intensity related to potash as coproduct.	67
Table 13. Confusion matrix relative to the NDWI (McFeeters) analysis.	83
Table 14. Confusion matrix relative to the NDWI (Gao) analysis.....	83

Table 15. Confusion matrix relative to the MNDWI (Xu) analysis.....	83
Table 16. Confusion matrix relative to the MNDWI (SWIR1) analysis.	83
Table 17. Confusion matrix relative to the MNDWI (SWIR2) analysis.	83
Table 18. Life Cycle Inventory Data used to perform the LCA analysis for lithium carbonate and for lithium hydroxide both for the brine pathway and for the ore pathway. The carbon dioxide data emissions to air have been retrieved from literature (Kelly et al., 2021).	95
Table 19. Life Cycle Impact Assessment results for lithium carbonate and lithium hydroxide both for the brine pathway and the ore pathway and for the ore near future scenario.....	97

Abbreviations

AOI: Area of Interest

DLE: Direct Lithium Extraction

EVs: electric vehicles

GDP: Gross Domestic Product

GIS: Geographic Information System

LCIA: Life Cycle Impact Assessment

LCA: Life Cycle Assessment

LUI: Land Use Intensity

MIR: Middle Infrared

MNDWI: Modified Normalized Difference Water Index

MOP: Muriate of Potash

NIR: Near Infrared

NDVI: Normalized Difference Vegetation Index

NDWI: Normalized Difference Water Index

NMC622: $\text{LiNi}_{0.6}\text{Mn}_{0.2}\text{Co}_{0.2}\text{O}_2$

NMC811: $\text{LiNi}_{0.8}\text{Mn}_{0.1}\text{Co}_{0.1}\text{O}_2$

OSM: Open Street Map

RS: Remote Sensing

RT: Road Transport

SDGs: Sustainable Development Goals

SDS: Sustainable Development Scenario

SQM: Sociedad Química y Minera de Chile

SWIR: Shortwave Infrared

ST: Ship Transport

USGS: United States Geological Survey

1 Introduction

The extraction of natural resources is fundamental to the current global economy: raw materials are needed to produce goods and commodities both for the industry and for everyday use. The increasing high-performance demand of objects and electronic devices has led to an increase of their complexity and of the number of the materials required as input. One of the main goals of the 2030 Agenda for Sustainable Development is to decouple the economic growth from the resource use intensity and from environmental degradation (Goal 8.4), improving the efficiency and promoting the transition to a circular economy. However, nowadays the economic development is still heavily dependent on primary raw materials extraction: future trends predict that the mining of mineral resources will increase in the next decades, also due to the increase in the global population and to the transition towards green energy (OECD, 2019). The Paris Agreement has set to 2°C the maximum limit for the global temperature rising with respect to the pre-industrial levels, making efforts to keep it below 1.5°C. The International Energy Agency (IEA) has estimated that four times more minerals are needed by 2040 to reach the target goals in what it is called the Sustainable Development Scenario (SDS) (IEA, 2021), as shown in the column graph (left) in Figure 1. Instead, to be net-zero by 2050, six times the amount of minerals extracted today will be required at the global level (IEA, 2021). United States and European Union objective is to be Net-Zero by 2050; instead, China aims to hit the carbon emissions peak before 2030 and to be carbon neutral by 2060. To perform a rapid and collective transition towards a clean energy, many materials are needed for renewable energy technologies and energy storage systems. However, there are not enough metals for a low carbon energy transition and at the same time there is not enough low carbon energy for metal supply expansion (Wang et al., 2022; Thiel et al., 2021). For this reason, there is the risk of shifting the burden of carbon emissions from consumption to production.

The transition towards a clean energy and the consequent high demand for electric vehicles and renewable energy technologies is increasing the rate of extraction of natural resources from the Earth's crust. Electric batteries need several materials to be produced, requiring a high grade of mineral purity to reach high performance. Lithium is one of the metals that can be found in lithium-ion batteries, thus becoming critical for the energy transition. In the report *Critical Minerals for the Clean Energy Transitions* published by the IEA (IEA, 2021), it is underlined how lithium demand is set to soar, estimating that it will be 42 times higher in 2040 with respect to 2020 in the Sustainable Development Scenario, as shown in the column graph (right) in Figure 1.

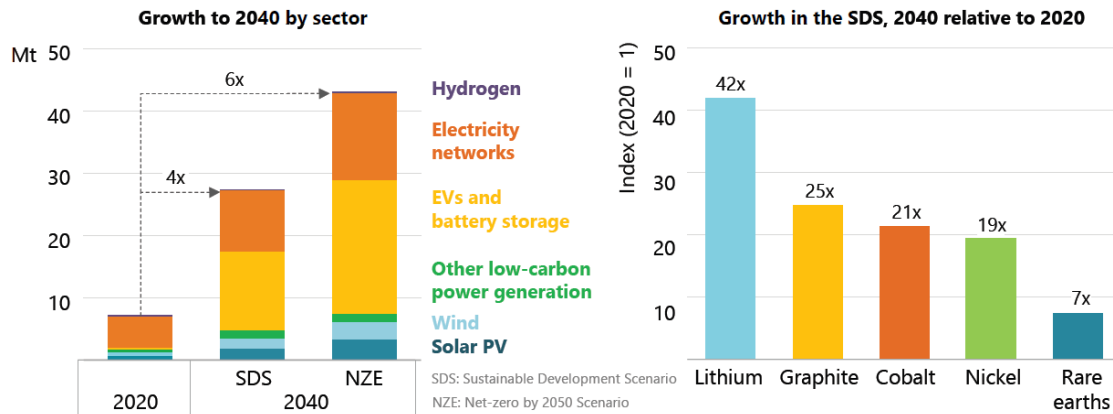


Figure 1. Mineral demand for clean energy technologies by scenario: Sustainable Development Scenario (SDS) and Net-zero by 2050 Scenario (NZE). (Source: IEA, 2021)

It is clear that natural resource extraction is expected to increase in the next decades, but mining activity has already become a pillar of the local economy of many countries over the years, generating jobs for the population and income for the nation. On the other hand, the extraction of natural resources is known to generate high pressures at the local level, causing many environmental and social impacts (Rudke et al., 2020). Water pollution, soil contamination, and land use are only some of the important issues linked to mining. There is a deep and complex interconnection between minerals extraction from the Earth's crust, energy and water needed for the process, and land required both for the extraction and for the waste disposal (Murguía et al., 2016). This "resource-nexus" generates competition for natural resources between the different parties that live or operate in a mine area. Protests of the local population often arise against both the private companies and against the government that gives concessions to the mining companies. Given the future resource demand in the Sustainable Development Goals (SDGs) framework, there is the needed to understand the critical and complex resource nexus of water, energy, food, land, and materials, through studies at different scales and contexts (Bleischwitz et al., 2018).

Environmental impacts are not usually completely understood because of the limited data available for the public at mine sites and since there is not a common methodology to assess them (Tost et al., 2018). Allocation methods, system boundaries, and input parameter can generate a large difference in the results obtained for the same area of analysis. Therefore, more studies to evaluate the environmental impacts caused by mining activity are needed. Remote Sensing and Geographic Information System (GIS) represent two important tools to study the mine areas, for example monitoring the changes in the land use or the eventual source of pollution in a region. Remote Sensing allows to study and cover large areas in a comprehensive and reliable way, being also an affordable cost technology (Charou et al., 2010). Thanks to historical data of multispectral satellites,

multitemporal analysis can be performed, generating databases, and retrieving important information on the variation of vegetation, built-up area, water bodies in the studied area. This kind of analysis could make the dynamics of an area clearer, representing a tool and a starting point to create management guidelines for the mine site and for the region itself. Therefore, spatial data can provide accurate information, especially on surface and land use changes, with a high potential in many environmental and social applications. However, there are no standardized methods to carry out environmental analysis that aim to quantify the environmental pressure of mining activity on land, thus limiting the comparison of the results between different studies (Tost et al., 2018). Therefore, there is the need to create common and coherent methods, that could be implemented integrating large spatial data to the environmental assessment. These methods should be designed to be applicable in different contexts, and should not require in situ measurements for validation, so that their implementation would be faster. Common criteria can allow comparisons of environmental impacts generated by different commodities or by the same material extracted in two different mine sites, with different extraction technologies. However, the creation of a shared methodology is a difficult and limited task because of the many types of extraction and production processes, sometimes also related to the same commodity. As mentioned before, another factor limiting the impact evaluations in mining activity is that there are not enough reliable environmental data available at mine site (Tost et al., 2018). Thanks to the Directive of the European Commission (2014/95/EU) delineating the Corporate Sustainability Reporting, non-financing report at company level often contains environmental quantitative data and information about sustainability. In Italy, the Directive has been implemented, requiring non-financial reporting to public institutes and private companies with more than 500 employees or with a certain asset. However, there is a large availability of economic and production data that can be retrieved from the main official mining databases such as the one of the United States Geological Survey (USGS) and of the S&P Global. Therefore, this information can be found more easily and can be integrated in the methodology for the environmental impact assessment, together with the geospatial data retrieved from Remote Sensing and GIS-based analysis.

1.1 Objectives of the study

The aim of this study is to show the importance of Remote Sensing and GIS-approach to study lithium mining and its production process. This work wants to underline the need to use geospatial data and tools to assess environmental impacts of mining activity on the land use, focusing on lithium extraction. In fact, lithium is a critical and strategic material for the energy transition, being fundamental to produce batteries used in electric vehicles. Two case studies have been considered,

representing two different lithium extraction technologies from brine and from ore. In particular, the land disturbed by the mine area has been linked to the production rate of the mine site, generating an indicator of the Land Use Intensity for each commodity considered. Remote Sensing techniques and GIS tools have been used to estimate the land use area, underlining the importance of the integration of these two disciplines. This work aims also to show the role of GIS tools to analyse the supply routes of lithium production, quantifying the kilometres travelled both on the land and on the sea. The global impact of carbon emissions generated from the transportation in lithium supply chain has been estimated, through the integration in a Life Cycle Assessment analysis.

2 Lithium in a nutshell

Lithium, identified with the chemical symbol Li, is the lightest metal and the least dense solid element at room temperature (around 0.53 g/cm³). It belongs to the alkali metal group, being in its pure form a soft grey metal. However, because of its high reactivity, it can occur in nature only in the form of inert mineral compounds or as chloride in brines and seawater (European Commission, 2020). There are different valuable lithium compounds: lithium carbonate (Li_2CO_3), lithium hydroxide ($LiOH$), lithium chloride ($LiCl$), and the metallic lithium (Li) (Meng et al, 2021). These compounds have different application, according to their quality and their degree of purity. The U.S. Geological Survey (USGS) estimated the global end-use of lithium markets in 2021: as shown in the pie chart in Figure 2, lithium is used mainly for batteries (74%), followed by glass and ceramics (14%), lubricating greases (3%), continuous casting mold flux powders (2%), polymer production (2%), air treatment (1%), and other uses (4%) (USGS, 2022). The market of lithium changes according to the location considered: for example, in Europe the glass and ceramic industries represents the main demand for lithium (European Commission, 2020).

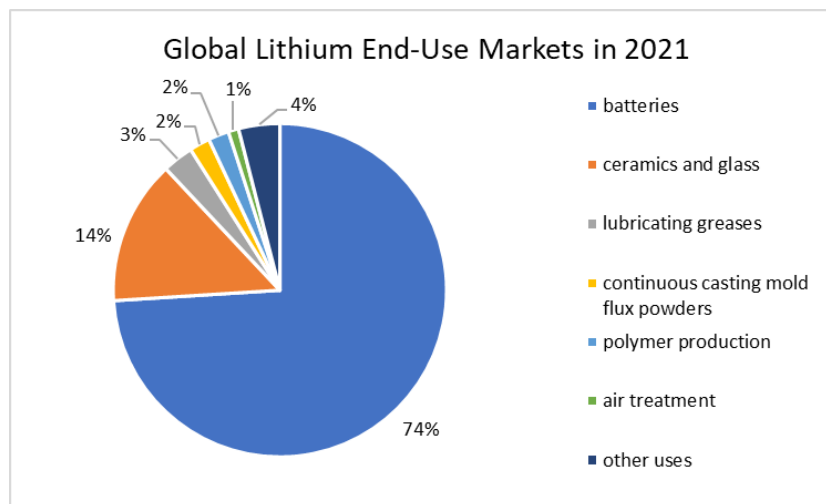


Figure 2. Main global end-use markets of lithium in 2021 according to USGS data (USGS, 2022).

There are two different kinds of lithium extraction: the hard rock mining process, which extracts mainly lithium in the form of spodumene and the brine evaporation process, which uses solar energy to let water evaporate leaving a high lithium concentration in the ponds (Tabelin et al, 2021). In the last years, new technologies have been studied for improving the process efficiency and lower the environmental impacts of the extraction. For example, the Direct Lithium Extraction (DLE) technologies which extract lithium through surfaces or membranes and then reinject the brine in the underground immediately after the mineral has been separated. It is a scale dependent

technology, making the process more difficult to be scaled up (Pálsdóttir et al, 2020), but it would allow to have faster production with high recoveries (Tabelin et al, 2021). Moreover, a new technology in the lithium extraction from geothermal brine is under studying. It uses supercritical fluid extraction process, which consists in transferring extracted components across a fluid interface. This method does not rely on solid extraction surfaces or membranes, making it less susceptible to surface scaling (Pálsdóttir et al, 2020).

According to data published annually by the USGS, lithium resources continue to increase, as shown in the timeseries graph in Figure 4, thanks to the higher exploration performed because of the current and future strategic importance of the mineral. In 2021, the main resources of lithium in the world have been estimated at 89 million tons, mainly located in Bolivia, Argentina, Chile, Australia, and China (USGS, 2022), as shown in the pie chart in Figure 3. In fact, one of the largest deposits of lithium in the world can be found in the so called “lithium triangle”, that is the area located between Bolivia, Chile, and Argentina, where lithium is contained in brines in the underground. At the time of writing, Bolivia has not started mining lithium at large scale, but there are projects in the development phase that plan to extract the mineral in the Salar de Uyuni in the next years (Reuters, 2022). The current global lithium reserves have been estimated at around 22 million metric tons, located mainly in Chile, Australia, Argentina, and China (USGS, 2022). Australia hosts the main sources of hard rock lithium, constituting a global lithium supply leader since 2018 (European Commission, 2020).

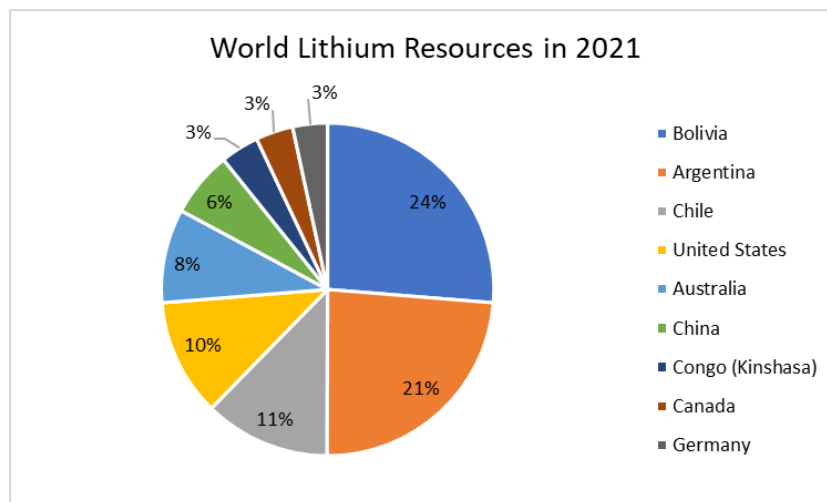


Figure 3. Main countries where lithium resources are located in 2021 according to USGS data (USGS, 2022).

Global lithium production has been constant for decades, being around 5 thousand tons per year, but it has started increasing since the last years of the XX century. As shown in the timeseries graph

in Figure 4, which summaries data published annually by USGS, in 2021 the global production of lithium has been estimated at around 100,000 tons per year, higher with respect to the year before, in 2020, when it has been around 82,500 tons (USGS, 2022). However, the lower production in 2020 has been a response to the low prices in the market and to the overproduction of that year (USGS, 2021). Therefore, the improvement of the pandemic emergency condition, the soaring demand of electric vehicles (EVs), and the higher price of lithium in the market have played key roles in the increase of the production in 2021.

The current recycling rate of lithium is almost negligible: the mineral cannot be recovered from glass and ceramics; instead, it could be recovered from Li-ion batteries, but the recycling process is still facing technical and economic challenges (Torres De Matos et al., 2020). Despite the collection rate of lithium is around 53%, the end-of-life recycling rate (EOL-RR), that is the ratio between the recycled mineral with respect to the amount collected from end-of-life products is around 0.4%. Instead, the end-of-life recycling input rate (EOL-RIR) that is the secondary material input in the European market demand is around 0.1% (Torres De Matos et al., 2020). According to the analysis of the European Commission and the Joint Research Centre (JRC), these low values of the indicators are a result of the low economic relevance obtained from lithium recycling due to the small quantities of the mineral present in products and to the low price of the primary material.

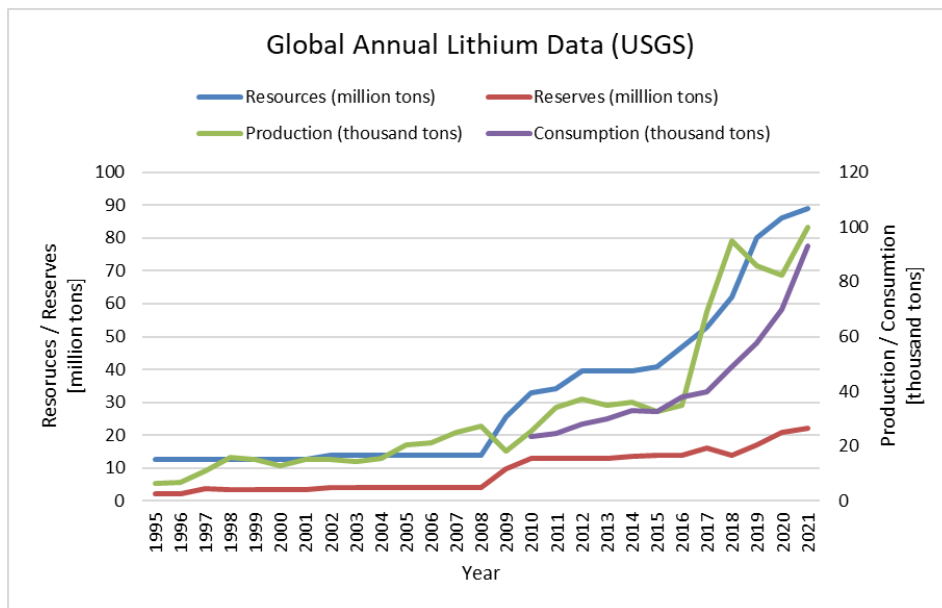


Figure 4. Timeseries of lithium resources and reserves, expressed in million tons (left axis), and of lithium production and consumption, expressed in thousand tons (right axis). Data shown in the graph come from the Annual Publication of Lithium Statistics and Information by National Minerals Information Center, USGS.

The main importer of lithium concentrates and of lithium carbonate is China, because it hosts the largest number of processing plants that refine the mineral in higher-value products, such as lithium hydroxide for EV's batteries. Therefore, China constitutes also one of the main exporters of such products that are destined mainly for domestic use and for countries such as Japan and South Korea, where batteries manufacture takes place.

In the long term, lithium prices are determined by fixed contracts, stipulated after a negotiation between the lithium producers and the buyers that are going to refine lithium products. Spot prices, instead, can have a high variability also in the short term, being more volatile than the previous mentioned (European Commission, 2020). For example, in 2021, fixed lithium carbonate average price has been equal to 17,000 US dollars per ton (USGS, 2022). In the same year, spot lithium carbonate prices in China have seen a rapid and consistent increase: from 7,000 US dollars per ton in January to 26,200 US dollar per ton in November (USGS, 2022). The price of lithium hydroxide has experienced almost the same growth, being around 9,000 US dollars per ton in January and reaching 27,400 US dollars per ton in November (USGS,2022). The cost of concentrated spodumene has also soared from 450 US dollars per ton in January to 2,300 US dollars per ton in November (USGS,2022). However, the price of this strategic mineral has been fixed at around 5,000 US dollars per ton until the 1990s, decade in which it started to slowly decrease, reaching a value of 4,200 US dollars per ton. After the collapse of lithium prices to 1,500 US dollars in 2001, it started increasing again starting from 2005, reaching a value of almost 3,500 US dollars per ton, but it experienced another drop due to the economic crisis of 2008. Since 2011, lithium prices have started rising again, with a higher rate starting from 2015 due to the increasing lithium importance in the global market. In 2018, lithium prices reached the value of 23,000 US dollars per ton, followed by a drop in 2019, that caused the halving of the cost (European Commission, 2020). In the last year, lithium prices have been soaring in the market: spot lithium carbonate price in China is around 69,906 US dollars per ton (Trading Economics, 2022), and lithium hydroxide one is around 81,500 US dollars per ton (London Metal Exchange, 2022).

Nowadays, lithium is one of the most discussed materials. It is the lightest of all metals, but it is also the most energy-dense, making it the ideal material for use in batteries and other technologies (European Commission, 2020). It is also essential in pharmaceutical applications and for industrial uses such as the glass and ceramic production, especially in the European market. Europe is highly dependent on imports of lithium concentrates: the EU Self-Sufficiency indicator for lithium has been estimated at 30.1% in 2018 by the statistical office of the European Union Eurostat (Eurostat, 2022). Imports come mainly from Australia (European Commission, 2020), instead a small amount comes

from Portugal, the only country mining lithium in Europe, that manage to satisfy only the 17% of the demand for the glass and ceramic industry (Torres De Matos et al., 2020). Instead, Europe is 100% reliant on imports of refined lithium compounds, coming mainly from Chile (European Commission, 2020). The only plant that refines lithium carbonate is in Germany and it is owned by the American Albemarle (Torres De Matos et al., 2020). In 2020, the European Commission has published the updated list of Critical Raw Materials (CRMs), by adding the lithium, because its increase in demand could lead to supply issues (European Commission, 2020). The Kyoto Protocol, the Paris Agreement, the UN Sustainable Development Goals (SDGs), and the Green Deal ask for lower CO₂ emissions to tackle with climate change. Therefore, with the increasing demand of batteries, lithium production must adapt to the high request from the market, otherwise its availability could limit the energy transition. One of the aims of the European Union in the field of critical raw materials is to diversify the source of supply to reduce the risk of disruption. In the case of lithium, Europe highly depends mainly on Chile and Australia. It is also worth to mention that the intensive lithium mining has important environmental and social impacts in the area in which the extraction process is operated. Therefore, diversify the sources of supply could avoid inequalities and high burdens on the countries where the mineral is extracted.

3 Characterization of the study sites

Lithium products such as lithium carbonate and lithium hydroxide can be produced through the extraction both from brine and from hard rock. Therefore, in this analysis, two case studies have been considered to assess the differences in these two lithium production pathways: brine extraction from the desertic area of the Salar de Atacama, in Chile and ore extraction from Greenbushes mine, in Western Australia. In this chapter, the characterization of the study sites is illustrated, pointing out also the environmental, social, and political critical aspects that are relevant to the analysis.

3.1 Salar de Atacama, Chile

Salar de Atacama is located in the Antofagasta Region in northern Chile, in South America, as shown in Figure 5. It is comprised between a latitude of 23°S and 24°S and a longitude of 65° W and 68° W. It has an extension of 3,000 km², being the third largest salt flat in the world, after Salar de Uyuni in Bolivia and Salinas Grandes in Argentina (Marazuela et al., 2019). It is an endorheic basin, that is a basin without outlet, surrounded by mountains range from each side: Cordillera de la Sal and Domeyko Range to the west, Andes Mountains to the east, and Cordòn de Lila in the south. Therefore, Salar de Atacama basin constitutes a unique morphologic feature that has been studied by hydrologists and other scientists through the years.

Four different zones can be identified in the area: salt flat nucleus, mixing zone, alluvial fans, and volcanic and basement rocks (Marazuela et al., 2020). Brine extraction takes place in the salt flat nucleus, that has an average elevation of 2,300 metres above the sea level. Two different companies operate in this area: the Chilean one Sociedad Química y Minera de Chile (SQM) and the American one Albemarle. SQM was a state-owned company which started producing fertilizer chemicals; then, in 1983, the military dictator Pinochet gave the company to his son-in-law. Nowadays, SQM is the world's largest lithium producer; it started mining lithium in the Salar de Atacama in 1994, signing a lease agreement with the Chilean Economic Development Agency Corporación de Fomento de la Producción (CORFO) to extract lithium and potassium-rich brine from the deposit. Instead, the other extraction plant located in the southern part of the salt flat nucleus started its operations already in 1980s, at that time owned by a company called Rockwood. Only in 2015, Albemarle acquired the company that was already extracting lithium in the Salar de Atacama.

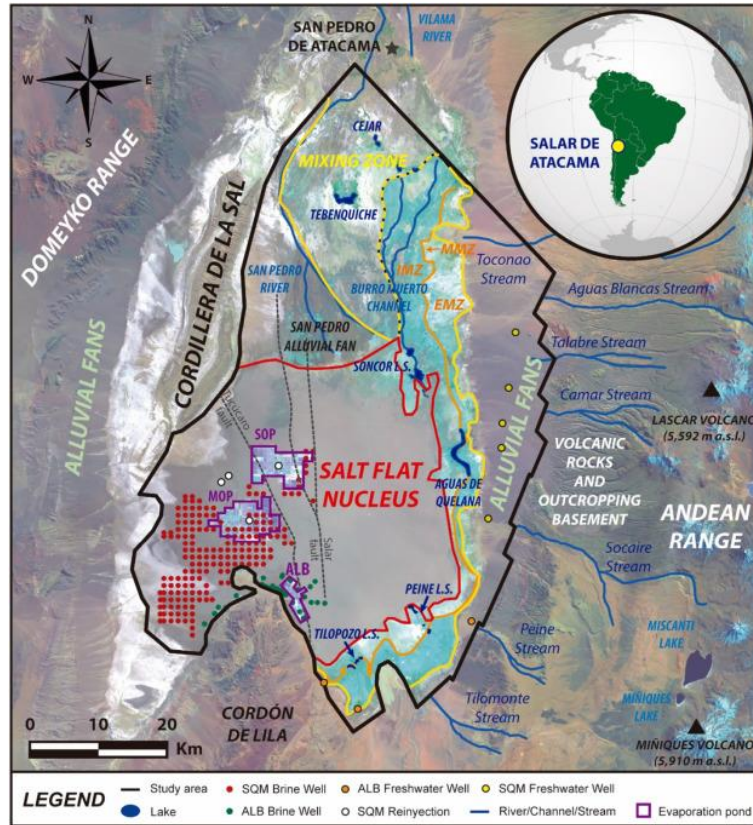


Figure 5. Location of the Salar de Atacama, in northern Chile, shown by a Landsat 8 satellite image acquired on the 27th of September 2016. (Source: Marazueta et al., 2020)

The climate of the salt flat area is arid and mild. Annual temperature ranges between -6°C and 33°C, delineating a cold desert environment because of the high elevation site. Precipitations are present both in winter and summer with an average of 10 mm/yr, but they are concentrated mainly during summer (January-March) (Liu et al., 2019). Therefore, the local climatic conditions are favourable of lithium production, allowing the evaporation of water from the ponds and the brine concentration. Instead, looking at the surrounding mountains range, rainfall rate is higher, with an average of 140 mm/yr, which constitutes a recharge for the endorheic basin.

3.1.1 Lithium extraction process from brine

Lithium production process starts in Salar de Atacama, in the salt flat nucleus, where pumping wells extract potassium and lithium-rich brine from the underground. Annual limit for brine extraction rate is set at 1600 L/s for the SQM company. The liquid is pumped into storage ponds, shown in Figure 6, where brine concentration takes place through sequential evaporation. There are evaporation ponds used for potassium production and others used for lithium one. Following the lithium production line, brine at around 0.17% lithium concentration (which contains 70% water by mass, the remainder is made of other minerals), undergoes several steps, being pumped through different ponds. Different salts are harvested during these concentration stages: potassium salts in

particular potassium chloride (KCl), are the most important ones. The concentration process last around one to two years, according to climatic conditions.



Figure 6. SQM mine plant in the Salar de Atacama, Chile. (Source: SQM, <https://www.sqmlithium.com/en/nosotros/>)

Concentrated brine at 6% lithium concentration is then pumped into tanker trucks and is sent to a refinement process, where lithium carbonate, lithium hydroxide and lithium chloride is produced. SQM owns a processing plant in the Salar de Carmen, a productive area located 20 km east of the city of Antofagasta. SQM plant is shown in the Sentinel-2A satellite image acquired on the 16th of January 2022 in Figure 7 (left). Instead, the processing plant owned by Albemarle, called Planta Química La Negra, is located 27km southeast of the city of Antofagasta and started operated in 1984. In the same satellite image acquired by Sentinel-2A on the 16th of January 2022, Albemarle processing plant is shown in Figure 7 (right). In both these plants, brine concentrate is processed to obtain lithium carbonate. The first step is the removal of boron using solvent extraction and of magnesium through chemical precipitation. Then, soda ash is added to the brine to make lithium carbonate precipitate. After that, it is refined and packed for export. Lithium carbonate could also be further processed to obtain lithium hydroxide through a reaction with a lime solution that also produces calcium carbonate as coproduct.

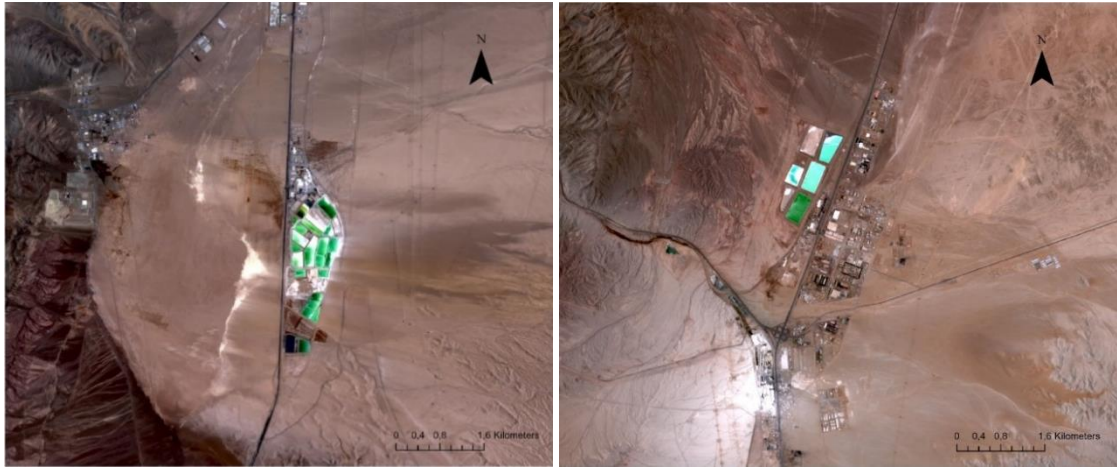


Figure 7. Sentinel-2 satellite image acquired on the 16th of January 2022 showing SQM processing plant in the Salar de Carmen (left) and Albemarle processing plant, called Planta Química La Negra (right).

3.1.2 The importance of the unique ecosystem

As mentioned before, the highest precipitation rate occurs on the high mountains in the upper part of the basin. Rainfall constitutes a replenishment for the basin storage: water infiltrates in the underground, then flows towards the low-elevation area, following the effect of the slope. Freshwater reaches an underground area where the salt brine is present (mixing zone), generating an interface called saline wedge due to the high difference in density. Freshwater flows above the brine, generating a shallow underground water table and allowing vegetation to exist in the marginal zone of the Salar. Lagoons are also generated by brackish water, with a high salinity because of the minerals that the water traps during its flow.

In the “lithium triangle” area, the brine evaporation process is performed to produce lithium compounds. The salt water is pumped out from the underground and is stored in ponds, letting the sun energy evaporate the water through a process of around one to two years. The main environmental concerns linked to the lithium production are related to the pollution of air, soil, and water. In particular, the conventional evaporation process could impact the animals and the vegetation of the area, the water availability, the land use, and the generation of waste (Kaunda, 2020). Moreover, in a desertic area, as the Salar de Atacama, the scarcity of water is one of the challenges that all the living species have to tackle with. Because of the high brine extraction rate, the groundwater levels have been lowered of one meter per year in some areas (Kaunda, 2020). Therefore, the intense extraction of brine from the underground represents the main environmental issue, that impacts both on the animals, on the vegetation, and on the communities living in the area. Moreover, the high-altitude hypersaline lagoons have unique biodiversity and are very sensitive to climate oscillation. The brine diversion contributes to compromise the structure

and the functioning of the lagoons, their ecological importance for the flamingos and for other migratory birds (Gajardo & Redón, 2019). Census made by the Chilean government underlined that the number of flamingos in the Atacama area has been decreasing since 1997; instead, it is stable in the rest of the country. Therefore, many National Reserves have been created in this area, as shown in the topographic map in Figure 8, managed by the Chilean National Forest Corporation CONAF (Corporación Nacional Forestal).

Salar de Atacama is a fragile ecosystem with unique biodiversity. It provides ecosystem services both to flora and fauna and to local communities. Water collected from the melting of Andean glaciers are used by indigenous communities as water resource for living. Human settlements in the salt area are shown with a red dot in the topographic map of the Salar de Atacama illustrated in Figure 8. The indigenous communities that live in the eastern part of the Salar, such as Camar, Socaire, Toconao and Peine, and the ones that live in the north, that are the communities of San Pedro de Atacama, highly depend on the tributaries for the water supply.

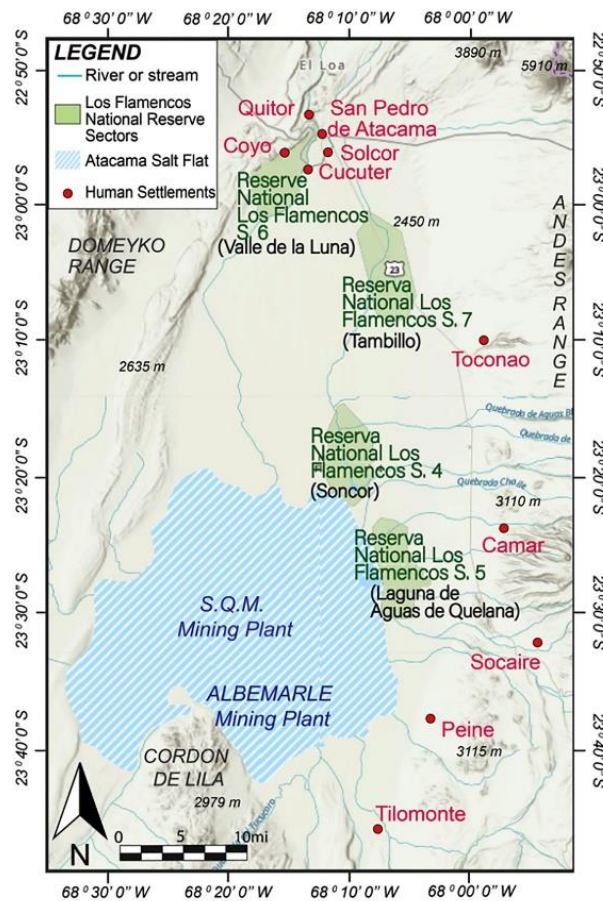


Figure 8. Topographic Map of the Salar de Atacama, showing National Reserves, Human Settlements, Rivers, and Streams. (Source: Liu et al., 2019).

The evaporation brine process has lower carbon emissions with respect to other materials: as mentioned before, the main issue is related to the intensive brine extraction from the underground, which causes concerns about the water depletion on the area. For this reason, the application of a Direct Lithium Extraction (DLE) technology in the Salar de Atacama could lower the impacts on the vegetation, on the animals, and on the communities living in the area. The DLE technology, in fact, would reinject the brine in the underground immediately after lithium has been extracted, avoiding the water to evaporate from one of the driest places on Earth. In this way, no evaporation ponds are required for the storage of the brine, also reducing the land use impacts. Moreover, the time required to produce lithium would be extremely reduced, the efficiency and the quality of lithium recovered (purity) are higher, avoiding further purification processes which requires chemicals. On the other hand, higher CO₂ emissions for the lithium production would be generated with a DLE technology. However, solar panels, wind turbines, and hydroelectric power plant can be used to generate electricity needed for the processes. In Chile, the current share of renewable energy in total electricity production is already at 45 percent (SQM, 2021).

3.1.3 Social and political framework

Nowadays, mining industry is a pillar for the Chilean economy, it contributes to a significant portion of the country's gross domestic product (GDP). The approach of basing an economy mainly on mining is called neoextractivism, a term which refers to the act of intensively exploiting natural resources in a state, making it the core of its economy (Babidge et al., 2018). Mainly copper, molybdenum, silver, and gold are mined in Chile; instead, copper and lithium are mostly extracted in the region of Antofagasta and then they are exported worldwide. The extraction of these commodities requires resources, such as energy, water, and land, that are shared with the local flora and fauna and with the communities living in the area. In the Antofagasta region, social conflicts and protest have been rising during the years against mining companies and against the Chilean government. Environmental policies have been introduced for the first time in Chile in the last decade of the XX century, without strict regulation for the extraction of water for the mining companies. The Water Code of 1981, part of the Chilean constitution written under the Pinochet dictatorship, set water rights as private, and still, they are today. The government aim was to incentivize the private investments in mining and agricultural activities. Copper and coal mining, avocados and salmon production were the goods that made Chile one of the richest countries of South America. In 2005, the Water Code was reformed, setting limits to the private allocation of water rights because of environmental concerns and monopolization of water rights. The first environmental legislation dates back to 1994. Local communities argue that Chilean regulations do not protect either their rights on natural resources or the environment as they should. National

Corporation for Indigenous Development (CONADI) has been established by the Indigenous law, International Labour Organization (ILO) Convention 169 in 1989 and ratified in 2008. This law gives indigenous people a voice and obliges the state must inform and consult indigenous communities when a project uses natural resources that are close to their territory. However, private companies often negotiate directly with indigenous communities, without the intervention of the State. Minera Escondida, the largest copper mine in the world, has been fined for causing irreparable environmental damage to in the Salar de Atacama because of water extraction exceeding the maximum level allowed in the period going from 2005 to 2019. In Chile, a national referendum was obtained thanks to continuous protests for social and environmental issues in 2019. A new constitution for the climate and ecological emergency will be written by 155 Chileans that have been elected. A draft of the new Constitution is expected to be ready for July 2022, followed by a national vote. After the last general elections held at the end of 2021, the young centre-left Gabriel Boric was elected as President of the Republic for the next four years. He aims to create a national lithium company and to set higher mining royalties and taxes. Therefore, in this new political context, in the new Constitution mining regulation will also be reshaped, together with communities' rights and roles in the sector. The Convention could probably make water a public good and brine considered legally as water, allowing stricter regulation for the mining companies. In fact, currently, brine is not considered as water, because of its impossibility to be used for drinking or irrigation purposes. Nowadays, brine is legally considered an ore resource, regulated by the mining code, allowing a high extraction rate and consequent environmental degradation to occur. A study demonstrated how vegetation has declined in the Salar de Atacama area in the last 20 years, together with an increase in the daily temperatures, a decrease in the soil moisture, and an increasing drought situation in the near national reserve area (Liu et al., 2019). Therefore, if from one side there is the urgent need to tackle with climate change, on the other hand it is worth to mention that biodiversity losses and social inequities are direct consequences of the intensive lithium extraction in this unique and extreme ecosystem of the salar.

3.2 Greenbushes, Western Australia

Western Australia is a rich mining region where several commodities are extracted and exported worldwide. Lithium deposits can be found mainly as spodumene, a mineral constitutes of lithium aluminium inosilicate $LiAl(SiO_3)_2$. Four large lithium mines have been identified in Western Australia: (1) Greenbushes, one of the largest active lithium production mines in the world, operated by the company Talison Lithium; its projected closure is expected in 2056; (2) Mount Marion, an active mine located 40 kilometres southwest of the city of Kalgoorlie. The production of

high-quality spodumene started in 2017, under the operation of the company Mineral Resources Ltd.; (3) Mt Cattlin, an active mine located in the south of Western Australia, where several commodities are mined: lithium, tantalum, copper, gold, niobium, spodumene, silica, zinc, lead, and manganese; (4) Pilgangoora, a mine project currently under expansion located in the north of Western Australia, where lithium, spodumene, and tantalum are extracted. Its closure is projected to be in 2047.

Greenbushes is the main lithium hard rock active mine in terms of production, located immediately south of the Greenbushes town, within the Shire of Bridgetown. It can be found around 250 kilometres south of Perth, in south-west of Western Australia, an area where mining is one of the main economic activities of the region, together with farming and tourism. Mining activities started in the area of Greenbushes in 1888 with the extraction of tin, followed by the extraction of tantalum in the 1940s since the geology of the region presents deposits of Lithium-Caesium-Tantalum pegmatites. Therefore, this mine site has been chosen for the analysis of lithium ore pathways because of its economic importance. The town of Greenbushes and its mine site are shown in the aerial picture in Figure 9.



Figure 9. Aerial image showing the town of Greenbushes and the close spodumene mine site. (Source: Talison Lithium <https://www.talisonlithium.com/greenbushes-project>)

The area of Greenbushes has a temperate climate. Annual maximum temperature in the mine area ranges between 14°C and 30°C; instead, annual minimum temperature ranges between 4°C and 13°C. The average precipitation rate is around 926 mm/yr, mostly falling in wintertime (Talison Lithium, 2019).

3.2.1 Lithium extraction process from ore

At Greenbushes mine site, lithium ore (called spodumene) is mined with a traditional drill and blast method. The fragmented rock generated from the explosion is carried to the in-situ plants. There are two lithium processing plants, a technical grade plant and a chemical grade plant. Two new chemical-grade processing plants (CGP3 and CGP4) are planned to be built, according to the mining expansion proposal published in 2019. After an initial crushing, the ore is transported through a conveyor belt to a final grinding in a mill with steel balls, which crush until the ore size is smaller than one tens of millimetres. Then, water is added to the mill which allow a slurry of fine particles called the pulp to be obtained. This step is followed by a physical separation of the rock and the spodumene by density difference in a floatation tank. Several processes, such as adjustment of the pH and addition of foaming agents, take place to make the process more efficient. The foam which float is collected at the top of the floatation tank, while the remaining pulp is fed into the next tank for a second step to recover the maximum lithium ore. This is done in multiple steps through the floatation tanks until there is no more lithium ore in the pulp. Therefore, the recovered foam contains a high concentration of spodumene. If iron ore is present, magnetic separation is used to remove it. Then, this mixture passes through a filter mat which allows liquid to flow and to dry the spodumene. The final product, depending on the desired quality, contains between 63% and 94% spodumene. Then, it could be packed in jumbo bags or shipped as bulk commodity all around the world, but mainly to China which converts the spodumene concentrate into high value lithium derivatives. Spodumene concentrates is shipped mainly from Port of Bunbury, specialised in bulk handling, and in limited volume from Fremantle Harbour, a main container shipping port. Storage of processed tailings takes place in storage facilities (TSF), located above ground in the southern part of the mine site. Instead, waste material from the mining activities is stored in designated areas within the site, called Floyd's Waste Rock Landform (WRL) and located in the eastern part of the mine site, where it is contoured and replanted as part of a rehabilitation plan.

According to the Western Australia Mineral and Petroleum Statistic Digest of the years 2020-2021, published by the Department of Mines, Industry Regulation and Safety, spodumene concentrate sales went up again after three years of decreasing trend. Australia is one of the main exporters of lithium in the world, but it has never refined spodumene concentrate in its own country. According to the last investments and joint ventures, Greenbushes spodumene concentrate will be delivered to two different processing plant in the future. One of them is called Kwinana plant, owned by the Chinese company Tianqui Lithium and the Australian one IGO. It has been completed in 2021 and it is located 20 km south the city of Fremantle. It is designed to produce up to 24,000 tonnes of lithium hydroxide per year and it is expected to produce at full capacity at the end of 2022. In Figure

10, the Sentinel-2 satellite image acquired on the 6th of April 2022 shows the area of Fremantle where the Kwinana processing plant is located.

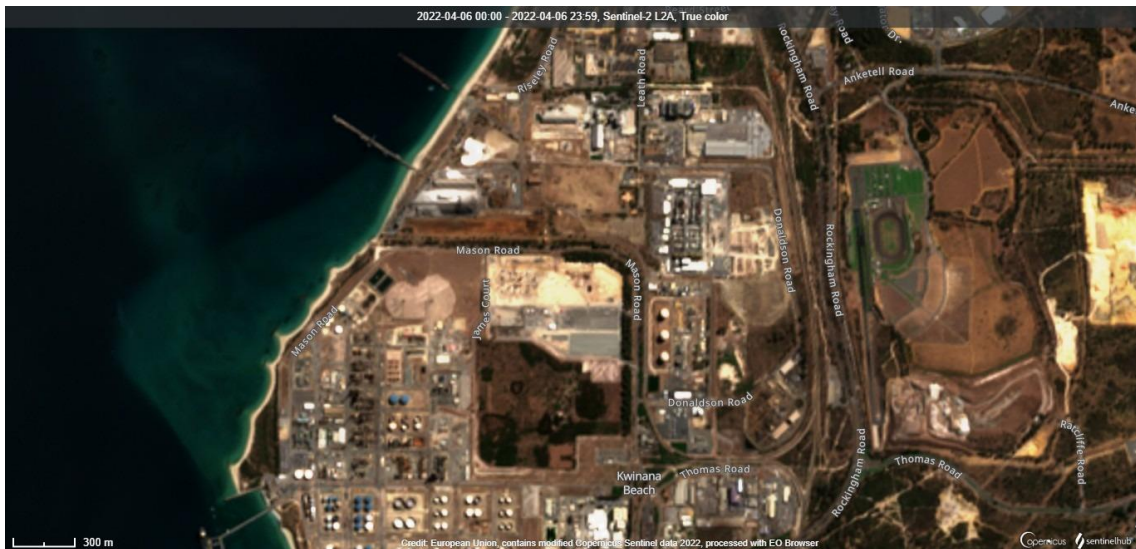


Figure 10. Sentinel-2 satellite image acquired on the 6th of April 2022 showing the area of Fremantle and the Kwinana processing plant.

The other lithium processing plant is called Kemerton and it is owned by the American company Albemarle. It is located approximately 17 kilometres north-east of the city of Bunbury. The plant constitutes the basis of the MARBL Lithium Operations joint venture with Mineral Resources Limited. Its designed production capacity is 1 million tonnes of spodumene ore concentrate. In Figure 11, the Sentinel-2 satellite image acquired by on the 11th of April 2022 shows the Kemerton lithium processing plant.



Figure 11. Sentinel-2 satellite image acquired on the 11th of April 2022 showing the Kemerton lithium processing plant.

These two plants are going to reach the design capacity in the next years, becoming an important asset for the mining region of Western Australia. Concentrated spodumene produced at Greenbushes mine will be processed in these two plants, obtaining lithium products that will be exported worldwide.

4 Data products

Satellite images and geographic information systems have been used in this analysis. Landsat products have been downloaded from USGS Earth Explorer (USGS Earth Explorer). Instead, Sentinel-2 satellites images have been downloaded from ESA Copernicus Open Access Hub (Copernicus Open Access Hub). Level-2 data products have been considered, because already processed for atmospheric correction.

Landsat 5

Landsat 5 is a satellite orbiting at 705 km from the Earth. There are two sensors mounted on board of the satellite: Multispectral Scanner (MSS) and Thematic Mapper (TM). MSS acquires four spectral bands in the Visible and Near Infrared, as Landsat 1 and 2. TM sensor acquires six spectral bands with a spatial resolution of 30 m and one thermal band with a resolution of 120 m, as shown in Table 1. Its temporal resolution is 16 days, and its swath width is 185 km. Landsat 5 was launched on the 1st of March 1984. It has been decommissioned in 2013, being the longest operating satellite in history.

Table 1. Spectral bands and spatial resolution of the Thematic Mapper (TM) sensor mounted on board of Landsat 5. (Source: USGS <https://www.usgs.gov/landsat-missions/landsat-5>)

Band Number	Band Name	μm	Resolution
1	Blue	0.45-0.52	30 m
2	Green	0.52-0.60	30 m
3	Red	0.63-0.69	30 m
4	Near-Infrared	0.76-0.90	30 m
5	Near-Infrared	1.55-1.75	30 m
6	Thermal	10.41-12.5	120 m
7	Mid-Infrared	2.08-2.35	30 m

Landsat 5 Level-2 data products have been considered for this analysis because atmospheric correction has been already carried out. Satellite images have been downloaded from the USGS Earth Explorer website (USGS Earth Explorer).

Landsat 8

Landsat 8 is a satellite that was launched on the 11th of February 2013. It orbits at an altitude of 705 km, a swath of 185 km, and it has a temporal resolution of 16 days. There are two sensors mounted on board of the satellite: the Operational Land Imager (OLI) and the Thermal Infrared Sensor (TIRS). Visible, Near Infrared, and Shortwave Infrared are acquired by the OLI instrument with a spatial resolution of 30 m for multispectral bands and of 15 m for the panchromatic one, as shown in Table 2. Instead, land surface temperature is measured by TIRS in two thermal bands at 100 m spatial resolution.

Table 2. Spectral bands and spatial resolution of the Operational Land Imager (OLI) sensor mounted on board of Landsat 8. (Source: USGS <https://www.usgs.gov/landsat-missions/landsat-8>)

Band Number	Band Name	μm	Resolution
1	Coastal Aerosol	0.43 - 0.45	30 m
2	Blue	0.45 - 0.51	30 m
3	Green	0.53 - 0.59	30 m
4	Red	0.64 - 0.67	30 m
5	Near-Infrared	0.85 - 0.88	30 m
6	SWIR1	1.57 - 1.65	120 m
7	SWIR2	2.11 - 2.29	30 m
8	Panchromatic (PAN)	0.50 - 0.68	15 m
9	Cirrus	1.36 - 1.38	30 m

Sentinel-2

The Copernicus Sentinel-2 is a multi-spectral imaging mission made of a constellation of two identical satellites (Sentinel-2A and Sentinel-2B). They are placed in the same orbit, phased at 180°, at a mean altitude of 786 km. They have a revisit time of five days in correspondence of the Equator in cloud-free condition and a 290 km swath width. They acquire optical images at high spatial resolution both of land and coastal areas with a radiometric resolution of 12-bit. The optical instrument mounted on board, called MultiSpectral Instrument (MSI), samples 13 spectral bands: four bands at 10 m spatial resolution, six bands at 20 m spatial resolution and three bands at 60 m spatial resolution, as shown in Table 3. MSI is a passive sensor that collects sunlight reflected from the Earth. Sentinel-2A was launched on the 23rd of June 2015; instead, Sentinel-2B was launched on the 7th of March 2017. Additional satellites (Sentinel-2C and Sentinel-2D) are planned to be launched in the next future to ensure continuity of multi-spectral imagery provided also by SPOT

and USGS Landsat TM. Sentinel-2 data products are mainly used to monitor variability in land surface. Main application can be found in agriculture, monitoring of ecosystems and water quality, forest management, disaster mapping and civil security.

Table 3. Wavelengths and Bandwidths of the three Spatial Resolutions of the MSI instruments mounted on board of Sentinel-2. (Source: <https://sentinel.esa.int/web/sentinel/missions/sentinel-2/instrument-payload/resolution-and-swath>)

Spatial Resolution (m)	Band Number	S2A			S2B	
		Band Name	Central Wavelength (nm)	Bandwidth (nm)	Central Wavelength (nm)	Bandwidth (nm)
10	2	Blue	492.4	66	492.1	66
	3	Green	559.8	36	559.0	36
	4	Red	664.6	31	664.9	31
	8	NIR	832.8	106	832.9	106
20	5	VNIR	704.1	15	703.8	16
	6	VNIR	740.5	15	739.1	15
	7	VNIR	782.8	20	779.7	20
	8a	VNIR	864.7	21	864.0	22
	11	SWIR	1613.7	91	1610.4	94
	12	SWIR	2202.4	175	2185.7	185
60	1	Aerosols	442.7	21	442.2	21
	9	Water Vapour	945.1	20	943.2	21
	10	Cirrus	1373.5	31	1376.9	30

Sentinel-5P

The Copernicus Sentinel-5 Precursor is a mission that aims to monitor the atmosphere, through emissions measurement of several compounds. It also provides continuity in the data availability of atmospheric measurement from Envisat and the future missions. It is a low Earth-orbit satellite, placed in an orbit at an altitude of around 824 km with a revisit time of 16 days. The sensor mounted on board of the satellite is called TROPOspheric Monitoring Instrument (TROPOMI). It is a passive imaging spectrometer with a swath width of 2600 km and a spatial sampling of 7x7 km². Sentinel-5P was launched on the 13th of October 2017. Sentinel-5P Level-2 data products have been

downloaded via the Copernicus Open Access Hub. Several compounds are measured by the TROPOMI: aerosols, clouds, methane, carbon monoxide, formaldehyde, nitrogen dioxide, ozone, and sulfur dioxide. Through their quantification, it is possible to monitor air quality, ozone, and UV radiation, and to perform climate forecasting. The level-2 products available for the users are shown in Table 4.

Table 4. Level 2 geophysical products of the TROPospheric Monitoring Instrument (TROPOMI) mounted on board of Sentinel 5P. (Source: <https://sentinels.copernicus.eu/web/sentinel/technical-guides/sentinel-5p/products-algorithms>)

Product	Parameter
L2__O3__	Ozone (O ₃) total column
L2__O3_TCL	Ozone (O ₃) tropospheric column
L2__O3__PR	Ozone (O ₃) profile
L2__NO2__	Nitrogen Dioxide (NO ₂), total and tropospheric columns
L2__SO2__	Sulfur Dioxide (SO ₂) total column
L2__CO__	Carbon Monoxide (CO) total column
L2__CH4__	Methane (CH ₄) total column
L2__HCHO__	Formaldehyde (HCHO) total column
L2__CLOUD_	Cloud fraction, albedo, top pressure
L2__AER_AI	UV Aerosol Index
L2__AER_LH	Aerosol Layer Height (mid-level pressure)
UV product	Surface Irradiance/erythemal dose
L2__NP_BDx	Suomi-NPP VIIRS Clouds
AUX_CTMFC	A-priori profile shapes for the NO ₂ , HCHO and SO ₂
AUX_CTMANA	vertical column retrievals

All the satellite images that have been used in this analysis are listed in Table 5, showing details about the date in which the satellite image has been acquired, the percentage of the cloud cover of the data product, and the type of sensor mounted on board of the satellite that has acquired the image.

Table 5. List of all the satellite images used for this analysis, showing the acquisition date, the sensor type, and the cloud cover of the data products.

Area	Acquisition date	Sensor type	Cloud cover (%)
Salar de Atacama	01/29/1992	Landsat 5 TM	1.0
	01/26/1997	Landsat 5 TM	1.0
	01/24/2002	Landsat 5 TM	1.0
	02/07/2007	Landsat 5 TM	3.0
	01/17/2011	Landsat 5 TM	1.0
	02/02/2017	Landsat 8 OLI	0.53
	01/03/2022	Sentinel-2A MSI	0.26
Antofagasta region	01/16/2022	Sentinel-2A MSI	0.44
Greenbushes mine	02/17/2022	Sentinel-2A MSI	1.66E-4

Ground truth data

To perform the Accuracy Assessment of the Index Analysis for the Chilean mining site, ground truth data have been generated to compare the results obtained with the index extraction with the real data. Polygons representing the evaporation ponds in the Salar de Atacama have been downloaded from OpenStreetMap, through QGIS software, using the QuickOSM Tool. QGIS has been used because of the possibility to obtain the temporal reference of data, that is the data of creation of a polygon.

Software

Different software have been used during this work. ArcGIS Pro has been used to work with satellite images, to perform Index Analysis and Accuracy Assessment, and to carry out Route Network Analysis. QGIS has been used only to retrieve information about the temporal generation of the ground truth data. ENVI Classic 5.3 has been used to obtain the histogram and the threshold values in the index analysis. OpenLCA has been used to perform the life cycle assessment to evaluate the contribution of transportation in the carbon emissions of lithium production.

5 Methodology

In this chapter, remote sensing, and GIS-based approach for analysing the two different study areas are illustrated in the first five paragraphs. In the first one, it is illustrated the index analysis carried out to extract the evaporation ponds area, evaluating which index performs better through an accuracy assessment. Then, an estimation of the area through the years has been carried out to detect how the land has been changing since 1992. In the second paragraph, an estimation of the Greenbushes mine area has been carried out through GIS software. In the third one, Sentinel-5P data products have been analysed to detect if emissions of several compounds can be quantified in correspondence of the mine areas to be integrated in the LCA analysis. In the fourth and fifth paragraphs, the methodology to identify the transportation routes on land and on sea and to quantify the km travelled respectively by trucks and by vessels is shown. Finally, the last two paragraphs show the approach followed for the integration of the obtained results in the land use intensity and in the LCA analysis. More details about the methodology are illustrated in the Appendix.

5.1 Indices analysis for evaporation ponds area extraction in Chile

An analysis has been performed to extract the evaporation ponds area in the Salar de Atacama with ArcGIS Pro and ENVI software. First, the analysis has been tested on the Sentinel-2 satellite image acquired on the 3rd of January 2022 over the salt flat nucleus in the Salar de Atacama. Several indices have been tested in this analysis to detect how each one could extract ponds area where brine is stored for one to two years. Then, evaporation ponds area has been evaluated for different years (1992, 1997, 2002, 2007, 2011, 2017, 2022) using NDVI index to study how it has expanded in time. NDVI index has been chosen to have the possibility to apply this methodology in other studies: Near Infrared Band and Red Band (Visible) - used to compute NDVI - are present in almost every sensing data product. Satellites images acquired during summer (January or February) have been chosen to minimize the seasonality effects (Liu et al., 2019). The date of acquisition, the sensor type, and the cloud cover percentage for each satellite image analysed are shown in Table 5 in Chapter 4.

The indices that have been evaluated in this analysis are: NDVI, NDWI (McFeeters), NDWI (Gao), MNDWI (Xu), MNDWI (SWIR1), MNDWI (SWIR2), tested through an accuracy assessment carried out to detect which of them perform better for this purpose. In this paragraph, each index will be defined, indicating the bands needed for computing it and its main applications. The bands' number is referred to Sentinel-2 satellite, but also Landsat data products have been used in this analysis, considering the corresponding spectral bands named with a different number.

NDVI

Normalized Difference Vegetation Index (NDVI) is the most used vegetation indices in the remote sensing applications, ranging between -1 and +1. It is computed through a simple mathematical formula that uses Near Infrared and the Red Band of the Visible. In fact, plants can absorb wavelengths in the visible, in particular the red light, and can reflect the ones in the near infrared at a strength that varies according to the growth of the plants and to the kind of species. The reason why NDVI is frequently used in remote sensing studies, is that nowadays almost all sensors on board of satellites can measure red and near infrared wavelengths. Therefore, mostly of the time, NDVI can be computed because of the certain data availability to study the health of vegetation in the area.

$$NDVI = \frac{NIR(B8) - Red(B4)}{NIR(B8) + Red(B4)}$$

NDWI

The Normalized Difference Water Index (NDWI) is used to identify water bodies and to measure moisture content through a satellite image. One of the first definitions of the NDWI has been done by McFeeters in 1996 (McFeeters, 1996) and it uses the green band of the visible and the near infrared band to detect changes in water features. In fact, water has a highly reflectivity in the green wavelengths and a high absorption in the NIR, attributing positive values for water bodies. It is computed as:

$$NDWI (McFeeters) = \frac{Green(B3) - NIR(B8)}{Green(B3) + NIR(B8)}$$

Another version of the index has been introduced by Gao in the same year: it uses the near infrared and the short-wave infrared band (Gao, 1996). It can detect water content in plant leaves, parameter that is changing during their growing period. Therefore, it is used for studying the water stress in crop analysis. It can also be used to monitor risk of combustion in dry areas subjected to fires. Its mathematical formula is equal to:

$$NDWI (Gao) = \frac{NIR(B8) - SWIR(B11)}{NIR(B8) + SWIR(B11)}$$

MNDWI

In 2006, the Modified Normalized Difference Water Index (MNDWI) has been defined by Xu to enhance open water features in satellite images (Xu, 2006). The NIR band present in the NDWI defined by McFeeters in 1996 has been substituted by a middle infrared band (MIR), resulting in a greater positive value for water bodies. Therefore, the modified formula can extract water features in a more accurate way, giving negative values to soil, vegetation, and built-up areas. It is defined as:

$$MNDWI (Xu) = \frac{Green(B3) - MIR(B8A)}{Green(B3) + MIR(B8A)}$$

Other two versions of the MNDWI have been considered in this analysis, substituting the MIR band in the index defined by Xu. The MIR band has been replaced with the first part of the short-wave infrared corresponding to Band 11 of Sentinel-2, as shown in the following formula.

$$MNDWI (SWIR1) = \frac{Green(B3) - SWIR(B11)}{Green(B3) + SWIR(B11)}$$

Then, the MIR band has been substituted with the second part of the short-wave infrared, corresponding to Band 12 of Sentinel-2.

$$MNDWI (SWIR2) = \frac{Green(B3) - SWIR(B12)}{Green(B3) + SWIR(B12)}$$

The latter two indices that considers the SWIR bands have been computed since a low reflectance of the evaporation ponds area in the short-wave infrared part of the spectrum has been detected through the analysis of the spectral signatures of evaporation ponds in ENVI software. A spectral signature is a graph that shows reflectivity as a function of the wavelength of a surface reflected electromagnetic energy. Three different evaporation ponds classes have been evaluated: one for ponds where brine is stored for evaporation, the other for ponds appearing white in the True Color Image since salts are predominant, and the other one where ponds appear brownish, linked to the potash production line. The spectral signatures of evaporation ponds classes are shown in Figure 12.

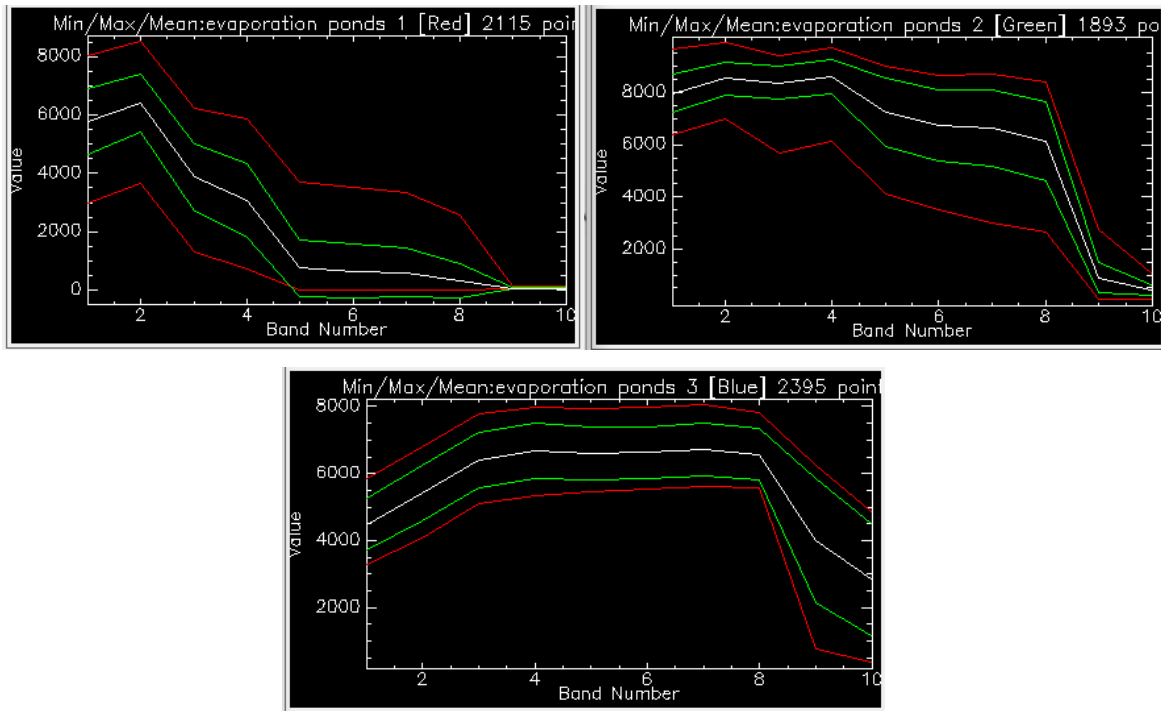


Figure 12. Spectral signatures of three different evaporation pond classes in ENVI software. On the x axis, the bands considered in the analysis are shown; on the y axis, the Surface Reflectance value acquired by the MSI sensor is shown.

In ENVI, Bands Number shown on the x-axis of the spectral signature corresponds to a different number of the nomenclature of Sentinel-2 bands since only some of them have been considered in this analysis. Therefore, to correctly interpret the spectral signatures shown in Figure 12, the Band Number assigned in ENVI, and the corresponding Sentinel-2 nomenclature is shown in Table 6.

Table 6. Bands correspondence between the Band Number proper of Sentinel-2 Nomenclature and the one assigned in ENVI during the analysis.

Band Name	ENVI	Sentinel-2 MSI
Blue	Band 1	Band 2
Green	Band 2	Band 3
Red	Band 3	Band 4
VNIR	Band 4	Band 5
VNIR	Band 5	Band 6
VNIR	Band 6	Band 7
NIR	Band 7	Band 8
VNIR	Band 8	Band 8A
SWIR 1	Band 9	Band 11
SWIR 2	Band 10	Band 12

As it can be noticed from the spectral signatures, all classes of evaporation ponds have a low reflectance in the SWIR part of the spectrum and a high reflectance in the green part of the visible.

Therefore, MNDWI has been evaluated also using SWIR 1 and SWIR 2 to detect if a better accuracy could be achieved.

Image processing

Each satellite image has followed several processes, shown in the flow diagram in Figure 13. This part of the analysis has been performed using ArcGIS Pro. First, each band of the Level-2 data product downloaded from the database has been opened in the software and a unique layer has been created using the command Composite Bands present in the Raster Section of Data Management Tools. A Resampling process has also been necessary for bands having different cell size, in a way that the following analysis could be performed. For example, this is the case of Sentinel 2 data product, whose spatial resolution is equal to 10 m and to 20 m according to the bands considered, as shown in Table 3. Having grouped all the bands of interest with the same cells size, in the case the area of interest (AOI) is located in two adjacent satellite images, the latter have been joined using the command Mosaic. After that, the satellite image has been cut using a shape file of the AOI of the study, using the Clip command. In this way, the size of the image has been reduced in a way that the following steps of the data analysis have been speeded up. Considering the reduced study area, the index has been computed using the command Band Arithmetic. The image obtained have values that ranges between the low and high limit of each index. For example, each value of the cells of an image generated computing NDVI has values raging between -1 and +1. To extract evaporation ponds area, threshold values have been identified for each index using ENVI software. Thresholds have been chosen through the integrated use of Interactive Stretching and Density Slice, allowing to correctly identify the evaporation ponds area in the image. Interactive Stretching is a function which can display the histogram distribution of the image. Instead, Density Slice is a Color Mapping Tool which allows the user to associate each interval of the histogram to a different colour. The latter is just a way to display the image on the screen, helping the user to identify features and analyse the image, but it does not modify its features.

After having identified all the thresholds, binary images (0, 1) have been created for each index with the command Raster Calculator in ArcGIS Pro. Binary images have cells values that can be equal to 0 or to 1: in this case 1 has been assigned to a cell identified as evaporation pond area, as defined choosing the different thresholds. The value of 0 has been assigned to cells that have not been classified before as evaporation ponds area.

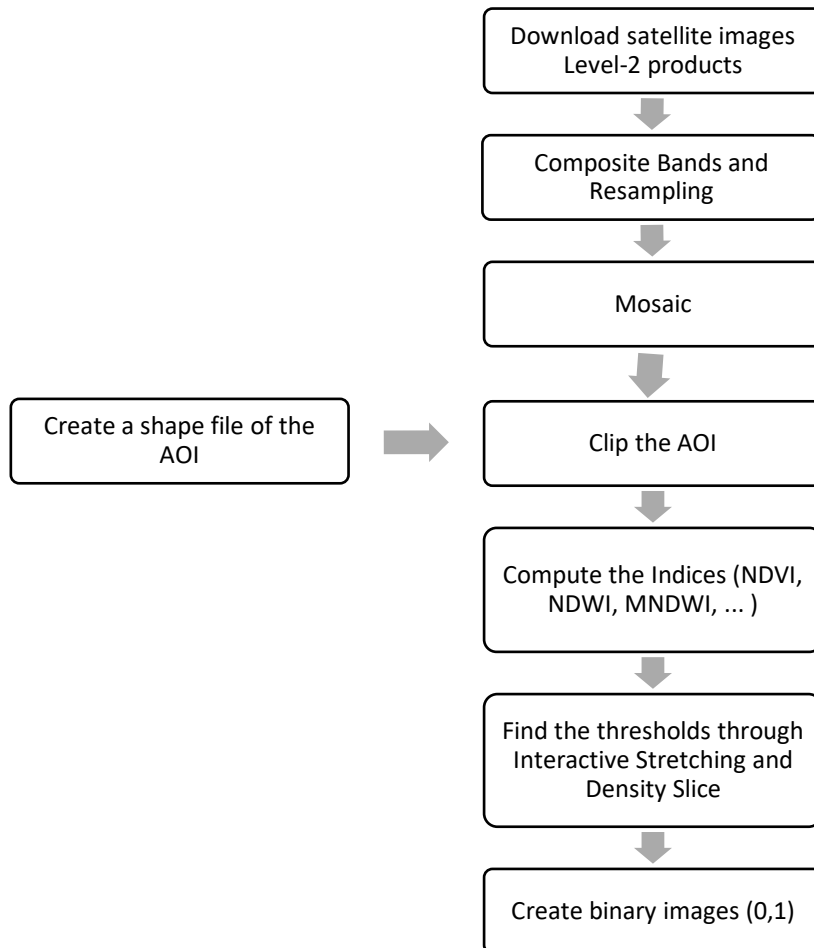


Figure 13. Flow diagram showing the steps carried out to process each satellite image in ArcGIS Pro and in ENVI.

Once the classified images have been generated, it is necessary to evaluate the quality of the process performed. Therefore, an accuracy assessment has been carried out generating Ground Control Points (GCPs) and comparing the image classified with a reference one. The latter is called ground truth, and, in this analysis, ground truth images have been generated following several steps, shown in the flow diagram in Figure 14. The final output of the accuracy assessment is a Confusion Matrix, which will be explained in more details later in this chapter. Ground truth data have been generated using OpenStreetMap (OSM) data. First, the Salar de Atacama area has been explored on OSM website to check the availability of digitalized polygons. Then, keys and tags of the features of interest have been retrieved to filter the data needed. Evaporation ponds polygons in the Salar de Atacama area have been filtered and downloaded through the Tool Quick OSM in QGIS software. Metadata have been checked to detect when polygons data have been created by users: if polygons were created after the year of the acquisition of the satellite image, the polygon

has not been considered. If data were missing, especially for the last years considered, new polygon features have been drawn manually. Binary images (0, 1) have been created to generate ground truth data, associating the value of 1 to cells inside the evaporation ponds polygons and the value of 0 to the remaining area.

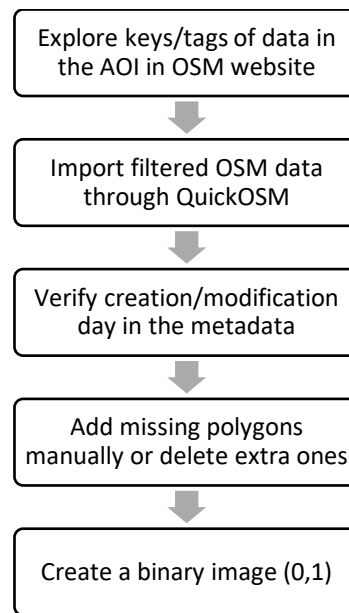


Figure 14. Flow diagram showing the steps followed to create ground truth data.

After having created ground truth data, Accuracy Assessment has been performed in ArcGIS Pro through several steps that are shown in Figure 15. To compare the evaporation ponds area extracted through index analysis and the reference one in the ground truth data, it is necessary that the cells value belonging to evaporation ponds have the same value. As mentioned before, a value of 1 has been assigned to evaporation ponds area in both images to perform the accuracy assessment. The function Create Accuracy Assessment Points has been used, and the Sample Strategy has been chosen as Random, in a way that ground control points are randomly distributed across the raster image. Then, the function Update Accuracy Assessment Point has been performed to also evaluate the points relative to the ground truth image. The last step is the validation of the results through the creation of the confusion matrix. The latter has been exported as table and the kappa value coefficient has been considered to describe the accuracy. Kappa coefficient is an indicator that compares the results of the classification performed to values assigned randomly. It ranges between 0 and 1, where 1 represents 100 percent accuracy, meaning that the classified image is identical to the ground truth one. Therefore, the higher is the kappa coefficient, the higher

is the quality of the classification performed. Other accuracy indicators are needed to have a complete description of the goodness of the analysis. They can be found in the confusion matrix, also called error matrix, that is a quantitative method to define classification accuracy, testing the correspondence of classification results with a reference data. It has the shape of a table, where rows show classified images classes to be tested and columns represent the ground truth classes. Crossing each column with each row, the corresponding cell contains the number of pixels for all correlations. Therefore, the diagonal cells of the matrix point out the cells that have been classified in a correct way. From this number it is possible to obtain the overall accuracy of the classification (OvAc), dividing that number for the total number of cells. Each class accuracy is assessed through non-diagonal cells of the matrix, which contain the number of the cells with an error in the classification. There are two kinds of error: underestimation, when an omission error has occurred or overestimation when a commission error has been done. The omission error can be found in the cells located left and right of the diagonal. Its value represents the number of errors caused by the fact that a cell that belongs to a certain class is not included in that class but is classified as part of other classes. User's Accuracy is an indicator of omission errors, because it counts the numbers of correctly identified cells with respect to the total number of cells in the classified image. Instead, the commission error can be found in the cells located above and below of the diagonal. Its value represents the number of errors caused by the fact that the classification attributes cells to a class that do not belong to that class. Producer's Accuracy is an indicator of commission errors, because it counts the numbers of correctly identified cells with respect to the total number of cells in the reference image.

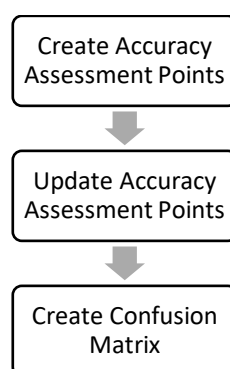


Figure 15. Flow diagram showing the steps followed to perform the accuracy assessment in ArcGIS Pro.

5.2 Mine area analysis in Western Australia

Active mine area at Greenbushes in Western Australia has been extracted manually generating a new feature class of polygons in ArcGIS Pro. The Sentinel-2 satellite image acquired on the 17th of

February 2022 has been used. The polygon has been digitalized following and integrating information about the mine extension available in Talison Lithium report (Talison Lithium, 2019).

5.3 Atmospheric emissions analysis

Sentinel 5P images have been analysed for both the Chilean mine site and the Western Australia one to understand if emissions can be detected and quantified through this data to be then integrated in the LCA analysis. EO Browser, that is a free functionality of the Sentinel Hub showcase, has been used to have a quick look of the eventual emissions over the area of interest. As mentioned before, Sentinel 5P sensor, called TROPOMI, can detect aerosols, clouds, methane, carbon monoxide, formaldehyde, nitrogen dioxide, ozone, and sulfur dioxide. Satellite images acquired over the same area but in different periods have been compared and analysed to see if emissions could be related to the process of lithium extraction and production.

5.4 Transportation Routes Analysis

Land Transport

To evaluate the contribution of transportation in the carbon footprint of lithium production, the distance travelled by trucks during all the production processes has been estimated through the Network Analyst Tool available in ArcGIS Pro. Route analysis has been performed in the software which give the possibility to find the best way to get from one location to another, adding intermediate stops. Several outputs can be chosen for a simple route analysis, such as driving distance or driving time, but it is also possible to optimize the route in terms of shortest time or shortest distance to travel or in terms of the best route given several intermediate stops. Brine and ore lithium pathway have been studied in detail, and mine site, processing plants, and harbour locations have been added to the Stops feature class in the Route Layer. The sequence of the stops has been previously fixed, and a simple route analysis with truck driving distance as output has been performed. It has also been necessary to retrieve information about how the lithium compounds are transported, if they are stored in bags, or as bulk products, or as liquid substances. Truck typology and dimensions for each route have also been retrieved through information coming from company reports to set limitation for the route analysis, because some roads cannot be used by trucks that have certain dimension or weight. Travel mode Properties set for the analysis are shown in Figure 39 in the Appendix (Section II).

Sea Transport

To perform the analysis on the contribution of transportation over the total carbon emission in lithium production, sea routes have been analysed, retrieving information about the distance

travelled by the vessels from Chile and Western Australia to their main lithium export countries. Therefore, it has been necessary to understand lithium routes in detail, looking for reliable information about export data. Main destination countries of lithium exported from Chile have been found in the database of the Chilean Custom. For Western Australia, data about the main lithium export countries have been retrieved through the World Integrated Trade Solution (WITS). WITS is a software that gives information about trade and tariffs developed by the World Bank, the United Nations Conference on Trade and Development (UNCTAD), International Trade Center, United Nations Statistical Division (UNSD), and the World Trade Organization (WTO). Distances have been quantified through the SeaRoute program, which has been used to retrieve the shortest sea route between two locations given as input. The database used by the programme is composed of the most frequent maritime routes in the world. An input file (in .csv format) with geographic coordinates in decimal degrees of origin and destination locations has been created and used as input. A resolution of 5 km has been set to compute all the different sea routes. The SeaRoute programme gives also the possibility to decide if the vessels can pass or not through a particular canal (such as the Suez Canal or the Panama one). Therefore, for the sea route analysis, information about the type and dimensions of the vessels have been retrieved, because fundamental to understand if the vessels can pass through Panama channel or not, determining a shorter route to go from the Chilean coast to the North of Europe. This kind of information have been found on the website of the main shipping companies operating in the ports considered in this analysis. Given all these data to the programme, a GeoJSON file has been obtained as output, which contains the same information of the input file, plus (1) the computed distance in km between the origin/destination, and (2) the distance between the coordinates of the origin location in the input file and the closest harbour node of the network. Then, the GeoJSON file has been imported in ArcGIS Pro to read the distance estimated and to visualize the sea routes obtained in a map.

5.5 Environmental impact assessment of lithium mining on land

Information retrieved through remote sensing and GIS analysis have been used to quantify the impact of lithium mining on the land use. The estimation of the mine area in Chile and Western Australia has been related to the production of lithium at the mine sites to create an indicator of land occupied for a unit mass of lithium compound produced. This indicator, called land use intensity is expressed in squared meters of land used per tonne of lithium produced, and has been computed as:

$$\text{Land Use Intensity (LUI)} \frac{m^2}{ton} = \frac{\text{Lithium Mining Area (2022)}}{\text{Annual Production (2022)}}$$

In the case of Chile, SQM operations in the Salar de Atacama have been considered for the analysis and company's reports have been used to retrieve information about annual production (SQM, 2022). The company extracts brine from the underground to produce lithium and potassium compounds. Therefore, allocation methods have been implemented to consider both production lines and split the land use burden. Mass allocation and economic allocation have been carried out and then compared to the indicator resulting from the analysis without potash allocation. Mass allocation coefficient $A_{mass,j}$ has been computed as:

$$A_{mass,j} = \frac{j - mass}{total\ mass} \cdot A_{tot} = \frac{m_j}{\sum m_i} \cdot A_{tot}$$

where m_j is the mass of the product considered for the calculation of the allocation coefficient and A_{tot} is the area burden related to the production of the j-product.

Economic allocation coefficient $A_{economic,j}$ has been computed as:

$$A_{economic,j} = \frac{j - product\ value}{total\ value} = \frac{m_j \cdot v_j}{\sum m_i \cdot v_i} \cdot A_{tot}$$

where v_j is the economic value of the j-product considered for the calculation of the allocation coefficient.

Therefore, the Land Use Intensity (LUI) estimated with allocation methods has been calculated with the following formula:

$$Land\ Use\ Intensity\ (LUI) \frac{m^2}{ton} = \frac{Allocation\ coefficient \cdot Evaporation\ Ponds\ Area\ (2022)}{Annual\ Production\ (2022)}$$

Instead, in the case of Western Australia, the area estimated through ArcGIS Pro has been used in this analysis and Tianqi's Lithium production data have been retrieved from the IGO's Quarterly Report for the period ended on the 31st of March 2022 (IGO, 2022). To compute the land use intensity analysis, no allocation method has been used because there are no other relevant coproducts as output from the Greenbushes mine operations. All the steps and the assumptions made for the analysis are illustrated in detail in the Appendix (Section III).

5.6 Carbon emissions from lithium products: the contribution of transportation

Goal and Scope definition

The goal of this life cycle assessment is to evaluate the contribution of transportation to the environmental impact of lithium production, with a focus on carbon emissions. The scope of this study is to integrate information retrieved through geographic information systems (GIS) in a life cycle assessment (LCA) to compute the carbon footprint of lithium production from mining to refinement of battery grade lithium products. Carbon emissions related to production from brine in Chile and from ore in Western Australia have been retrieved from a paper published Kelly et al. in 2021. They have collected and analysed data about the energy, greenhouse gases, and water needed for lithium carbonate and lithium hydroxide production (Kelly et al., 2021). The contribution of transportation that is already present in the carbon emissions results of the paper has been estimated and removed, using the detailed data that have been provided by the authors in the Supplementary Materials. Therefore, the inputs used in this analysis are (1) the elementary flow of carbon emission of lithium production, coming from literature, and (2) the transportation distance retrieved from the previous GIS analysis. The functional unit has been chosen as 1 tonne of lithium carbonate/lithium hydroxide. The system boundary is from cradle-to-gate: 1 tonne of lithium carbonate/lithium hydroxide shipped to a refinement plant in China has been considered. The latter has been chosen because it produces two battery cathode materials: $\text{LiNi}_{0.6}\text{Mn}_{0.2}\text{Co}_{0.2}\text{O}_2$ (NMC622) and $\text{LiNi}_{0.8}\text{Mn}_{0.1}\text{Co}_{0.1}\text{O}_2$ (NMC811) that are used in electric vehicle batteries. In Figure 16, the flow processes and system boundaries for the brine pathway are shown, together with transportation stages (RT: Road Transport, ST: Ship Transport).

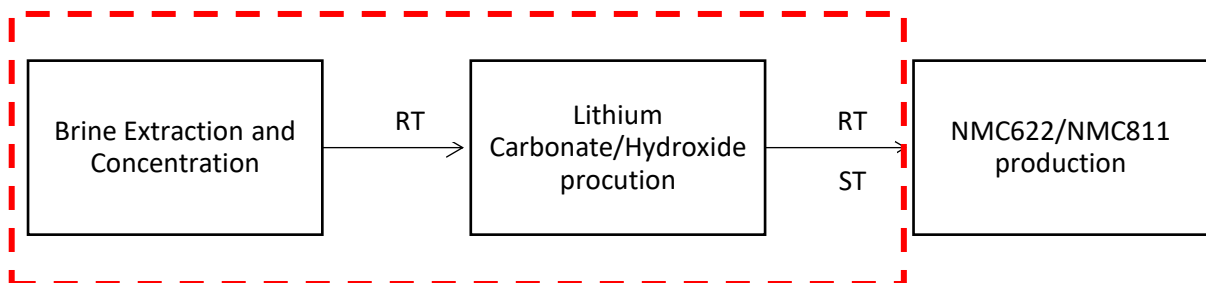


Figure 16. Flow processes and system boundaries for the Chilean brine pathway. Road Transport (RT) in Chile and in China and Ship Transport (ST) are also indicated.

In Figure 17, the flow processes and system boundaries are shown for the ore pathway, together with transportation stages (RT: Road Transport, ST: Ship Transport). The analysis has been performed using OpenLCA as software and Ecoinvent as database.

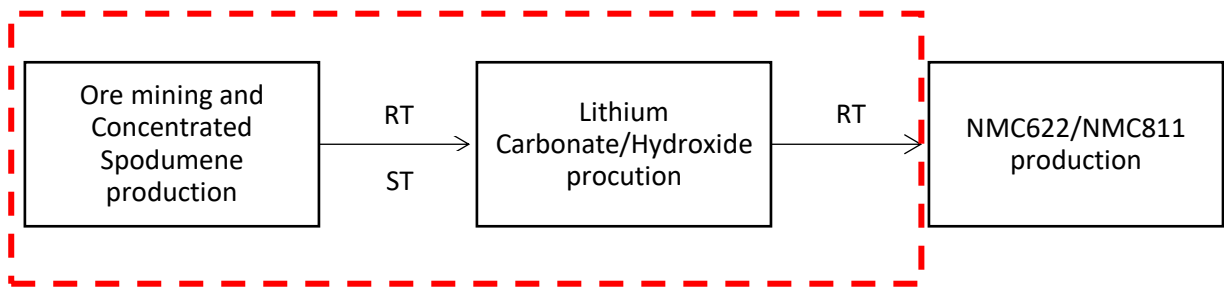


Figure 17. Flow processes and system boundaries for the Australian ore pathway. Road Transport (RT) in Western Australia and in China and Ship Transport (ST) are also indicated.

Life Cycle Inventory Analysis

For the Chilean pathway (brine), road transportation of concentrated lithium brine in tanker trucks from Salar de Atacama extraction site to the processing plant in Salar de Carmen has been considered. After that, shipment of lithium carbonate/lithium hydroxide stored in jumbo bags in container trucks from Salar de Carmen to the port of Mejillones has been evaluated. Then, shipping in cargo vessels to the main export destination country (China) has been considered, in particular to the port of Shanghai. Finally, road transportation in container trucks to a refinement plant that produces cathode materials for battery production has been estimated. Shandong Gelon has been chosen as reference refinement plant because is one of the largest companies in China that refines lithium compounds to produce lithium nickel manganese cobalt oxide. It refines lithium carbonate in NMC622 and lithium hydroxide in NMC811. In the process graph illustrated in Figure 18, the origin and destination locations for each transport stage are shown for the Chilean brine pathway. The quantitative inputs used to generate the process are shown in Table 18 in the Appendix (Section IV).



Figure 18. Graph illustrating all the origin and destination locations for each transportation stage for the Chilean brine pathway.

For the Australian pathway (ore), road transportation of concentrated spodumene from Greenbushes mine site to the port of Bunbury has been considered. Shipping of concentrated spodumene from the Australian port to the port of Shanghai, in China, that is the main export destination country, has been estimated. Then, road transportation in container trucks from the

Chinese port to the Tianqui Lithium processing plant in Shehong, Sichuan has been considered. The plant of Shehong has been chosen as processing plant because it produces both lithium carbonate and lithium hydroxide from concentrated spodumene extracted at Greenbushes. Instead, Zhangjiagang plant, in Jiangsu, owned by Tianqui Lithium, produces lithium carbonate only. Finally, road transportation from the latter to the refinement plant that produces cathode materials (NMC622 and NMC811) has been considered. In the process graph illustrated in Figure 19, the origin and destination locations for each transport stage are shown for the Western Australian ore pathway. The inputs used to generate the process are shown in Table 18 in the Appendix (Section IV).

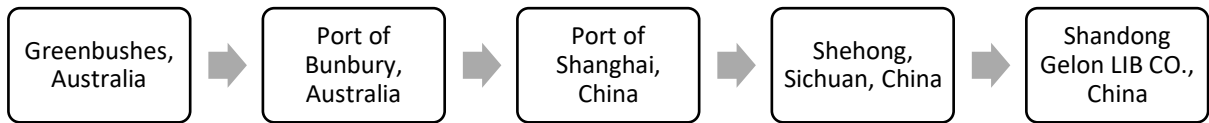


Figure 19. Graph showing all the origin and destination locations for each transport stage for the Western Australian ore pathway.

The supply chain of lithium is currently experiencing many changes and it will be reshaped a lot in the future due to the soaring demand of the critical mineral all over the world. As shown in the previous analysis, the Chinese company Tianqui Lithium and the American one Albemarle have been investing in processing plants in Western Australia. These plants are going to produce lithium hydroxide and lithium carbonate from concentrated spodumene extracted from Greenbushes mine. In this way, lithium compounds with a higher economic value in the market will be exported from the country. Therefore, this analysis evaluates how the transport would change according to this near future scenario. For the ore pathway, road transportation of concentrated spodumene in trucks has been considered from Greenbushes mine to the Kiwana processing plant, owned by Tianqui Lithium. Then, shipment of lithium carbonate and lithium hydroxide from the Kiwana plant to the port of Bunbury has been considered. Shipping of lithium carbonate and lithium hydroxide from the Australian port to the Chinese port of Qingdao has been considered. Qingdao port has been chosen as destination port because of the proximity to the processing plant. Road transportation from the Chinese port to the refinement plant that produces NMC622 and NMC811 for battery production has been considered. In the flow diagram in Figure 20, the origin and destination locations for each transport stage are shown for the near future Western Australian ore

pathway. The inputs used to generate the process are shown in Table 18 in the Appendix (Section IV).

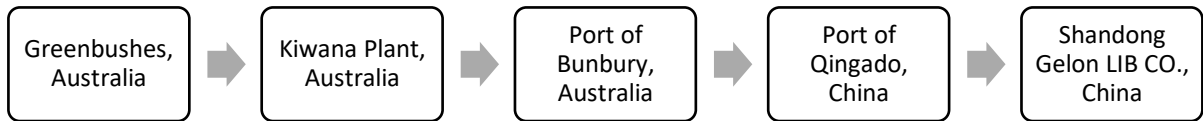


Figure 20. Graph showing all the origin and destination locations for each transport stage for the near future Western Australian ore pathway.

Life Cycle Impact Assessment

The life cycle impact assessment (LCIA) has been carried out using the ILCD 2011 Midpoint+ method. It is a characterization method created by the Joint Research Centre (JRC) of the European Commission. Midpoint impact categories such as climate change, ozone depletion, human toxicity-cancer effects, acidification, freshwater ecotoxicity, land use, water resource depletion could be evaluated through this method. In this study, the midpoint impact category of Climate Change has been considered to evaluate the carbon emission of transportation in lithium production.

6 Results and discussions

In this Chapter, all results obtained are presented through a division that follows the same subchapters of the Methodology section. Therefore, in the first part, the results of the analysis performed on satellites images are illustrated, followed by the outputs of the study on the transportation routes. In the last part, the results of the land use intensity and LCA analysis are shown.

6.1 Indices analysis for evaporation ponds area extraction in Chile

Brine extraction and evaporation process takes place in the salt flat nucleus in the Salar de Atacama, shown in Figure 21 by the True Color Image Sentinel-2 satellite images acquired on the 3rd of January 2022. The latter is the result of the pre-processing steps illustrated before in the Chapter 5.1. Band 4 (Red), Band 3 (Green), and Band 2 (Blue) of the Visible Spectrum have respectively been associated to the red, green, and blue display colour setting to have a Natural Colour representation of the area. All the True Color satellite images used for the analysis are shown in Figure 35 in the Appendix (Section I).

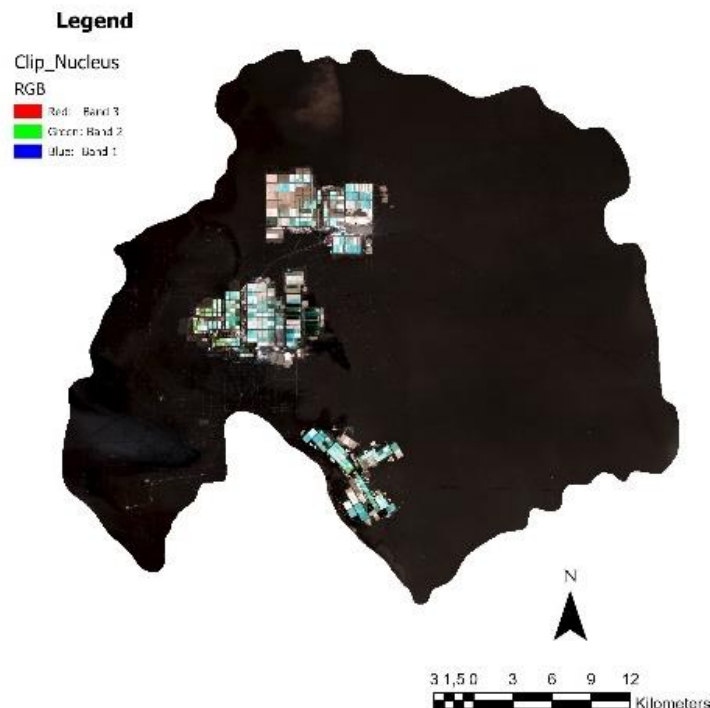


Figure 21. True Color Image Sentinel-2 satellite images acquired on the 3rd of January 2022 showing the area over the Salar de Atacama, Chile.

The raster obtained computing the NDVI on the satellite image is shown in Figure 22 (left). As it can be noticed, the evaporation ponds are identified with a negative NDVI, depicted in brownish in the map. This is due to the presence of water in the brine that absorbs more in the NIR than in the Red spectrum. Therefore, having a lower reflectance in the NIR with respect to the Red, the brine shows a negative NDVI. Some ponds do not have a negative NDVI value, because they do not store brine but salt waste, where no water is present. They can be identified in white in Figure 22 (left), because their NDVI ranges between 0 and low positive values. Instead, bare soil presents a positive NDVI value allowing the identification and the separation of the two characteristic features. The opposite happens for all the other indices used (NDWI, MNDWI, ...), as shown in Figure 22 (right). The water reflects more in the green than in the NIR, resulting in positive NDWI values. All the raster obtained computing respectively the NDVI (for the different years) and the different indices are shown in Figure 36 and in Figure 37 in the Appendix (Section I).

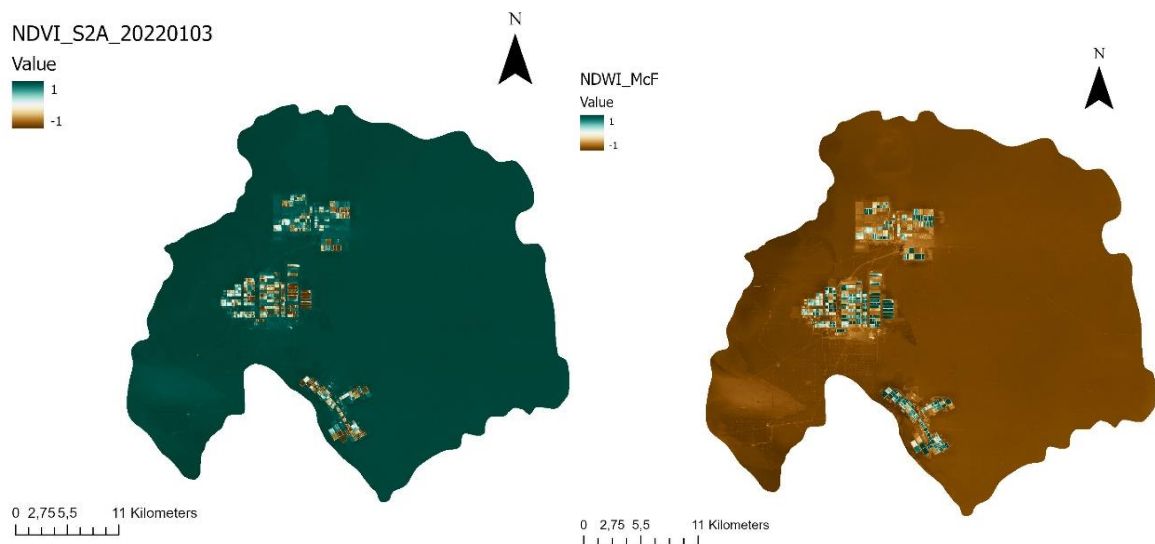


Figure 22. NDVI image (left) and NDWI (McFeeter) image (right) showing the Salar de Atacama area.

Table 7 shows the thresholds selected through the Interactive Stretching and the Density Slice Tools in ENVI. These thresholds have been used to obtain all the binary images (0, 1) that can be found attached in Figure 38 in the Appendix (Section I), together with an example of the ground truth for the year 2022 and its relative binary image (0, 1) in Figure 37. Table 7 also shows the resulted estimated area (in squared kilometres) occupied by the evaporation ponds in 2022 and the Kappa Coefficient resulting from the accuracy analysis for each index.

Table 7. Thresholds that have been used to create all the binary images, estimated area (in squared kilometres) occupied by the evaporation ponds, and Kappa Coefficient resulting from the accuracy analysis shown for each index in relation to the Sentinel-2 satellite image acquired in 2022.

Index	Threshold	Evaporation Ponds Area	Kappa coefficient
-	-	km ²	-
NDVI	$x \leq +0.01$	53.43	0.81
NDWI (McFeeters)	$x \geq -0.045$	47.47	0.75
NDWI (Gao)	$x \geq +0.15$	58.05	0.81
MNDWI (Xu)	$x \geq -0.005$	44.74	0.79
MNDWI (SWIR1)	$x \geq +0.10$	60.50	0.85
MNDWI (SWIR2)	$x \geq +0.25$	61.42	0.84

As it can be noticed in Table 7, the values of the estimated ponds area ranges between 45 km² and 61 km². The highest accuracy of 0.84 and 0.85 has been reached by the MNDWI that uses the short-wave infrared band, as already expected thanks to the analysis of the spectral signatures of the pond's classes. NDVI, which is the index that has been considered for the estimation of the ponds area in the past, has a value of the kappa coefficient equal to 0.81 for the analysis of the satellite image acquired on the 3rd of January 2022. The NDVI confusion matrix obtained is shown in Table 8. As it can be noticed, 846 cells belonging to the evaporation ponds area have been correctly classified, 172 cells belonging to evaporation ponds have wrongly been assigned to the other class, generating an underestimation or omission error, and 202 cells not belonging to evaporation pond have wrongly been assigned to ponds area, generating an overestimation or commission error. The other confusion matrices relative to all the indices can be found attached in Table 13-17 in the Appendix (Section I).

Table 8. Confusion matrix relative to the NDVI analysis.

ClassValue	C_0	C_1	Total	User's Accuracy	Kappa Coefficient
C_0	18780	202	18982	0,989	0
C_1	172	846	1018	0,831	0
Total	18952	1048	20000	0	0
Producer's Accuracy	0,991	0,807	0	0,981	0
Kappa Coefficient	0	0	0	0	0,809

The results of the evaporation ponds area estimated for the years 1992, 1997, 2002, 2007, 2011, 2017, and 2022 through NDVI are shown in Table 9. Brine extraction has started in the salt flat nucleus in 1983, but the first satellite image available in the area has been acquired on the 24th of December 1984 by Landsat 5. The evaporation ponds area has been increasing during the years following the increase in lithium global demand.

Table 9. Results of the estimated area according to the multitemporal NDVI analysis, together with the Kappa Coefficient accuracy indicator.

Year	Evaporation Ponds Area (NDVI)	Kappa Coefficient
-	km2	-
1992	1.95	0.70
1997	12.93	0.88
2002	26.97	0.73
2007	41.95	0.78
2011	51.53	0.84
2017	52.04	0.77
2022	53.43	0.81

The evaporation ponds area that has been estimated through the NDVI analysing the Sentinel-2 satellite image acquired on the 3rd of January 2022 has been integrated in the land use intensity analysis that will be illustrated in Chapter 6.5.

6.2 Mine area analysis in Western Australia

Analysing the Sentinel-2 satellite image acquired on the 17th of February 2022, the area disturbed by the mining operations at Greenbushes has been estimated through ArcGIS Pro. Polygons have been digitalized covering open pits, tailing storage facilities, and waste rock landform. In Figure 23, the mine site of Greenbushes is shown in a map with the identified active area that will be integrated in the land use intensity analysis illustrated in Chapter 6.5. The area disturbed by the mine activity, shown with a red dotted line in Figure 23, has been estimated at 7,657,970.53 m².

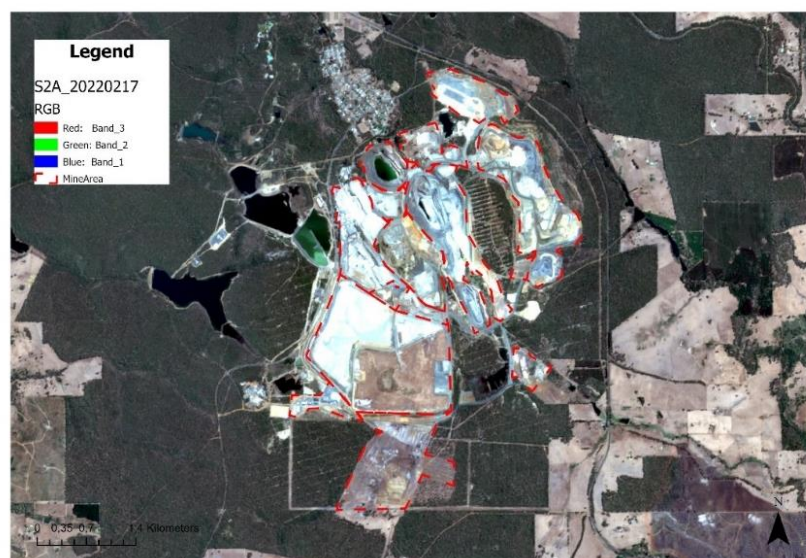


Figure 23. Sentinel-2 satellite image acquired on the 17th of February 2022 showing the mine site of Greenbushes and the identified active area with a red dotted line.

Analysing the satellite image acquired on the 17th of February 2022, a disturbed area has been detected in the southeast part of the mine site, as shown in the False Color Image in Figure 24. Remote Sensing is widely used for monitoring the mine sites, for verifying that the active area effectively used by companies that have won a concession in a place is the one declared in the legal agreements. Checking the acquisition before and after this disturbed area appeared, it has been possible to understand that the disturbances has been generated in a couple of days. Therefore, the hypothesis of a fire has been considered, confirmed by the news of the Greenbushes local newspapers (ABC News, 2022). In the Quarterly Report for the period ended on the 31st of March 2022, the Australian company IGO has also announced that the first quarter production of 2022 has been lower of around 23,000 tons because of a damage to the powerline caused by a bushfire in the southeast of the mine site at the beginning of February 2022 (IGO, 2022).

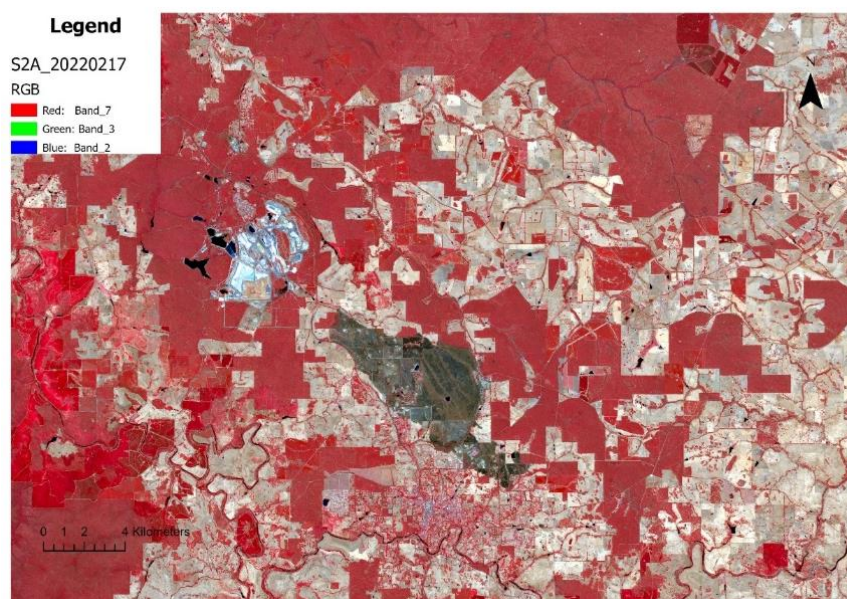


Figure 24. False Color of the satellite image acquired by Sentinel-2 on the 17th of February 2022 showing the Greenbushes mine site and the area affected by the fire (in brownish).

In Figure 24, the False Color Image acquired on the 17th of February 2022 of the mine site and of the area affected by the fire is shown. The area has been estimated at 17,000 m². The False Colour Image has been created using near infrared, red and green bands. The latter is a widely used combination, commonly implemented to assess plant density and health, since plants reflect near infrared and green light, while they absorb red. Therefore, in Figure 24, the vegetation results depicted in red, cultivated fields in light brownish, clearly delineating the area after the bushfire which is depicted in dark brown. Remote Sensing is commonly used to analyse and prevent natural

disaster as fire events, also studying the post-event land conditions and rehabilitation behaviours. Nowadays, integrating these applications with the monitoring of mine sites is of extreme importance to better understand the dynamics of the minerals supply chain.

6.3 Atmospheric emissions analysis

Results of the analysis of the Sentinel 5P satellite images show that it is not possible to correctly attribute emissions to a particular mine site, because the spatial resolution of the sensor TROPOMI is too low, being the sensor pixels dimension larger than the extension of the eventual emissions sources. The spatial resolution limits the application of these measurements, but some studies managed to quantify methane emissions combining Sentinel-5P data with Sentinel-2 data (The European Space Agency, 2020).

However, in this study, it has been possible to detect emissions over larger areas analysing the satellite images. Figure 25 shows the Aerosol Index (AER AI) obtained over Chilean area. The AER AI is obtained considering two wavelengths, through a calculation based on the changes in the Rayleigh scattering in the UV spectral range, where the ozone is absorbed in small quantities. It is a quantitative index, where a positive value indicates the presence of elevated layers of aerosols that absorbs UV rays. Typically, desert dust, volcanic ashes and biomass burning can cause the presence of this aerosols in the atmosphere. As it can be noticed in the eastern part of the image shown in Figure 25, over the Salar de Atacama basin, higher values of the AER AI can be detected, indicated by yellow, orange, and red pixels. The AER AI shown has been computed for the pair of wavelengths 340/380 nm. Being a desertic region, the presence of aerosols in this area can be connected to the presence of desert dust.

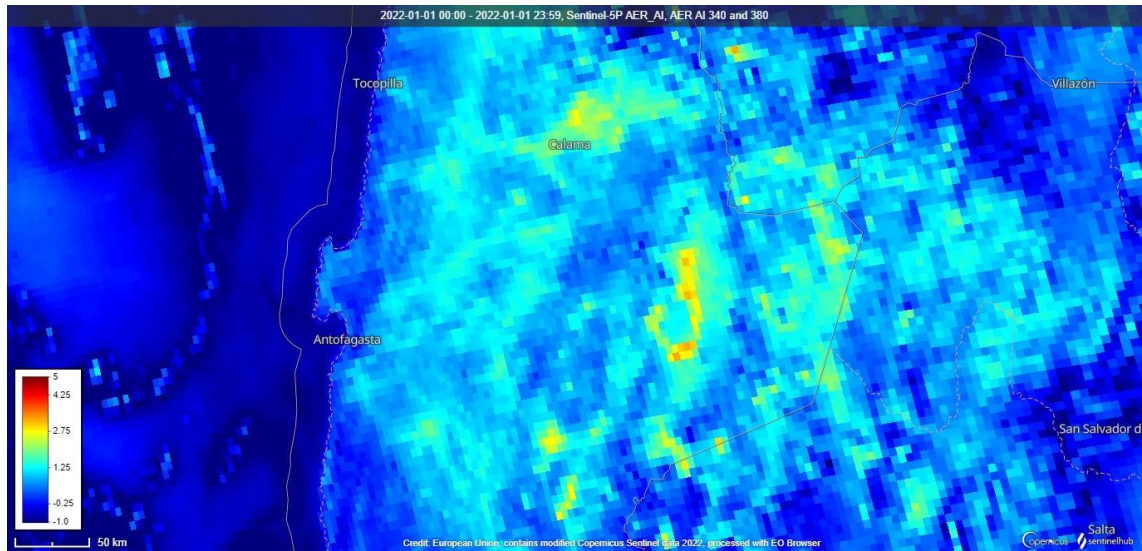


Figure 25. Aerosol Index (AER AI) image obtained from TOPOMI sensor (Sentinel-5P), acquired on the 1st of January 2022 over the Chilean area.

Figure 26 shows the Nitrogen Dioxide (NO₂) values expressed in mol/m² over the Chilean area. Tropospheric and stratospheric Nitrogen Dioxide and Nitrogen Oxide column products are obtained by the TROPOMI sensor in a passive way, measuring the solar radiation reflected and emitted by the Earth. These two gases are naturally present in the Earth atmosphere because of wildfires and microbiological processes in soil. However, anthropogenic activities such as fossil fuel combustion and biomass burning causes more NO_x emissions to enter the environment. As it can be noticed in the south-east part of the image, high values of NO₂ tropospheric column can be identified by red pixels, surrounded by orange and yellow ones. That area is located over the copper mine Minera Escondida, where fossil fuels combustion occurs for the mining activities.

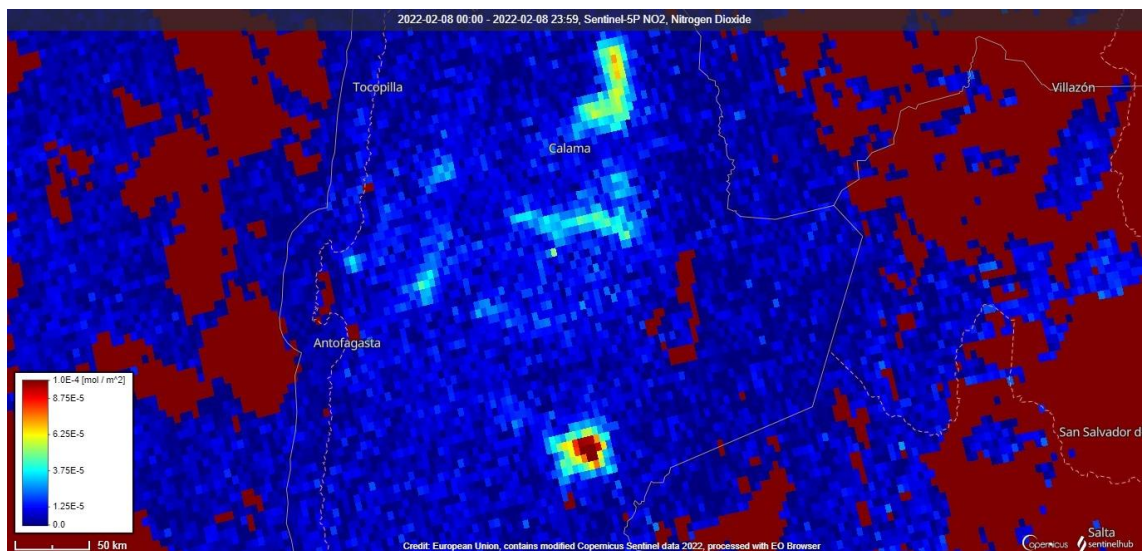


Figure 26. Nitrogen Dioxide (NO₂) image obtained from TOPOMI sensor (Sentinel-5P), acquired on the 8th of February 2022 over the Chilean area.

In Figure 27, NO₂ measurement acquired by Sentinel-5P over the area of Greenbushes in Western Australian is shown during the wildfire event that started in the afternoon of the 5th of February 2022. As it can be noticed by the red pixel in the middle of the image, the amount of NO₂ (measured in mol/m²) that have been emitted in the air is high in the fire site and in the surrounding area.

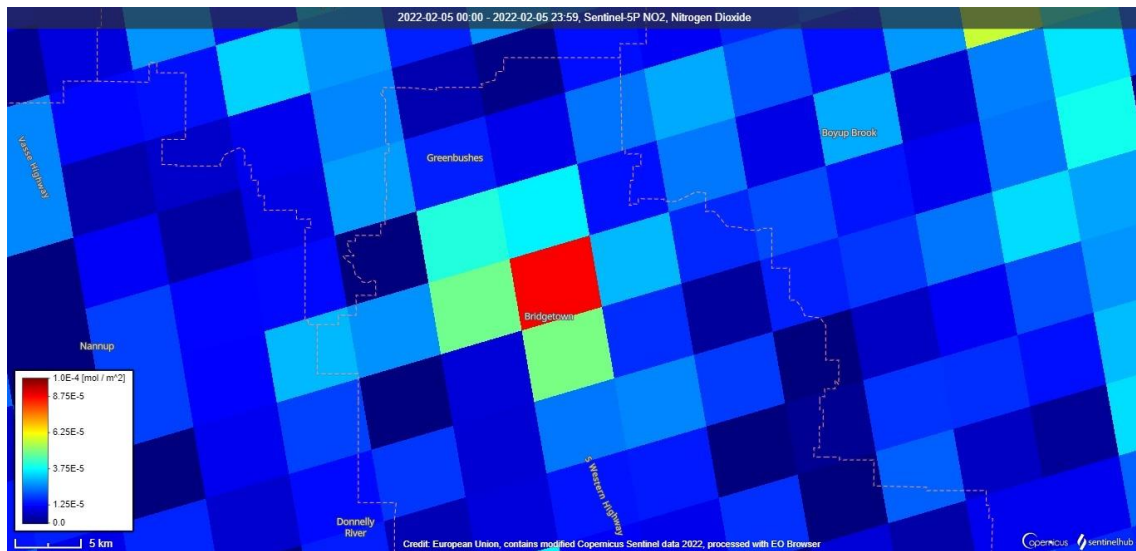


Figure 27. Nitrogen Dioxide (NO₂) image obtained from TOPOMI sensor (Sentinel-5P), acquired on the 5th of February 2022 over the Greenbushes area in Western Australia.

6.4 Transportation Routes Analysis

Land Transport

The Network Analysis Tool has been used in ArcGIS Pro to compute the distance in km travelled by the trucks. The 'Truck distance' has been set as variable to be computed and several paths have been estimated for both the brine and ore pathway:

1. Brine trucks' path (SQM): from the extraction site in the Salar de Atacama, to the processing plant in the Salar de Carmen and to the shipping at Puerto de Mejillones in Chile. SQM has won concession for the extraction of brine in the Salar de Atacama, where it produces both lithium concentrated brine and other products to obtain potash compounds. The lithium concentrated brine (6%) is then transported by tanker trucks in the Salar de Carmen, close to the city of Antofagasta, where there is a processing plant that transform brine in lithium carbonate and then in lithium hydroxide. Then, container trucks transport lithium products stored in jumbo bags from the plant to the close port of Mejillones, as shown by the green route in the map in Figure 28.

2. Brine trucks' path (Albemarle): from the extraction site in Salar de Atacama, to the processing plant Planta Química La Negra and to the shipping at Puerto de Mejillones in Chile. Albemarle was the first company to extract brine in the Salar de Atacama, despite it was under the name of Rockwood. Its mining plant is located in the southern part of the salt flat nucleus, where the evaporation process takes place in ponds. The concentrated brine is then transported to the refinement plant called Planta Química La Negra, located close to the city of Antofagasta. Then, produced lithium compounds are stored in bags and transported to the port of Mejillones, that is close to the processing plant, as shown by the brown route in the map in Figure 28.

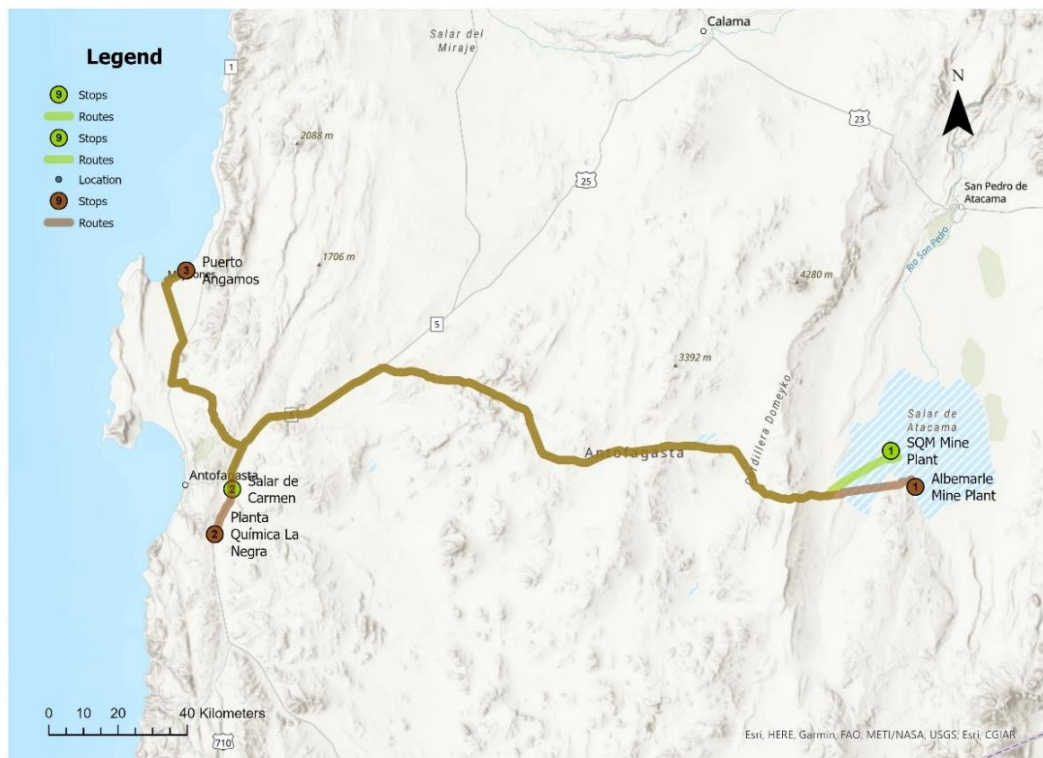


Figure 28. Map showing the stops and the transportation routes in Chile for the SQM trucks (green) and for the Albemarle ones (brown).

3. Ore truck's path (Tianqui): from the Greenbushes mine to Bunbury Port in Western Australia. Annual export volume of spodumene concentrate has been around 767,000 tonnes in 2018-2019 from the Port of Bunbury. The material is transported through the South Western Highway road from Greenbushes mine to the harbour, as shown in the route map in Figure 29. Talison Lithium, the South West Development Commission and Arc Infrastructure have been carrying out a feasibility study for a railway line construction that

will connect Greenbushes mine site to the Port of Bunbury and to the two lithium refinery plants. There is an abandoned line that connects Greenbushes to the town of Picton (located at 10 km from the Port of Bunbury) that has not been active since 2005. Infrastructures investments would be required for the loading facilities at Greenbushes mine and for the unloading ones at Bunbury and Kwinana. Nowadays, in the context of an increasing demand for lithium products, the project would support the transformation to a rail-based lithium supply chain, lowering the traffic pressure on the highway. At the same time, it would be an opportunity also for the tourism development of the area.

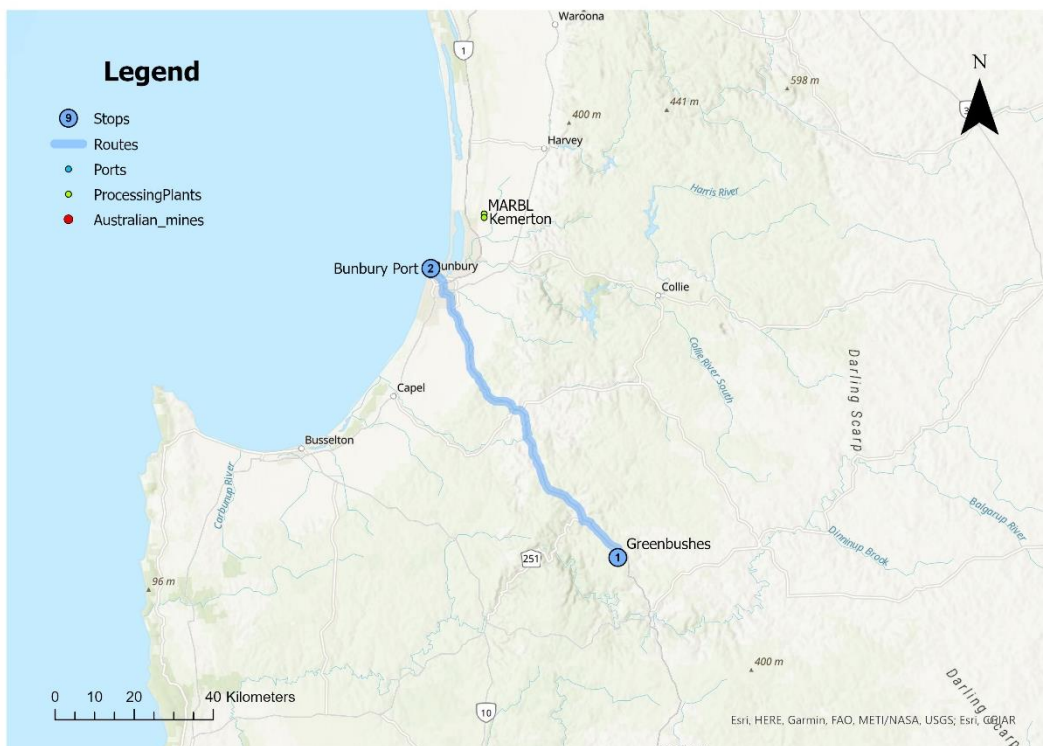


Figure 29. Map showing the stops and the transportation route in Western Australia for the trucks transporting concentrated spodumene from the Greenbushes mine site.

4. Lithium products from brine: from the Port of Shanghai to Shandong Gelon. in China. It has been supposed that lithium products are imported from Chile through one of the main ports of China that is in Shanghai. Then, lithium carbonate and hydroxide are refined in cathode materials by the company Shandong Gelon. The route is shown in yellow in Figure 30. More details about this pathway can be found in Chapter 5.6.
5. Concentrated spodumene (Tianqi): from the Port of Shanghai to Shehong, in Sichuan, and then to Shandong Gelon. in China. It has been supposed that concentrated spodumene

from the Greenbushes mine is imported from Australia through one of the main ports of China that is in Shanghai. Then, lithium carbonate and hydroxide are produced in the Tianqui's processing plant at Shehong, in Sichuan. After that, it has been assumed that lithium compounds are refined in cathode materials by the company Shandong Gelon. The route is shown in brown in Figure 30. More details about this pathway can be found in Chapter 5.6.

6. Lithium products from ore (Tianqui): from the Port of Qingdao to Shandong Gelon. in China. It has been supposed that lithium products are imported from Australia through the main port of Qingdao. Then, lithium carbonate and hydroxide are refined in cathode materials by the company Shandong Gelon LIB CO. The route is shown in green in Figure 30. More details about this pathway can be found in Chapter 5.6.

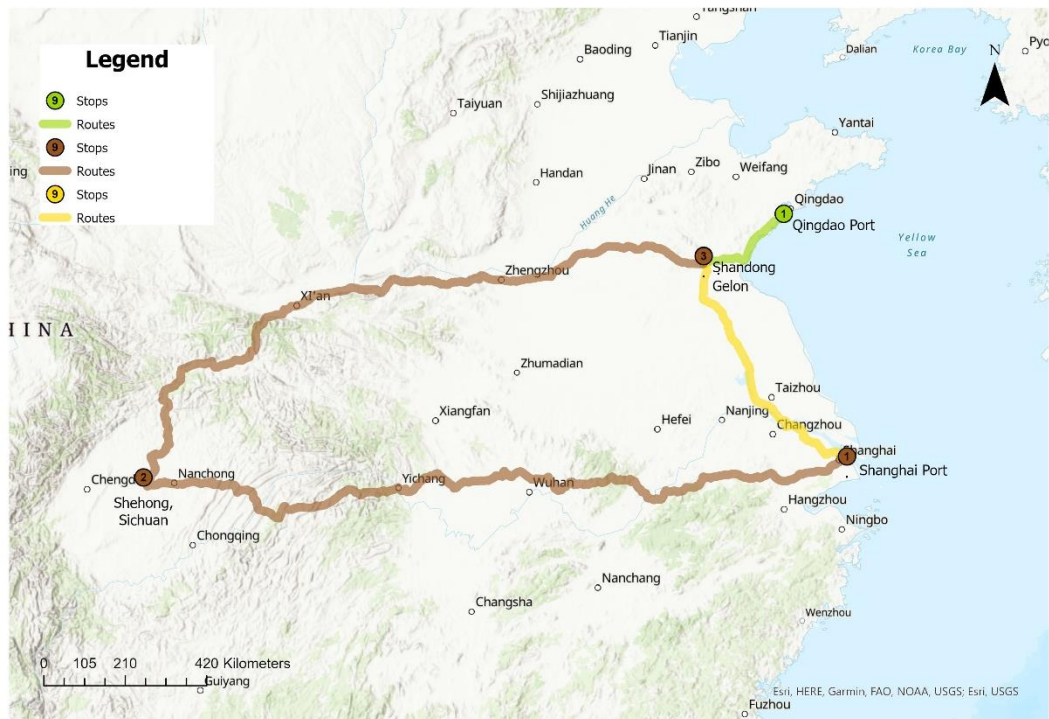


Figure 30. Map showing the stops and the transportation routes in China for the trucks in the Chilean lithium brine pathway (yellow), in the Australian ore pathway (brown), and in the near future Australian ore pathway (green).

Results obtained through the Route analysis in Network Analyst Tool in ArcGIS Pro are shown in Table 10. All distances needed for the following LCA analysis are expressed in kilometres.

Table 10. Results of the Land Routes Transportation Analysis, showing distances expressed in kilometres.

Route ID	Route	Total Kilometres
1	Salar de Atacama – Salar de Carmen – Puerto de Mejillones, Chile	324
2	Salar de Atacama - Planta Química La Negra – Puerto de Mejillones, Chile	353
3	Greenbushes – Port Bunbury, Western Australia	83
4	Port of Shanghai – Shandong Gelon, China	652
5	Port of Shanghai – Shehong, Sichuan – Shandong Gelon, China	3,700
6	Port of Qingdao – Shandong Gelon, China	250

The largest distance travelled by the trucks is the one relative to the ore pathway, because the plant that refines concentrated spodumene in lithium hydroxide and carbonate is far away from the coast. Moreover, then the refined products have to travel back to the plants that refines lithium compounds in cathode materials for battery production.

Sea Transport

According to official data on the Chilean Custom website, lithium compounds produced in the Antofagasta region are exported mainly from Puerto Angamos, located in Mejillones. Therefore, the latter has been chosen as port of origin in the sea route analysis for the brine pathway. Basing on the information available on the same database, the main destination countries where Chile export lithium products are China, Japan, South Korea, Belgium, USA, and Germany. Instead, according to the database of the World Integrated Trade Solution (WITS), in 2019, Australia exported minerals mainly to China, Japan, and South Korea. In 2020, main exporters of lithium oxide and hydroxide are China, Chile, Russian Federation, United States, Netherlands. Considering carbonates and lithium carbonates, the global leader exporters in 2020 were Chile, China, Argentina, European Union, Netherlands. Australia is not in the lead of the main exporter of refined lithium, underlining the fact that the country exports mainly spodumene concentrates. The main destination countries of lithium export from Chile and Western Australia have been represented on a map, shown in Figure 31.

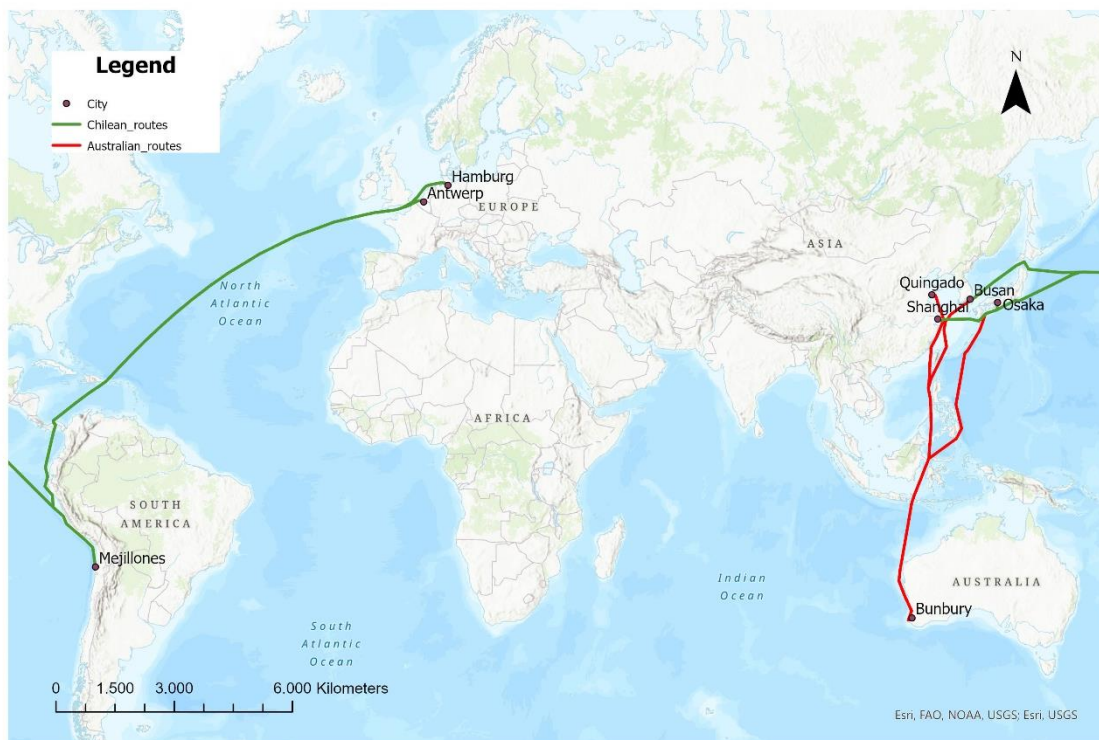


Figure 31. Sea routes travelled by the vessels both for lithium production from brine in Chile (green) and from ore in Western Australia (red).

Results of the sea route analysis are shown in Table 11, where distances are expressed in kilometres and the estimated travel time in days. The distance travelled by vessels to reach China has been implemented in the LCA analysis to evaluate the contribution of transportation on the total carbon footprint of lithium production.

Table 11. Results of the Sea Routes Transportation Analysis, showing the distance covered by the vessels in kilometres, together with the days of travelling.

Route Name	Distance	Travelling Time
-	km	days
Mejillones – Hamburg	13,552	23
Mejillones – Antwerpen (Belgium)	13,053	22
Mejillones – Osaka (Japan)	14,069	30
Mejillones – Busan (South Korea)	18,282	31
Mejillones – Shanghai (China)	17,277	32
Bunbury – Shanghai (China)	7,683	13
Bunbury – Osaka (Japan)	8,592	14
Bunbury – Busan (South Korea)	8,275	14
Bunbury – Quingado (China)	8,177	15

The export of minerals is usually an important trigger for the development of local infrastructure in a region. In remote places of the Salar de Atacama, where only indigenous communities live, roads and other type of infrastructures have been constructed only because of brine extraction for lithium and potash production in the late 1980s. Ports represent the main example of this mechanism: the increase in mining activity of a region is reflected by the development of the closer strategic harbours, where further refinement plants of the materials are constructed together with all the infrastructure related to the fuel supply and to the shipping management operations. For example, the port of Angamos, chosen for the brine pathway analysis, is located in the city of Mejillones, around 65 kilometres north of the city of Antofagasta. In the 80s, its economy started to grow thanks to the fishing sector. Then, since the last years of the XX century, given its location in the middle of what is today the world’s largest copper mining region, the city of Mejillones has rapidly developed into an important industrial centre servicing the mining industry. In Figure 32, the evolution of the area of Mejillones is shown through the multitemporal land use database Globeland30 (Globeland).

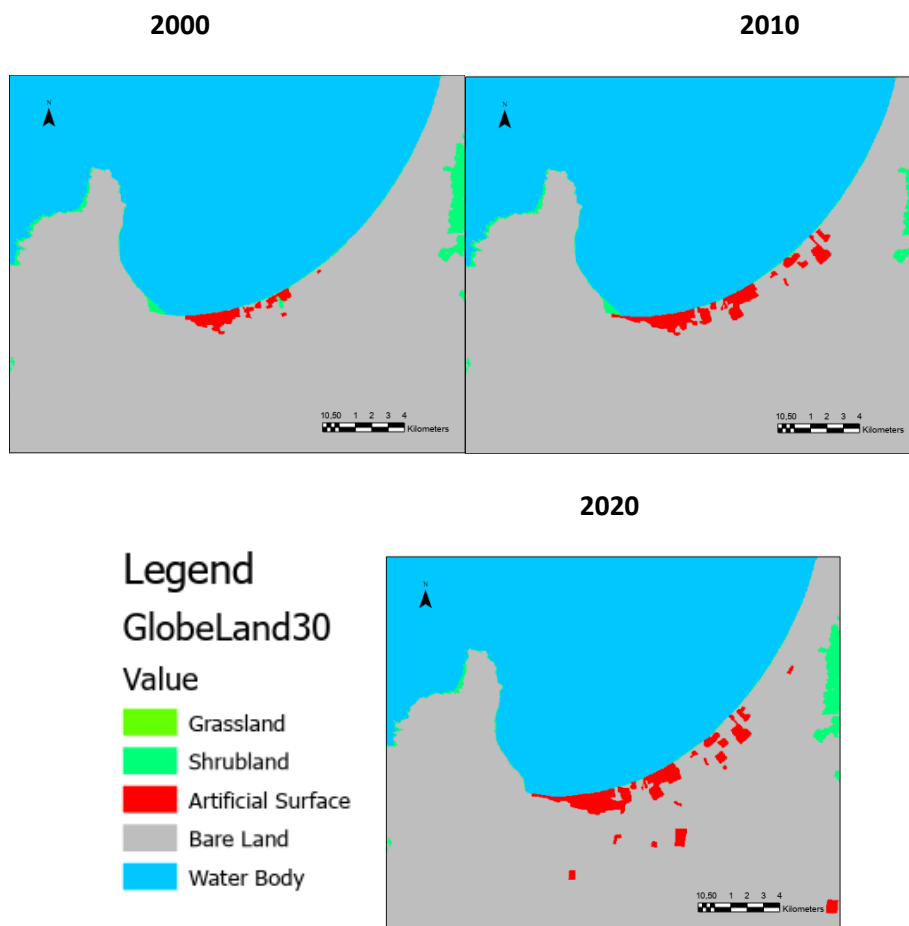


Figure 32. Multitemporal land use images showing the area of the port of Mejillones in Chile, retrieved from the Globeland30 database. The upper left image refers to the year 2000, the upper right one to the year 2010, and the bottom one to the year 2020.

The multitemporal land use maps show an increase in the artificial surface area since the year 2000. The main companies close to the ports have been identified to detect if they are also related to the production or shipping of lithium compounds. There are no plants that could be related to further lithium processing in the port location. The only plants related to lithium shipping are the ones concerning the fuel supply for the ships.

6.5 Environmental impact assessment of lithium mining on land

Integrating the area obtained through the indices analysis performed using satellite images, an indicator of the land used for lithium production has been computed. The Land Use Intensity (LUI) has been calculated for lithium carbonate and lithium hydroxide, both for the brine extraction pathway and for the ore one. Moreover, in the Chilean case, mass and economic allocation methods have been performed to consider the coproduction of potash. The methodology followed is described in detail in the Chapter 5.5 and in the Appendix (Section III). All the results of the land use intensity analysis have been summarised in Table 12.

Table 12. Results of the Land Use Intensity (LUI) analysis, showing the squared metres per ton of product of lithium carbonate and of lithium hydroxide both for the brine extraction in the Salar de Atacama and for the ore extraction at Greenbushes. Mass allocation and economic allocation results are also shown for the brine extraction in Chile, together with the land use intensity related to potash as coproduct.

		Land Use Intensity (LUI)		
		No Allocation	Mass Allocation	Economic Allocation
		m ² /ton	m ² /ton	m ² /ton
Brine	Lithium Carbonate	169.9	4.93	133.4
	Potash	-	4.84	1.07
	Lithium Hydroxide	179.9	4.80	142.7
	Potash	-	4.84	0.98
Hard Rock	Lithium Carbonate		48.58	
	Lithium Hydroxide		42.72	

As it can be noticed in Table 12, considering the values obtained without and with economic allocation, the land use intensity of the lithium extracted from concentrated brine in Chile results higher both for lithium carbonate and lithium hydroxide compared to the ones produced starting from spodumene ore in Western Australia. Chilean lithium compounds would have a lower LUI only

if mass allocation of potash is considered because of the high amount of potash (8.52 tons) produced starting from 1 ton of concentrated lithium brine (6%).

Considering the values obtained without allocation method, lithium hydroxide land use intensity (m²/ton) results higher because of the slightly higher amount of brine needed to produce it respect to lithium carbonate. This approach does not consider the potash production (*KCl*) as coproduct of the process in the production line. Therefore, a further analysis has been carried out allocating the burden of the land use also to potash production.

For the Chilean brine pathway, the land use intensity computed with the mass allocation method is two orders of magnitude lower than the previous ones that do not consider potash allocation. In this case, the land use intensity of lithium hydroxide results lower than the lithium carbonate one. The reason behind these results is that the amount of potash generated as coproduct (per ton of Li product) in the lithium hydroxide production is higher than the *KCl* generated in the lithium carbonate process because of the higher amount of concentrated brine needed for the process. Therefore, in the case of lithium hydroxide, the land burden is allocated in slightly higher amount to potash coproducts.

Land Use Intensity computed with economic allocation is higher than the values obtained from the analysis performed with mass allocation, because of the higher economic value of lithium products in the market with respect to the potassium chloride one. Land use intensity related to lithium hydroxide result slightly higher than lithium carbonate one also because of its higher economic value. However, the values computed with economic allocation method result of the same order of magnitude - slightly lower - than the ones that do not consider allocation of potash. These results underline how the choice of the allocation method is important for the land use intensity analysis and it could determine a huge difference in the final outputs.

LUI of potash computed with the economic allocation method results equal to 0.98-1.07 m²/ton, lower than the one obtained through the mass allocation method (4.84 m²/ton), but in the same order of magnitude. These results underline how the lower market value of potash shifts the burden of land to the strategic and more expensive lithium products. Instead, the mass allocation approach splits almost equally the burden of the land use between lithium compounds and potash coproducts since the economic market values are not considered in the mass allocation coefficient.

Considering compounds obtained through hard rock extraction in Western Australia, the land use intensity related to lithium hydroxide results lower than the lithium carbonate one because of the lower amount of spodumene ore needed to produce it. The superficial land disturbed by mining

per ton produced results lower than the ones related to brine production in Chile, if considering the ones obtained without allocation and with economic one. However, it is worth to mention that the hard rock mining goes also deep down in the underground, disturbance that is not considered with this indicator.

The Land Use Intensity (LUI) is a way to quantify the environmental impact on land generated by the mining of a commodity in an area. Since it is computed per unit of tonne extracted, it could be also used to predict the area of a mine site that would be affected by mining activity according to planned future production, assuming that the conditions of extraction and processing of the mineral at the time of the analysis will be implemented also in the future. Moreover, quantifying the environmental pressure on land could represent a tool also for people that live close to the mining area. In fact, this kind of indicators could provide a framework for the development of policies with the aim of reducing the land used for mining purposes or using it in a sustainable way, especially when the mine site is located close to a town, as in the case of Greenbushes, or in the middle of a unique ecosystem, in which land use generates pressure on local biodiversity and indigenous communities.

For a sustainable future, it is necessary to find other sources of lithium to decrease the impacts of the extraction on the supply countries, both on the environment and on the local population. Part of the solution to the problem could be geothermal lithium, stored in the brine: this type of extraction could reduce the environmental impact related to current extraction methods. However, this is a supply chain that has yet to be defined and of which costs and actual feasibility must be verified. Many sites are under study in the United States and only few in Europe. For example, the Vulcan Energy Resources is currently developing a project to produce battery-quality Zero Carbon Lithium hydroxide, by harnessing renewable geothermal energy to drive lithium production, without using evaporation, mining or fossil fuels. The aim is to use deep geothermal and lithium brine resource, which is Europe's largest lithium resource, in the Upper Rhine Valley of Germany.

Another route for a sustainable use of the resources is the recycling of lithium. The current lithium recycling rates, both the end of life (EOL) and the recycled content (RC) are close to zero (World Bank Group, 2020). There is high future potential for recycling to grow in this area, reducing overall mineral demand. There is, however, little current evidence of these processes occurring at a commercial level, despite much research and interest in the area.

In the future, the brine extraction process could be improved with Direct Lithium Extraction (DLE) technologies, currently under research. The implementation of this innovative solutions would reinject brine in the underground after lithium has been separated by the membranes, reducing

the impact of water use in the desertic areas such as the Salar de Atacama. Moreover, the land required for this process would be drastically reduced because no evaporation process would be needed, also reducing the time necessary to produce lithium compounds. The disadvantage of this technology is that it is scale dependent since it relies on surface separation of minerals from brine through the presence of a membrane, the choice of which is under studying to improve its efficiency.

6.6 Carbon emissions from lithium products: the contribution of transportation

The aim of the LCA analysis is to evaluate the contribution of transportation to the carbon footprint in lithium production. As mentioned before, the ILCD 2011 Midpoint+ method has been used to perform LCIA, through the midpoint impact category of Climate Change, expressed in tons of carbon dioxide equivalent (tCO₂eq). Results of the Life Cycle Impact Assessment are shown in Table 19 in the Appendix (Section IV). In Figure 33, the results of this analysis are shown both for the Chilean brine and for the Western Australian ore pathway, and carbon emissions are expressed in tCO₂eq/ton product. The absolute value of transportation emissions is depicted in yellow in the column graph in Figure 33; instead, the production ones retrieved from literature are shown in light blue.

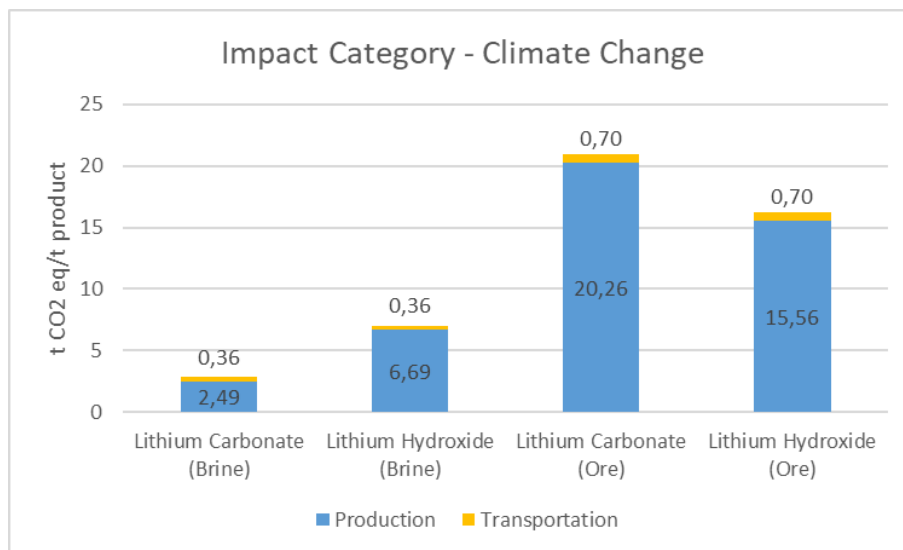


Figure 33. Results of the LCA analysis, where the absolute value of carbon emission related to transport is shown in yellow. Carbon emissions coming from the lithium production, shown in blue, have been retrieved from literature (Kelly et al., 2021).

Carbon emissions are higher for the transportation stage related to lithium production from ore (0.70 tCO₂eq/ton), because of the longer distance that the concentrated spodumene travels in trucks in China to be refined. In the brine pathway, instead, lithium compounds are processed close

to the mine site and on the way to the port for shipment. Therefore, despite the longer shipping distance from Chile to China respect to the one from Western Australia to China, the overall transport emissions are lower for the lithium products obtained from brine (0.36 tCO₂/ton). As shown in Figure 34, transportation accounts for a small percentage over the total carbon emissions in lithium production for both the pathways considered. Transportation represents 12.50% and 5.05% of the total carbon emissions respectively in lithium carbonate and in lithium hydroxide production from brine. The share of transportation emissions for the ore pathway is lower: they account for 3.32% of the total carbon footprint for lithium carbonate and 4.29% for lithium hydroxide.

Results obtained for the near future scenario, that is changing the location of the refinement plant from China to Western Australia to produce lithium carbonate and hydroxide from concentrated spodumene, are reported in Table 19 in the Appendix (Section IV). In this case, carbon emissions related to transportation results lower because of the lower distance the concentrated spodumene and the lithium compounds travel to the refinement plants in China. Carbon emission related to transport would be around 184.5 kgCO₂eq, 512.6 kg lower than transport emission of the process that takes place in China (696.14 kgCO₂eq). Moreover, considering that China heavily relies on fossil fuels, a change in the location of processing of spodumene concentrate would also lower the amount of carbon emissions related to the production process.

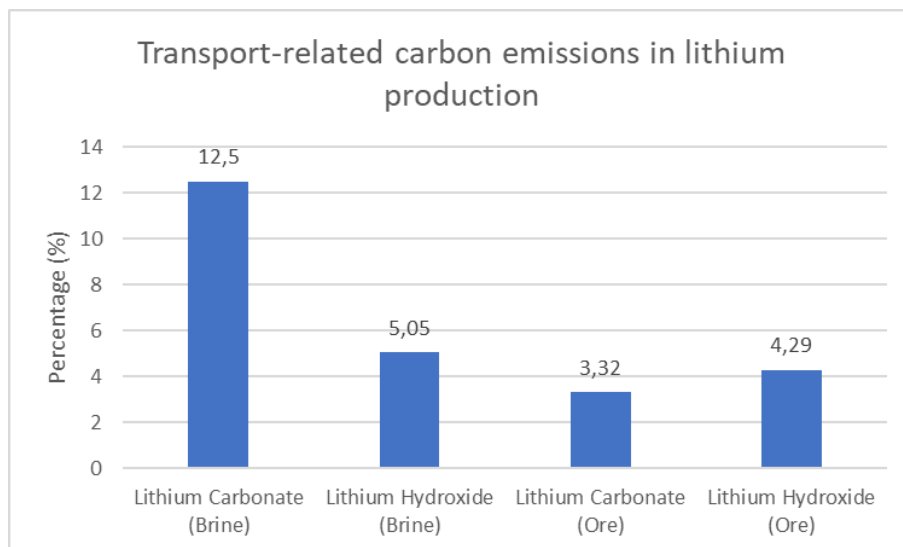


Figure 34. Percentage of carbon emissions related to transport in lithium production for lithium carbonate and for lithium hydroxide extracted from brine in Chile and from ore in Western Australia.

Transportation accounts for a small percentage of the total carbon emissions in lithium production, both for the brine and the ore pathway. It could be lowered reducing the distances that the

compounds travel to be processed, refining the minerals close to the mine site, as it has been demonstrated. Moreover, processing a raw material in the same country where the resource is extracted would allow the country to export a higher market value product, generating a higher GDP, creating jobs for local communities, and a fair extraction of natural resources.

However, it is worth to mention that the highest rate of carbon emissions is related to the production process of lithium compound. According to literature, lithium products produced from brine have a lower carbon footprint with respect to the ones obtained from ore. This is due to the less energy intensity process that takes place in Salar de Atacama which uses solar radiation to concentrate the brine. Moreover, the production of lithium compounds from concentrated spodumene takes place in China and is performed using fossil fuels, which have a higher carbon footprint respect to the Chilean electricity grid. Therefore, more needs to be done to lower the amount of carbon emitted to make the carbon footprint of lithium products as lower as possible.

7 Conclusions

In this study, the integration of Remote Sensing and GIS-based approach to analyse lithium mining activities and its related environmental impacts have been performed. The two main way of extraction from brine and from ore have been analysed, considering the most relevant mine sites for both pathways: the Salar de Atacama in Chile and the Greenbushes mine in Western Australia. The area disturbed by the mine activities has been evaluated using satellite images, through Remote Sensing methods and GIS tools. Among all the indices used to extract the mine area in Chile, the MNDWI computed with the SWIR shows the highest accuracy, followed by the NDVI. The latter has been used to perform a multitemporal evaluation of the mining area every five years since 1992. NDVI has been chosen because of the availability of red and near infrared bands in almost every remote sensing data product, thus allowing a general proposal for the evaluation on the environmental impact of mining on the land use. The area estimated has been implemented in the calculation of an indicator called Land Use Intensity (LUI): this analysis has shown the high variability of the results according to the allocation methods chosen, underlining the need to develop common criteria to assess the land disturbed by mining. A shared methodology would allow results to be comparable between different commodities, extraction and production processes, and contexts. However, it has not been possible to detect and attribute atmospheric emissions to the mining activity since the resolution of the Sentinel-5P data product is not high enough, underlining the need to develop high-resolution sensors. Land and sea routes have been studied and identified; then, kilometres travelled by trucks and vessels have been quantified using geomatics tools. Data about transport have been integrated in the Life Cycle Assessment analysis, which showed how the transportation emissions in lithium production do not represent a large share of the total carbon emissions. However, shortening the routes of the supply chain can be a solution for the future development of lithium production.

The results of this study represent only an example of the research that can be carried out in the field of mining activity with a geomatic approach. The rising demand of minerals for the energy transition and the population increase are generating the expansion of mining all over the world, but especially in natural resources rich countries. The decoupling of economic growth from the raw material extraction is one of the objectives set by the 2030 Agenda for Sustainable Development. However, future projection shows that the increasing trend of mining activity will not change in the next years. Therefore, it is necessary to support this process through policies and regulations to perform mining in a sustainable way. More studies analysing local environmental and social impacts are needed to give reliable information and instruments to policymakers, decision makers of the

mining industry and all the stakeholders. A multidisciplinary approach using Remotes Sensing and GIS tools represent a powerful instrument in the research field to give the opportunity to better understand the mining field, studying the effects at the local and global level and retrieving quantitative information about the supply chain of critical commodities.

References

- Babidge, S., & Bolados, P. (2018). Neextractivism and Indigenous Water Ritual in Salar de Atacama, Chile. *Latin American Perspectives*, 45(5), 170–185. <https://doi.org/10.1177/0094582X18782673>
- Bleischwitz, R., Spataru, C., VanDeveer, S. D., Obersteiner, M., van der Voet, E., Johnson, C., Andrews-Speed, P., Boersma, T., Hoff, H., & van Vuuren, D. P. (2018). Resource nexus perspectives towards the United Nations Sustainable Development Goals. *Nature Sustainability*, 1(12), 737–743. <https://doi.org/10.1038/s41893-018-0173-2>
- Charou, E., Stefouli, M., Dimitrakopoulos, D., Vasiliou, E., & Mavrantza, O. D. (2010). Using Remote Sensing to Assess Impact of Mining Activities on Land and Water Resources. *Mine Water and the Environment*, 29(1), 45–52. <https://doi.org/10.1007/s10230-010-0098-0>
- European Commission (2020). Study on the EU's list of Critical Raw Materials (2020), Factsheets on Critical Raw Materials. <https://op.europa.eu/en/publication-detail/-/publication/ff34ea21-ee55-11ea-991b-01aa75ed71a1/language-en>
- Gajardo, G., & Redón, S. (2019). Andean hypersaline lakes in the Atacama Desert , northern Chile: Between lithium exploitation and unique biodiversity conservation. *Conservation Science and Practice*, 1(9). <https://doi.org/10.1111/csp2.94>
- Gao, B. (1996). NDWI—A normalized difference water index for remote sensing of vegetation liquid water from space. *Remote Sensing of Environment*, 58(3), 257–266. [https://doi.org/10.1016/S0034-4257\(96\)00067-3](https://doi.org/10.1016/S0034-4257(96)00067-3)
- IEA (2021), The Role of Critical Minerals in Clean Energy Transitions, IEA, Paris <https://www.iea.org/reports/the-role-of-critical-minerals-in-clean-energy-transitions>
- Kaunda, R. B. (2020). Potential environmental impacts of lithium mining. *Journal of Energy & Natural Resources Law*, 38(3), 237–244. <https://doi.org/10.1080/02646811.2020.1754596>
- IGO (2022) Quarterly Report. Period Ended 31st March 2022. <https://www.igo.com.au/site/PDF/d57bab33-2b5c-4443-999a-82a370865820/March2022QuarterlyActivitiesReport>
- Torres De Matos, C., Ciacci, L., Godoy Leon, M.F., Lundhaug, M., Dewulf, J., Müller, D.B., Georgitzikis, K., Wittmer, D. and Mathieux, F., European Commission, & Joint Research Centre. (2020). Material system analysis of five battery-related raw materials: Cobalt, lithium, manganese, natural graphite, nickel. https://op.europa.eu/publication/manifestation_identifier/PUB_KJNA30103ENN

- Kelly, J. C., Wang, M., Dai, Q., & Winjobi, O. (2021). Energy, greenhouse gas, and water life cycle analysis of lithium carbonate and lithium hydroxide monohydrate from brine and ore resources and their use in lithium ion battery cathodes and lithium ion batteries. *Resources, Conservation and Recycling*, 174, 105762. <https://doi.org/10.1016/j.resconrec.2021.105762>
- Liu, W., Agusdinata, D. B., & Myint, S. W. (2019). Spatiotemporal patterns of lithium mining and environmental degradation in the Atacama Salt Flat, Chile. *International Journal of Applied Earth Observation and Geoinformation*, 80, 145–156. <https://doi.org/10.1016/j.jag.2019.04.016>
- Liu, W., & Agusdinata, D. B. (2020). Interdependencies of lithium mining and communities sustainability in Salar de Atacama, Chile. *Journal of Cleaner Production*, 260, 120838. <https://doi.org/10.1016/j.jclepro.2020.120838>
- Marazuela, M. A., Vázquez-Suñé, E., Ayora, C., García-Gil, A., & Palma, T. (2019). Hydrodynamics of salt flat basins: The Salar de Atacama example. *Science of The Total Environment*, 651, 668–683. <https://doi.org/10.1016/j.scitotenv.2018.09.190>
- Marazuela, M. A., Vázquez-Suñé, E., Ayora, C., & García-Gil, A. (2020). Towards more sustainable brine extraction in salt flats: Learning from the Salar de Atacama. *Science of The Total Environment*, 703, 135605. <https://doi.org/10.1016/j.scitotenv.2019.135605>
- McFeeters, S.K. (1996) The Use of the Normalized Difference Water Index (NDWI) in the Delineation of Open Water Features. *International Journal of Remote Sensing*, 17, 1425-1432. <http://dx.doi.org/10.1080/01431169608948714>
- Meng, F., McNeice, J., Zadeh, S. S., & Ghahreman, A. (2021). Review of Lithium Production and Recovery from Minerals, Brines, and Lithium-Ion Batteries. *Mineral Processing and Extractive Metallurgy Review*, 42(2), 123–141. <https://doi.org/10.1080/08827508.2019.1668387>
- Murguía, D.I. and Bringezu, S. (2016). Measuring the specific land requirements of large-scale metal mines for iron, bauxite, copper, gold and silver, *Progress in Industrial Ecology – An International Journal*, Vol. 10, Nos. 2/3, pp.264–285.
- Organization for Economic Cooperation and Development (OECD). (2019). *Global Material Resources Outlook to 2060. Economic drivers and environmental consequences*, OECD Publishing, Paris. <https://www.oecd.org/publications/global-material-resources-outlook-to-2060-9789264307452-en.htm>

Pálsdóttir, A., Alabi, C. A., Thompson, J. F. H., and Tester, J. W. (2020). Valorization of Geothermal Waters: The Development and Testing of a Supercritical Fluid Extraction Process for the Recovery of Lithium. Proceedings World Geothermal Congress 2020. Reykjavik, Iceland.

Rudke, A. P., Sikora de Souza, V. A., Santos, A. M. dos, Freitas Xavier, A. C., Rotunno Filho, O. C., & Martins, J. A. (2020). Impact of mining activities on areas of environmental protection in the southwest of the Amazon: A GIS- and remote sensing-based assessment. *Journal of Environmental Management*, 263, 110392. <https://doi.org/10.1016/j.jenvman.2020.110392>

SQM (2021) Sustainability of lithium production in Chile. How SQM organizes the extraction of the coveted raw material of Electromobility ecologically and socially. https://download.crossrelations.de/SQM_SustainableLithium_Eng.pdf

SQM (2022) Technical Report Summary. Operation Report. Salar de Atacama. <https://ir.sqm.com/English/news/news-details/2022/SQM-Files-Technical-Report-Summaries/default.aspx>

Tabelin, C. B., Dallas, J., Casanova, S., Pelech, T., Bournival, G., Saydam, S., and Canbulat, I. (2021). Towards a low-carbon society: A review of lithium resource availability, challenges and innovations in mining, extraction and recycling, and future perspectives. *Minerals Engineering*, 163, 106743. <https://doi.org/10.1016/j.mineng.2020.106743>

Talison Lithium (2019) Greenbushes Lithium Mine Expansion. Mining Proposal Surface Water Assessment. <https://www.epa.wa.gov.au/proposals/greenbushes-lithium-mine-expansion>

Thiel, G. P., & Stark, A. K. (2021). To decarbonize industry, we must decarbonize heat. *Joule*, 5(3), 531–550. <https://doi.org/10.1016/j.joule.2020.12.007>

Tost, M., Bayer, B., Hitch, M., Lutter, S., Moser, P., & Feiel, S. (2018). Metal Mining's Environmental Pressures: A Review and Updated Estimates on CO₂ Emissions, Water Use, and Land Requirements. *Sustainability*, 10(8), 2881. <https://doi.org/10.3390/su10082881>

USGS (2021) Lithium Statistics and Information. National Minerals Information Center. <https://pubs.usgs.gov/periodicals/mcs2021/mcs2021-lithium.pdf>

USGS (2022) Lithium Statistics and Information. National Minerals Information Center. <https://pubs.usgs.gov/periodicals/mcs2022/mcs2022-lithium.pdf>

Xu, H. (2006). Modification of normalised difference water index (NDWI) to enhance open water features in remotely sensed imagery. *International Journal of Remote Sensing*, 27(14), 3025–3033. <https://doi.org/10.1080/01431160600589179>

Wang, P., Wang, H., Chen, W.-Q., & Pauliuk, S. (2022). Carbon neutrality needs a circular metal-energy nexus. *Fundamental Research*, 2(3), 392–395. <https://doi.org/10.1016/j.fmre.2022.02.003>

World Bank Group (2020). Minerals for Climate Action: The Mineral Intensity of the Clean Energy Transition. <https://pubdocs.worldbank.org/en/961711588875536384/Minerals-for-Climate-Action-The-Mineral-Intensity-of-the-Clean-Energy-Transition.pdf>

World Bank Group (2022). Commodity Markets Outlook: The Impact of the War in Ukraine on Commodity Markets, April 2022. World Bank, Washington, DC. License: Creative Commons Attribution CC BY 3.0 IGO. <https://openknowledge.worldbank.org/handle/10986/37223>

Websites

ABC News, 6th February 2022. <https://www.abc.net.au/news/2022-02-06/bridgetown-and-denmark-bushfire-update/100808380>

Copernicus Open Access Hub - ESA, <https://scihub.copernicus.eu/dhus/#/home>

Earth Explorer – USGS, <https://earthexplorer.usgs.gov/>

Eurostat, https://ec.europa.eu/eurostat/databrowser/view/cei_srm010/default/table?lang=en, accessed on the 31st of May 2022

GlobeLand30, http://www.globallandcover.com/defaults_en.html?src=/Scripts/map/defaults/En/download_en.html&head=download&type=data

Reuters, 18th of June 2022. <https://www.reuters.com/markets/commodities/bolivia-delays-decision-lithium-mining-tie-ups-december-2022-06-17/>

The London Metal Exchange - an HKEX Company, <https://www.lme.com/en/Metals/EV/LME-Lithium-Hydroxide-CIF-Fastmarkets-MB#Price+graph>, accessed on the 5th of May 2022

Trading Economics, <https://tradingeconomics.com/commodity/lithium>, accessed on the 5th of May 2022

The European Space Agency, 14th December 2020. Mapping high-resolution methane emissions from space. https://www.esa.int/Applications/Observing_the_Earth/Copernicus/Sentinel-5P/Mapping_high-resolution_methane_emissions_from_space

Appendix

I. Indices Analysis for evaporation ponds area extraction in Chile

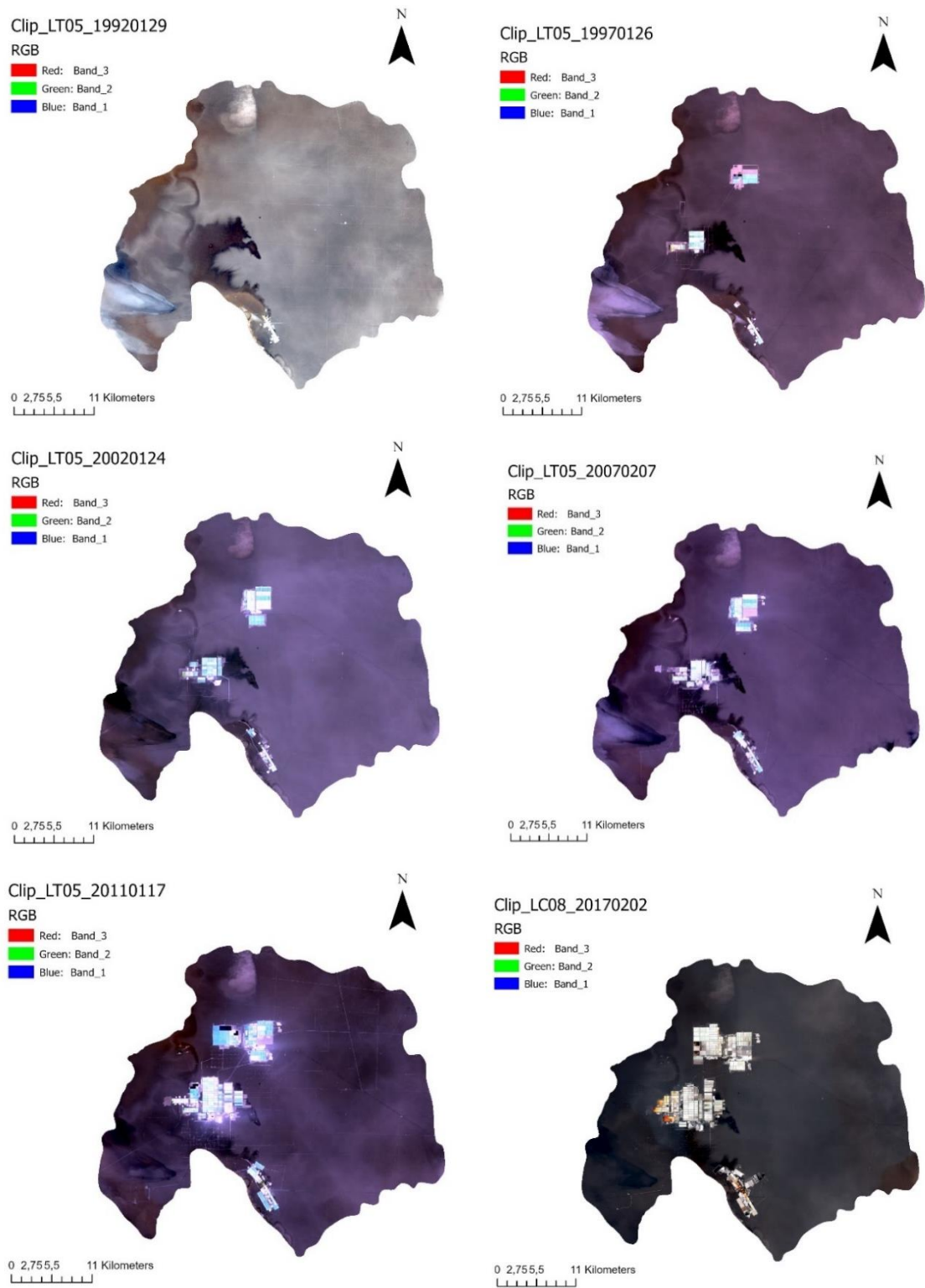


Figure 35. True Color Images of the processed satellite images showing the Salar de Atacama during the years.

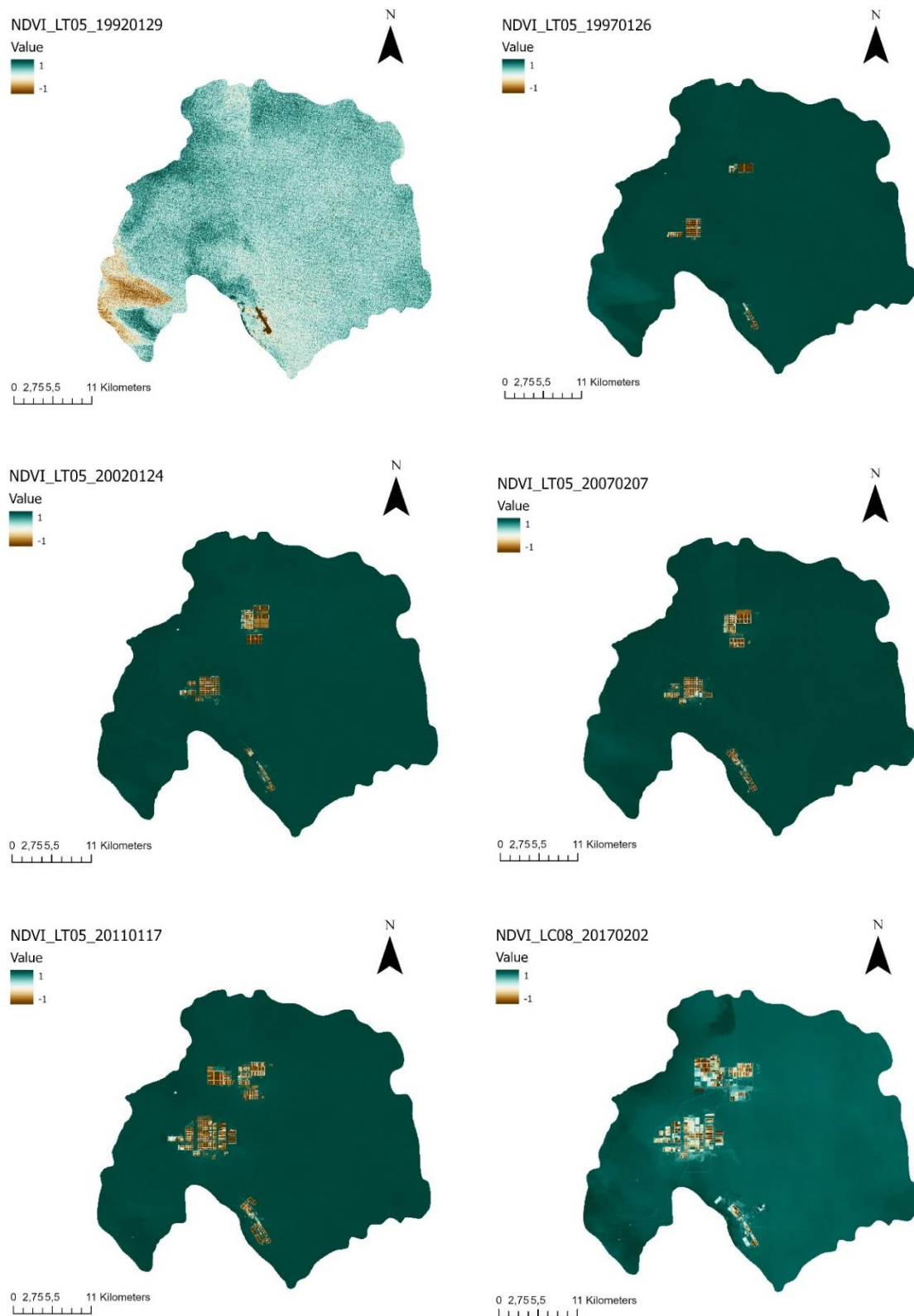


Figure 36. NDVI image computed for each year considered in the analysis.

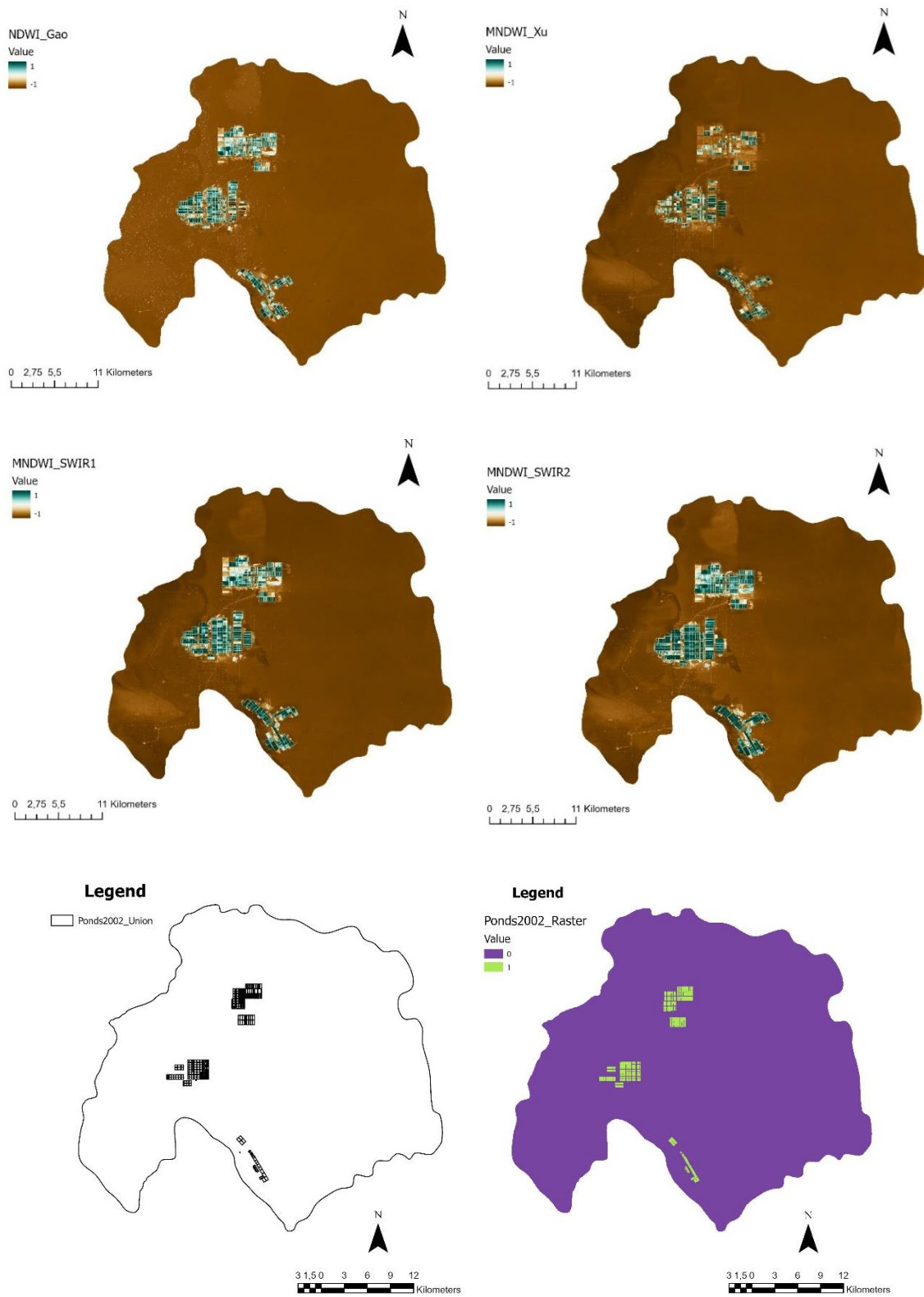


Figure 37. Indices image (NDWI, MNDWI, ...) computed for the satellite image related to the year 2022. The two bottom images show the ground truth data (left) and the binary image (right) for the year 2022.

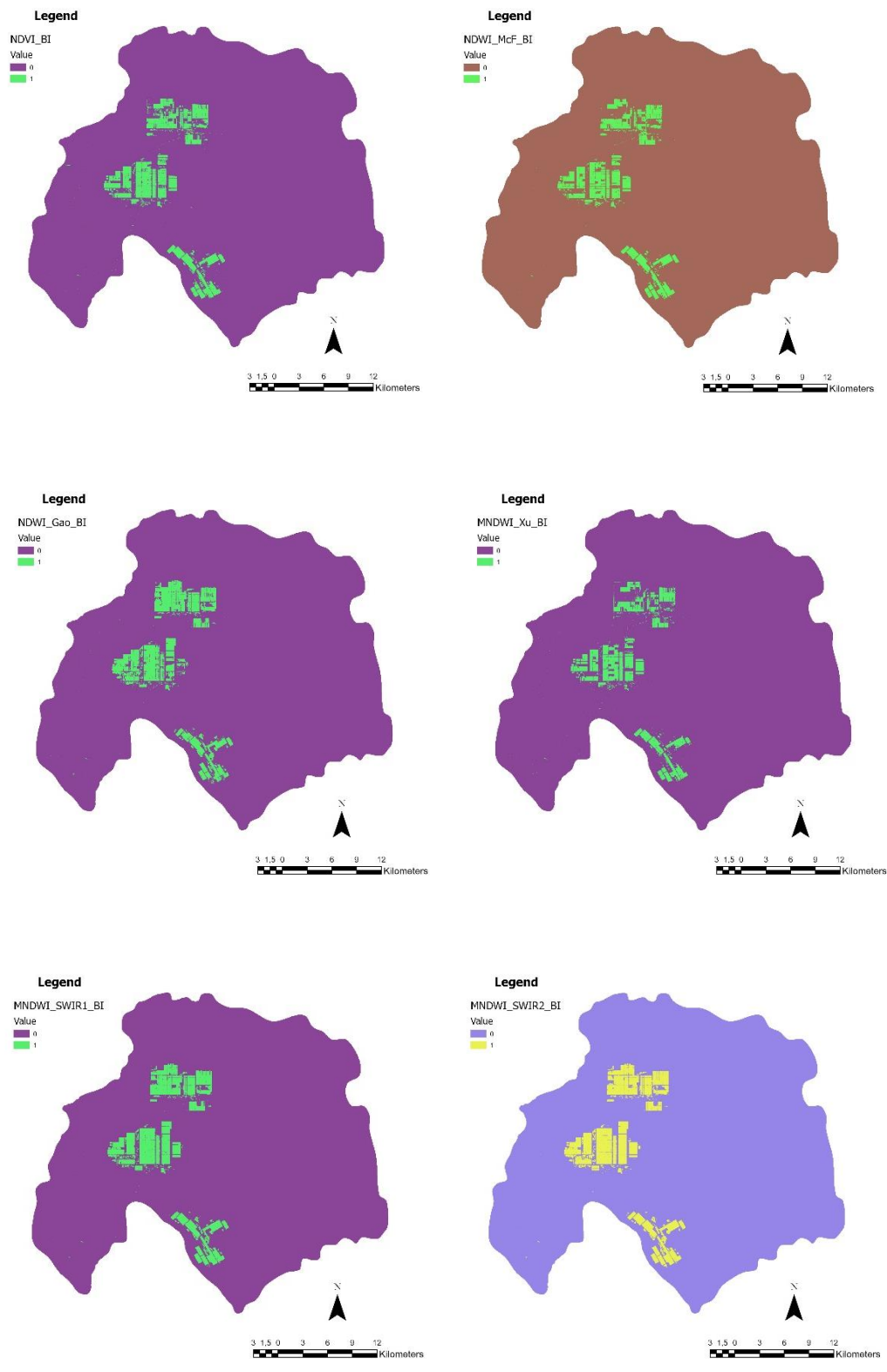


Figure 38. Binary images (0,1) for all the indices considered (NDVI, NDWI, MNDWI, ...) for the analysis of the satellite image relative to the year 2022.

Table 13. Confusion matrix relative to the NDWI (McFeeters) analysis.

ClassValue	C_0	C_1	Total	User's Accuracy	Kappa Coefficient
C_0	18852	264	19116	0,986	0
C_1	172	712	884	0,805	0
Total	19024	976	20000	0	0
Producer's Accuracy	0,991	0,729	0	0,978	0
Kappa Coefficient	0	0	0	0	0,75

Table 14. Confusion matrix relative to the NDWI (Gao) analysis.

ClassValue	C_0	C_1	Total	User's Accuracy	Kappa Coefficient
C_0	18812	151	18963	0,992	0
C_1	214	823	1037	0,794	0
Total	19026	974	20000	0	0
Producer's Accuracy	0,989	0,845	0	0,982	0
Kappa Coefficient	0	0	0	0	0,809

Table 15. Confusion matrix relative to the MNDWI (Xu) analysis.

ClassValue	C_0	C_1	Total	User's Accuracy	Kappa Coefficient
C_0	18850	295	19145	0,985	0
C_1	96	759	855	0,888	0
Total	18946	1054	20000	0	0
Producer's Accuracy	0,995	0,720	0	0,980	0
Kappa Coefficient	0	0	0	0	0,785

Table 16. Confusion matrix relative to the MNDWI (SWIR1) analysis.

ClassValue	C_0	C_1	Total	User's Accuracy	Kappa Coefficient
C_0	18788	80	18868	0,996	0
C_1	219	913	1132	0,806	0
Total	19007	993	20000	0	0
Producer's Accuracy	0,988	0,919	0	0,985	0
Kappa Coefficient	0	0	0	0	0,851

Table 17. Confusion matrix relative to the MNDWI (SWIR2) analysis.

ClassValue	C_0	C_1	Total	User's Accuracy	Kappa Coefficient
C_0	94066	361	94427	0,996	0
C_1	1216	4357	5573	0,782	0
Total	95282	4718	100000	0	0
Producer's Accuracy	0,987	0,923	0	0,984	0
Kappa Coefficient	0	0	0	0	0,838

II. Transportation Routes Analysis

The network analysis has been carried out using information and making assumptions on the kinds of trucks used to transport the material from the Salar de Atacama to the processing plants in Antofagasta and then to the port. After the water evaporates from the ponds, the concentrated solution of lithium chloride is transported from Salar de Atacama to Antofagasta by means of tanker trucks. The trucks have length of approximately of 11 m, height of 3 m and width of 2.5 m. For the analysis, ISO-compliant dimensions which are the ones of Front axle weight (FAW) tankers trucks have been used: length of 39.03 feet (11.89 m), width of 8.2 feet (2.5 m) and depth of 11.15 feet (3.39 m). These tanker trucks typically have a tank volume between 396 gallons (1499 L) and 792 gallons (2998 L).

The truck route analysis carried out to estimate the average km travelled from the Salar de Atacama to Antofagasta has been performed in ArcGIS Pro, considering the height, width, and length of the trucks. In Figure 39, the Travel Mode Restrictions are shown. They have been set before the Network Analysis has been performed.

In both the processing plants owned by the SQM and Albemarle company, lithium compounds are stored in jumbo bags of different weights. Then, each bag is labelled to be identified along all the transport process. Then, the different lithium products contained in the jumbo bags are stored into container trucks, ready to be transported to the port where the lithium compounds are shipped worldwide. Some of the trucks used by SQM are owned by Hapag-Lloyd company, that is a German international shipping and container transportation company. On the Hapag-Lloyd website, information about the dimensions of the containers used to carry lithium bags have been retrieved. The dimensions of these container trucks have been used to assume the dimensions of the trucks and to set the parameters for the Route Network Analysis in ArcGIS Pro.

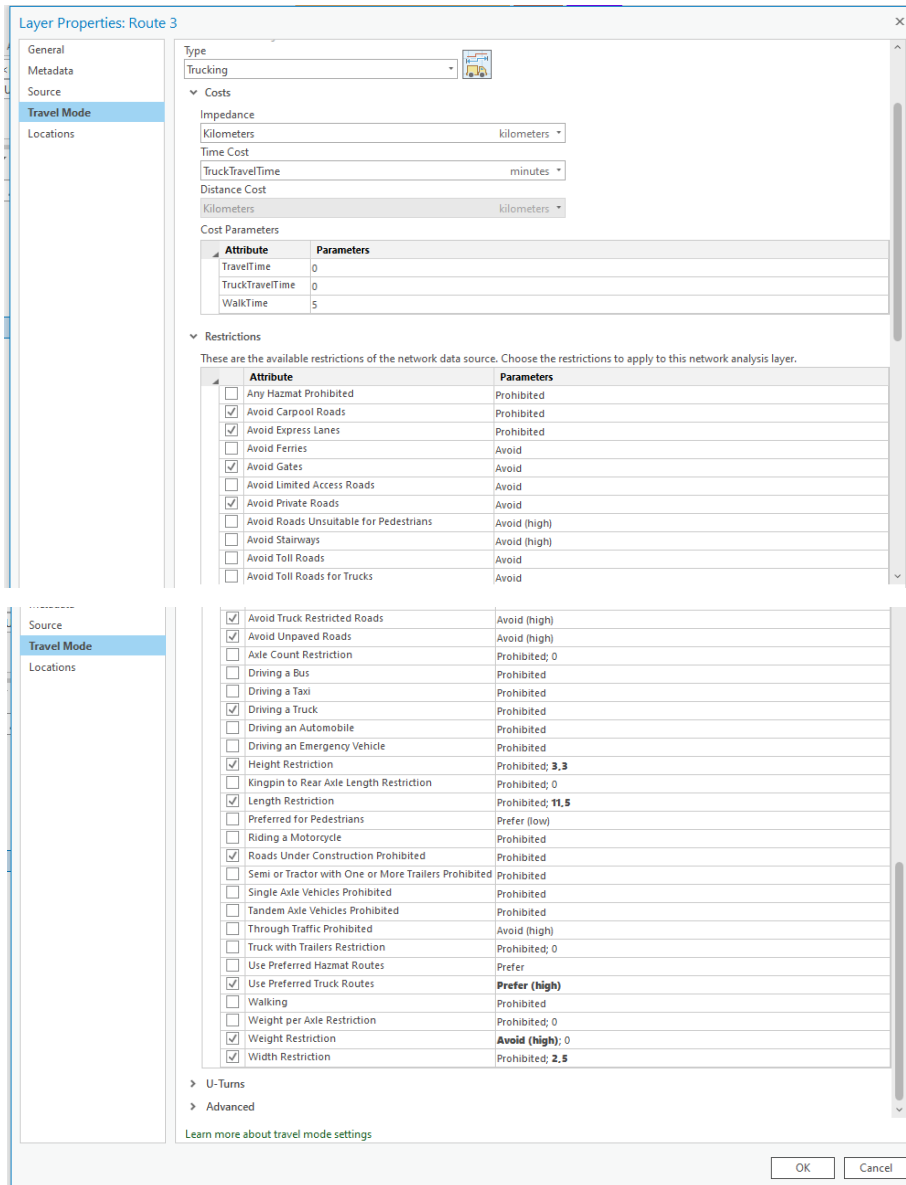


Figure 39. Travel Mode properties and Restriction settings related to the trucks transportation route analysis computed in ArcGIS Pro.

III. Environmental impact assessment of lithium mining on land

Brine – Salar de Atacama, Chile

According to the results of the indices analysis performed in ArcGIS Pro, the total area occupied by the evaporation ponds in 2022 has been estimated at 53.43 km². The latter refers to both the mine operations in the area owned by the SQM and Albemarle companies. Evaporation ponds owned by SQM are located in the central and northern part of the Salar de Atacama, as shown in Figure 40. According to the satellite image analysis, SQM evaporation ponds cover around 42.07 km².

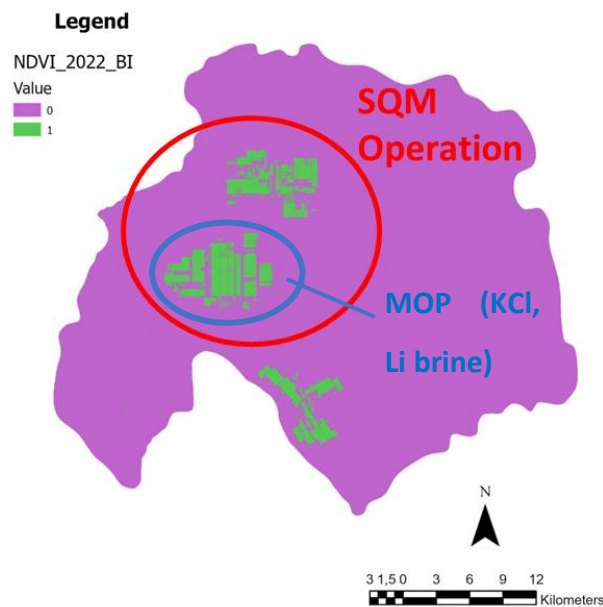


Figure 40. Binary Image obtained through the NDVI analysis showing the Salar de Atacama area, identifying the SQM operations (red circle) and the lithium evaporation ponds section (blue circle).

According to SQM data, in total, roughly 39 million m³ of brine is pumped to the surface annually for the production of concentrated lithium brine and potash. The area related to both is:

$$SQM \text{ Total Evaporation Ponds Area} = 42,071,100 \text{ m}^2$$

Approximately 60% of the brine is used to produce lithium, and the remainder is used to produce potash (40%). Lithium brine is produced in the MOP (muriate of potash) section, located in the southern part of SQM operation, as shown in Figure 40. In the MOP area, also potassium chloride (KCl) process takes place. Instead, the northern part of SQM operation, is called SOP (sulphate of potash) section, where both potassium sulphate (K₂SO₄) and potassium chloride (KCl) are produced. According to the satellite image analysis, the evaporation ponds area related to lithium production is equal to:

$$MOP \text{ Evaporation Ponds Area} = 24,212,600 \text{ m}^2$$

According to the Technical Report Summary published by SQM and related to Salar de Atacama mine operations, the annual production capacity of the lithium carbonate plant at the Salar del Carmen is around 120,000 metric tonnes per year. SQM is increasing the production capacity to 180,000 metric tonnes per year. Instead, the lithium hydroxide facility has a production capacity of 21,500 metric tonnes per year and SQM is increasing this production capacity to 30,000 metric tonnes per year. Considering the production capacity and basing on the satellite images analysed acquired in 2022, the following analysis has been carried out.

In Figure 41, the mass required for the SQM process are shown (Kelly et al., 2021). To produce 1 ton of brine at 6% concentration of lithium chloride, SQM needs to extract 24.1 tons of brine from the underground (0.17% lithium concentration). Moreover, each ton of brine (6% concentration) produce 8.52 ton of potash as coproduct. To produce 1 ton of lithium carbonate, 4 tons of concentrated brine (6%) are needed, resulting in 34.08 tons of potash as coproduct. Instead, to produce 1 ton of lithium hydroxide, which is obtained by further processing of lithium carbonate, 1.05 tons of the latter are needed, resulting in 35.78 ton of potash as coproduct.

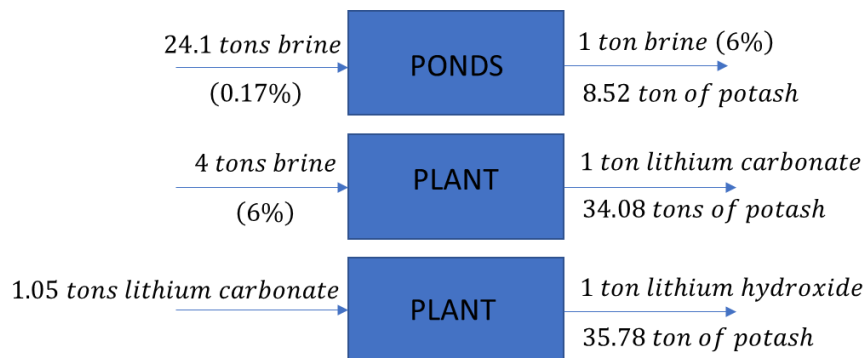


Figure 41. Flow chart showing the different mass required to produce 1 ton of lithium carbonate and lithium hydroxide, starting from the mass of the extracted brine from the Salar de Atacama.

Therefore, to produce 120 kiloton of lithium carbonate per year, as projected by the SQM Technical Report, the brine mass needed to be extracted from the underground and the potash coproduced in 2022 is equal to:

$$120 \text{ ktpy of Lithium Carbonate} \rightarrow 11,568,000 \text{ tons of brine (0.17\%)}$$

$$120 \text{ ktpy of Lithium Carbonate} \rightarrow 4,089,600 \text{ tons of potash as coproduct}$$

Instead, to produce 21.5 kiloton of lithium hydroxide per year, the mass of brine required, and the potash coproduced is:

$$21.5 \text{ ktpy of Lithium Hydroxide} \rightarrow 2,176,230 \text{ tons of brine (0.17\%)}$$

21.5 ktpy of Lithium Hydroxide → 769,260 tons of potash as coproduct

The lithium carbonate production over the total lithium production is equal to:

$$\text{Lithium Carbonate: } \frac{11,568,000 \text{ tons of brine}}{11,568,000 \text{ tons} + 2,176,230 \text{ tons of brine}} = 0,842 \rightarrow 84.2\%$$

Therefore, the lithium hydroxide one is equal to:

$$\text{Lithium Hydroxide: } \frac{2,176,230 \text{ tons of brine}}{11,568,000 \text{ tons} + 2,176,230 \text{ tons of brine}} = 0,158 \rightarrow 15.8\%$$

The computed factors are based on the mass of brine required to produce a certain amount of product and on the capacity production. Therefore, the following land use allocation also consider the current market demand and the company's refining infrastructure. Lithium hydroxide is produced with further refinement of lithium carbonate; therefore, the starting point for both lithium products is the concentrate brine (6%). The land used respectively for lithium carbonate production and lithium hydroxide production has been assigned according to the previous computed production factors:

$$A_{Li_2CO_3} = 0,842 \cdot 24,212,600 \text{ m}^2 = 20,387,009 \text{ m}^2$$

$$A_{LiOH} = 0.158 \cdot 24,212,600 \text{ m}^2 = 3,825,591 \text{ m}^2$$

Then, the land use intensity expressed in squared meters of land used per tonne of lithium produced has been computed:

$$\text{Land Use Intensity (LUI)} \frac{\text{m}^2}{\text{ton}} = \frac{\text{Lithium Evaporation Ponds Area (2022)}}{\text{Annual Production (2022)}}$$

$$LUI_{Li_2CO_3} = \frac{20,387,009 \text{ m}^2}{120 \cdot 10^3 \text{ tons}} = 169.9 \frac{\text{m}^2}{\text{ton}}$$

$$LUI_{LiOH} = \frac{3,825,591 \text{ m}^2}{21.5 \cdot 10^3 \text{ tons}} = 177.9 \frac{\text{m}^2}{\text{ton}}$$

Through a mass allocation method, the total land use associated respectively with lithium production and potash production are split among the outputs based on their mass shares of the total output.

$$A_j = \frac{j - \text{mass}}{\text{total mass}} \cdot A_{tot} = \frac{m_j}{\sum m_i} \cdot A_{tot}$$

In this case, the coefficient has been computed for both lithium carbonate and lithium hydroxide:

$$\text{Lithium Carbonate: } \frac{1 \text{ ton}}{1 \text{ ton} + 34.08 \text{ ton}} = 0.029$$

$$\text{Potash (Li}_2\text{CO}_3 \text{ production): } \frac{34.08 \text{ ton}}{1 \text{ ton} + 34.08 \text{ ton}} = 0.971$$

$$\text{Lithium Hydroxide: } \frac{1 \text{ ton}}{1 \text{ ton} + 35.78 \text{ ton}} = 0.027$$

$$\text{Potash (LiOH production): } \frac{35.78 \text{ ton}}{1 \text{ ton} + 35.78 \text{ ton}} = 0.973$$

Then, the land use intensity has been computed as:

$$\text{Land Use Intensity (LUI) } \frac{\text{m}^2}{\text{ton}} = \frac{\text{Allocation mass coefficient} \cdot \text{Evaporation Ponds Area (2022)}}{\text{Annual Production (2022)}}$$

$$LUI_{\text{Li}_2\text{CO}_3} = \frac{0.029 \cdot 20,387,009 \text{ m}^2}{120 \cdot 10^3 \text{ tons}} = \frac{591,223 \text{ m}^2}{120 \cdot 10^3 \text{ tons}} = 4.93 \frac{\text{m}^2}{\text{ton}}$$

$$LUI_{\text{Potash, Li}_2\text{CO}_3} = \frac{0.971 \cdot 20,387,009 \text{ m}^2}{4,089,600 \text{ tons of potash}} = \frac{19,795,786 \text{ m}^2}{4,089,600 \text{ tons}} = 4.84 \frac{\text{m}^2}{\text{ton}}$$

$$LUI_{\text{LiOH}} = \frac{0.027 \cdot 3,825,591 \text{ m}^2}{21.5 \cdot 10^3 \text{ tons}} = \frac{103,291 \text{ m}^2}{21.5 \cdot 10^3 \text{ tons}} = 4.80 \frac{\text{m}^2}{\text{ton}}$$

$$LUI_{\text{Potash, LiOH}} = \frac{0.973 \cdot 3,825,591 \text{ m}^2}{769,260 \text{ tons of potash}} = \frac{3,722,300 \text{ m}^2}{769,260 \text{ tons of potash}} = 4.84 \frac{\text{m}^2}{\text{ton}}$$

However, potash products and lithium products have different economic value. Therefore, economic allocation has been carried out to detect how the land use intensity would change according to the market price of the products.

Economic value allocation assigns the land used for the production process based on the economic value of the products of a process. The total area, A_{tot} , has been allocated to the different outputs based on the ratio of the single j -product value to the total system's output value. Single product value is the product's mass, m_j , and the per-mass value (market price) of product v_j . The total value is the sum of the product of mass and per-mass value of all other system outputs:

$$A_j = \frac{j \text{ - product value}}{\text{total value}} = \frac{m_j \cdot v_j}{\sum m_i \cdot v_i} \cdot A_{tot}$$

At the time of writing, lithium carbonate price has soared to 69,906 \$USD/ton (Trading Economics, 2022) and lithium hydroxide to 81,500 \$USD/ton (The London Metal Exchange, 2022). Prices has been increasing through the last period, because of the high demand of lithium compounds for EV's

batteries. SQM refines potash brine to obtain two different value products: potassium chloride KCl and potassium sulphate K_2SO_4 , which currently have a value of 562.5 USD/ton and 755.4 USD/ton respectively. These potash compounds are used for fertilizers production all around the world. In the last month their price has soared because of the sanctions that EU has imposed on imports from Belarus and Russia, important suppliers of fertilizers (World Bank Group, 2022). It is worth to mention that price volatility of minerals is high; therefore, the scenario presented in this analysis could change rapidly in the next years.

To perform the economic allocation, only KCl has been considered because it is the coproduct obtained in the MOP section, which is the one linked to lithium production:

$$\text{potassium chloride value} = 562.5 \text{ USD/ton}$$

Then, lithium carbonate economic coefficient for the allocation process has been computed:

$$\begin{aligned} \text{Lithium Carbonate: } & \frac{\text{Li}_2\text{CO}_3 \text{ value}}{\text{Li}_2\text{CO}_3 \text{ value} + \text{KCl value}} = \frac{m_{\text{Li}_2\text{CO}_3} \cdot v_{\text{Li}_2\text{CO}_3}}{m_{\text{Li}_2\text{CO}_3} \cdot v_{\text{Li}_2\text{CO}_3} + m_{\text{KCl}} \cdot v_{\text{KCl}}} = \\ & = \frac{1 \text{ ton Li}_2\text{CO}_3 \cdot 69,906 \frac{\$}{\text{ton}} \text{Li}_2\text{CO}_3}{1 \text{ ton Li}_2\text{CO}_3 \cdot 69,906 \frac{\$}{\text{ton}} + 34.08 \text{ ton KCl} \cdot 562.5 \frac{\$}{\text{ton}} \text{KCl}} = 0.785 \end{aligned}$$

Also, potassium chloride economic coefficient for the allocation process has been computed for the lithium carbonate production process analysis:

$$\begin{aligned} \text{Potassium Chloride (Li}_2\text{CO}_3 \text{ prod): } & \frac{\text{KCl value}}{\text{Li}_2\text{CO}_3 \text{ value} + \text{KCl value}} \\ & = \frac{m_{\text{KCl}} \cdot v_{\text{KCl}}}{m_{\text{Li}_2\text{CO}_3} \cdot v_{\text{Li}_2\text{CO}_3} + m_{\text{KCl}} \cdot v_{\text{KCl}}} \\ & = \frac{34.08 \text{ ton KCl} \cdot 562.5 \frac{\$}{\text{ton}} \text{KCl}}{1 \text{ ton Li}_2\text{CO}_3 \cdot 69,906 \frac{\$}{\text{ton}} + 34.08 \text{ ton KCl} \cdot 562.5 \frac{\$}{\text{ton}} \text{KCl}} = 0.215 \end{aligned}$$

Moreover, lithium hydroxide economic coefficient for the allocation process has been computed:

$$\begin{aligned} \text{Lithium Hydroxide: } & \frac{\text{LiOH value}}{\text{LiOH value} + \text{KCl value}} = \frac{m_{\text{LiOH}} \cdot v_{\text{LiOH}}}{m_{\text{LiOH}} \cdot v_{\text{LiOH}} + m_{\text{KCl}} \cdot v_{\text{KCl}}} = \\ & = \frac{1 \text{ ton LiOH} \cdot 81,500 \frac{\$}{\text{ton}} \text{LiOH}}{1 \text{ ton LiOH} \cdot 81,500 \frac{\$}{\text{ton}} + 35.78 \text{ ton KCl} \cdot 562.5 \frac{\$}{\text{ton}} \text{KCl}} = 0.802 \end{aligned}$$

Also, potassium chloride economic coefficient for the allocation process has been computed for the lithium hydroxide production process analysis:

$$\begin{aligned} \text{Potassium Chloride (LiOH prod.):} & \frac{KCl \text{ value}}{LiOH \text{ value} + KCl \text{ value}} = \frac{m_{KCl} \cdot v_{KCl}}{m_{LiOH} \cdot v_{LiOH} + m_{KCl} \cdot v_{KCl}} = \\ & = \frac{35.78 \text{ ton KCl} \cdot 562.5 \frac{\$}{\text{ton}} KCl}{1 \text{ ton LiOH} \cdot 81,500 \frac{\$}{\text{ton}} + 35.78 \text{ ton KCl} \cdot 562.5 \frac{\$}{\text{ton}} KCl} = 0.198 \end{aligned}$$

Then, land use intensity has been computed for lithium carbonate, lithium hydroxide, and for potassium chloride:

$$\begin{aligned} \text{Land Use Intensity (LUI)} & \frac{m^2}{\text{ton}} \\ & = \frac{\text{Allocation value coefficient} \cdot \text{Evaporation Ponds Area (2022)}}{\text{Annual Production (2022)}} \end{aligned}$$

$$LUI_{Li_2CO_3} = \frac{0.785 \cdot 20,387,009 \text{ m}^2}{120 \cdot 10^3 \text{ tons}} = \frac{16,003,802 \text{ m}^2}{120 \cdot 10^3 \text{ tons}} = 133.4 \frac{\text{m}^2}{\text{ton}}$$

$$LUI_{KCl, Li_2CO_3} = \frac{0.215 \cdot 20,387,009 \text{ m}^2}{4,089,600 \text{ tons}} = \frac{4,383,207 \text{ m}^2}{4,089,600 \text{ tons}} = 1.07 \frac{\text{m}^2}{\text{ton}}$$

$$LUI_{LiOH} = \frac{0.802 \cdot 3,825,591 \text{ m}^2}{21.5 \cdot 10^3 \text{ tons}} = \frac{3,068,124 \text{ m}^2}{21.5 \cdot 10^3 \text{ tons}} = 142.7 \frac{\text{m}^2}{\text{ton}}$$

$$LUI_{KCl, LiOH} = \frac{0.198 \cdot 3,825,591 \text{ m}^2}{769,260 \text{ tons}} = \frac{757,467 \text{ m}^2}{769,260 \text{ tons}} = 0.98 \frac{\text{m}^2}{\text{ton}}$$

All the previous results are summarised in the Table 12 in Chapter 6.5.

Hard Rock – Greenbushes, Western Australia

According to the Quarterly Report published by IGO Ltd. for the period ended on the 31st of March 2022, total spodumene concentrate production was 270,464 tons, up 5% respect to the previous quarter. This value includes both technical grade and chemical grade spodumene concentrate produced from Greenbushes mine. The first quarter production of 2022 has been lower of around 23,000 tons because of a damage to the powerline caused by a bushfire in the southeast of the mine site at the beginning of February 2022. Considering the lower production due to the bushfire, total projected spodumene concentrate production for the year 2022 has been computed as:

$$270,464 \text{ tons} \cdot 1 \text{ quarter} + (270,464 + 23,000) \text{ tons} \cdot 3 \text{ quarters} = 1,150,856 \text{ tons}$$

Considering the projected production for the year 2022 and basing on the satellite image analysed acquired in 2022, the following analysis has been carried out.

In Figure 42, the mass required for the process are shown (Kelly et al., 2021). To produce 1 ton of concentrated spodumene (at 6% Li_2O), 4.5 tons of spodumene ore with a concentration of around 0.8-0.9% Li_2O are needed. To obtain 4.5 tons of spodumene ore, around 31.5 tons of materials need to be extracted from the underground, generating a considerable amount of rock waste. To produce 1 ton of lithium carbonate, 7.3 tons of concentrated spodumene (6%) are needed. Instead, 6.42 tons of concentrated spodumene (6%) are needed to produce 1 ton of lithium hydroxide.

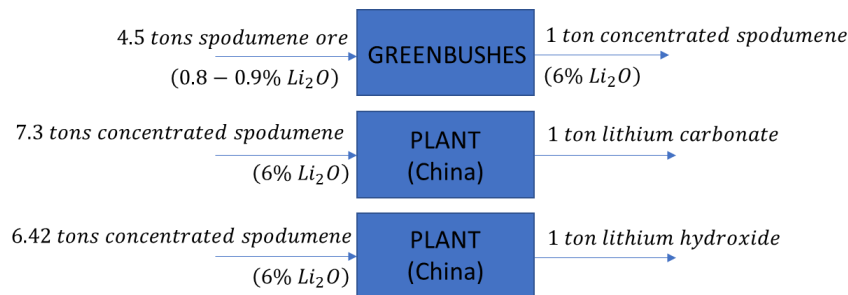


Figure 42. Flow chart showing the different mass required to produce 1 ton of lithium carbonate and lithium hydroxide, starting from the mass of the spodumene ore extracted at Greenbushes mine site.

According to Tianqi's Lithium Report 2021, the mid-term planned compound production capacity will be of around 54.5 ktpy for lithium carbonate and of 53 ktpy for lithium hydroxide. Therefore, it has been assumed that the concentrated spodumene exported from the Greenbushes mine would be refined into these two different compounds according to this proportion. To produce 54.5 kiloton of lithium carbonate per year, as projected by Tianqi's Lithium Report, the following concentrated spodumene mass is needed:

$$54.5 \text{ ktpy of Lithium Carbonate} \rightarrow 397,850 \text{ tons of concentrated spodumene (6\%)}$$

Instead, to produce 53 kiloton of lithium hydroxide per year, the mass of concentrated spodumene required is:

$$53 \text{ ktpy of Lithium Hydroxide} \rightarrow 340,260 \text{ tons of concentrated spodumene (6\%)}$$

The lithium carbonate production over the total lithium production is equal to:

$$\text{Lithium Carbonate: } \frac{397,850 \text{ tons of conc. spodumene (6\%)}}{397,850 \text{ tons} + 340,260 \text{ tons of brine}} = 0.539 \rightarrow 53.9\%$$

Therefore, the lithium hydroxide one is equal to:

$$\text{Lithium Hydroxide: } \frac{340,260 \text{ tons of conc. spodumene (6\%)}}{397,850 \text{ tons} + 340,260 \text{ tons of conc. spodumene (6\%)}} = 0.461$$

$$\rightarrow 46.1\%$$

The previous factors are based on the mass of concentrated spodumene (6%) required to produce a certain amount of product and on the expected refinement of the exported spodumene from the Greenbushes mine in lithium carbonate or hydroxide. Therefore, this proportion is completely assumed and could change according to the market demand and to the refinement infrastructure of different companies. The land use burden and the projected concentrated spodumene production at Greenbushes in 2022 have been divided according to these factors. Lithium carbonate and lithium hydroxide are both produced starting from concentrated spodumene (6%); therefore, the spodumene allocated to lithium carbonate production in 2022 from the Greenbushes mine is equal to:

$$\text{concentrated spodumene}_{Li_2CO_3} = 0.539 \cdot 1,150,856 \text{ tons} = 620,311.33 \text{ tons}$$

which corresponds to:

$$\begin{aligned} & \text{lithium carbonate production (2022)} \\ &= \frac{620,311.33 \text{ tons conc. spodumene (6\%)}}{7.3 \text{ tons conc. spodumene (6\%)/ton lithium carbonate}} \\ &= 84,974.15 \text{ tons of } Li_2CO_3 \end{aligned}$$

Instead, the spodumene allocated to lithium hydroxide production in 2022 from the Greenbushes mine is equal to:

$$\text{concentrated spodumene}_{LiOH} = 0.461 \cdot 1,150,856 \text{ tons} = 530,544.62 \text{ tons}$$

which corresponds to:

$$\begin{aligned} & \text{lithium hydroxide production (2022)} \\ &= \frac{530,544.62 \text{ tons conc. spodumene (6\%)}}{6.42 \text{ tons conc. spodumene (6\%)/ton lithium hydroxide}} \\ &= 82,639.35 \text{ tons of } LiOH \end{aligned}$$

The land used respectively for lithium carbonate production and lithium hydroxide production has been assigned according to the previous computed factors:

$$A_{Li_2CO_3} = 0.539 \cdot 7,657,970.53 \text{ m}^2 = 4,127,646.12 \text{ m}^2$$

$$A_{LiOH} = 0.461 \cdot 7,657,970.53 \text{ m}^2 = 3,530,324.41 \text{ m}^2$$

Then, the land use intensity expressed in squared meters of land used per tonne of lithium produced has been computed:

$$\text{Land Use Intensity (LUI)} \frac{m^2}{ton} = \frac{\text{Lithium Mining Area (2022)}}{\text{Annual Production (2022)}}$$

$$LUI_{Li_2CO_3} = \frac{4,127,646.12 m^2}{84,974.15 tons Li_2CO_3} = 48.58 \frac{m^2}{ton}$$

$$LUI_{LiOH} = \frac{3,530,324.41 m^2}{82,639.35 tons} = 42.72 \frac{m^2}{ton}$$

To compute the land use intensity analysis, no allocation method has been used because there are no other relevant coproducts as output from the Greenbushes mine operations.

IV. Carbon emissions from lithium products: the contribution of transportation

Table 18 illustrates the life cycle inventory datasets which have been used to perform the life cycle assessment.

Table 18. Life Cycle Inventory Data used to perform the LCA analysis for lithium carbonate and for lithium hydroxide both for the brine pathway and for the ore pathway. The carbon dioxide data emissions to air have been retrieved from literature (Kelly et al., 2021).

	Input	Category	Amount	Unit
Lithium Carbonate - Brine	Carbon dioxide	Emission to air/unspecified	2.4933 ¹	t
	Transport, lorry > 16t, fleet average – RER	Transport system/road	1.0*247+1.0*92	t*km
	Transport, transoceanic freight ship – OCE	Transport system/ship	1.0*17277	t*km
	Transport, lorry 20-28t, fleet average - CH	Transport system/road	1.0*652	t*km
Lithium Hydroxide - Brine	Carbon dioxide	Emission to air/unspecified	6.691 ¹	t
	Transport, lorry > 16t, fleet average – RER	Transport system/road	1.0*247+1.0*92	t*km
	Transport, transoceanic freight ship – OCE	Transport system/ship	1.0*17277	t*km
	Transport, lorry 20-28t, fleet average - CH	Transport system/road	1.0*652	t*km
Lithium Carbonate - Ore	Carbon dioxide	Emission to air/unspecified	20.263 ¹	t
	Transport, lorry > 16t, fleet average – RER	Transport system/road	1.0*83	t*km
	Transport, transoceanic freight ship – OCE	Transport system/ship	1.0*7683	t*km
	Transport, lorry 20-28t, fleet average - CH	Transport system/road	1.0*1708	t*km
	Transport, lorry > 28t, fleet average - CH	Transport system/road	1.0*1992	t*km
Lithium Hydroxide - Ore	Carbon dioxide	Emission to air/unspecified	15.563 ¹	t
	Transport, lorry > 16t, fleet average – RER	Transport system/road	1.0*83	t*km

	Transport, transoceanic freight ship – OCE	Transport system/ship	1.0*7683	t*km
	Transport, lorry 20-28t, fleet average - CH	Transport system/road	1.0*1708	t*km
	Transport, lorry > 28t, fleet average - CH	Transport system/road	1.0*1992	t*km
Transportation Lithium Carbonate – Ore (NF)	Transport, lorry > 16t, fleet average – RER	Transport system/road	1.0*365	t*km
	Transport, transoceanic freight ship – OCE	Transport system/ship	1.0*8177	t*km
	Transport, lorry 20-28t, fleet average - CH	Transport system/road	1.0*250	t*km
Transportation Lithium Hydroxide – Ore (NF)	Transport, lorry > 16t, fleet average – RER	Transport system/road	1.0*365	t*km
	Transport, transoceanic freight ship – OCE	Transport system/ship	1.0*8177	t*km
	Transport, lorry 20-28t, fleet average - CH	Transport system/road	1.0*250	t*km

¹ Value retrieved from literature (Kelly e al., 2021)

Table 19 illustrates the results of the life cycle impact assessment which has been performed using the ILCD Midpoint+ 2011 characterization method.

Table 19. Life Cycle Impact Assessment results for lithium carbonate and lithium hydroxide both for the brine pathway and the ore pathway and for the ore near future scenario.

Impact category - Climate Change				
	Contribution (%)	Process	Amount	Unit
Lithium Carbonate (Brine)	87,50	Production	2.493,30	kg CO2 eq
	6,49	transport, transoceanic freight ship - OCE	184,93	kg CO2 eq
	4,43	transport, lorry 20-28t, fleet average - CH	126,31	kg CO2 eq
	1,58	transport, lorry >16t, fleet average - RER	45,09	kg CO2 eq
	100	Total	2849,621	kg CO2 eq
Lithium Hydroxide (Brine)	94,95	Production	6.691,0	kg CO2 eq
	2,62	transport, transoceanic freight ship - OCE	184,93	kg CO2 eq
	1,79	transport, lorry 20-28t, fleet average - CH	126,31	kg CO2 eq
	0,64	transport, lorry >16t, fleet average - RER	45,09	kg CO2 eq
	100	Total	7047,321	kg CO2 eq
Lithium Carbonate (Ore)	96,68	Production	20263	kg CO2 eq
	1,58	transport, lorry 20-28t, fleet average - CH	330,875	kg CO2 eq
	1,30	transport, lorry >28t, fleet average - CH	271,993	kg CO2 eq
	0,39	transport, transoceanic freight ship - OCE	82,236	kg CO2 eq
	0,05	transport, lorry >16t, fleet average - RER	11,039	kg CO2 eq
	100	Total	20959,144	kg CO2 eq
Lithium Hydroxide (Ore)	95,71	Production	15563	kg CO2 eq
	2,04	transport, lorry 20-28t, fleet average - CH	330,87	kg CO2 eq

	1,67	transport, lorry >28t, fleet average - CH	271,99	kg CO2 eq
	0,51	transport, transoceanic freight ship - OCE	82,24	kg CO2 eq
	0,07	transport, lorry >16t, fleet average - RER	11,04	kg CO2 eq
	100	Total	16259,144	kg CO2 eq
Transportation Lithium (Ore) - NF	47	transport, transoceanic freight ship - OCE	87,52	kg CO2 eq
	26	transport, lorry >16t, fleet average - RER	48,55	kg CO2 eq
	26	transport, lorry 20-28t, fleet average - CH	48,43	kg CO2 eq
	100	Total	184,50	kg CO2 eq